LABORATORY-SCALE FRACTURE CONDUCTIVITY CREATED BY ACID ETCHING

A Dissertation

by

MAYSAM POURNIK

Submitted to the Office of Graduate Studies of
Texas A&M University
in partial fulfillment of the requirements for the degree of

DOCTOR OF PHILOSOPHY

December 2008

Major Subject: Petroleum Engineering

LABORATORY-SCALE FRACTURE CONDUCTIVITY

CREATED BY ACID ETCHING

A Dissertation

by

MAYSAM POURNIK

Submitted to the Office of Graduate Studies of
Texas A&M University
in partial fulfillment of the requirements for the degree of

DOCTOR OF PHILOSOPHY

Approved by:

Chair of Committee,	A. Daniel Hill
Committee Members,	Ding Zhu
	Peter Valko
	Zhengdong Cheng
Head of Department,	Stephen A. Holditch

December 2008

Major Subject: Petroleum Engineering

ABSTRACT

Laboratory-Scale Fracture Conductivity Created by Acid Etching. (December 2008)

Maysam Pournik, M.En., University of Birmingham;

M.S., The University of Texas at Austin

Chair of Advisory Committee: Dr. A. Daniel Hill

Success of acid fracturing treatment depends greatly on the created conductivity under closure stress. In order to have sufficient conductivity, the fracture face must be non-uniformly etched while the fracture strength maintained to withstand the closure stress. While there have been several experimental studies conducted on acid fracturing, most of these have not scaled experiments to field conditions and did not account for the effect of rock weakening and etching pattern. Hence, acid fracture conductivity predictions based on the above works have not been able to match actual results.

In order to develop a more appropriate and accurate prediction of acid fracturing treatment outcome, a laboratory facility was developed that is properly scaled to field conditions and enables analysis of etching pattern and rock strength. A systematic experimental study that covered a variety of formations, acid types, and acid contact times was conducted. An acid fracture conductivity correlation was developed based on etched volume, etched pattern, and fracture strength under closure stress.

Results suggested that there is an optimal time of acid exposure resulting in maximum fracture conductivity. There were large differences in the conductivity created

with the different acid systems tested due to different etching patterns and degree of rock strength weakening. There was an optimal acid system depending on formation type, contact time and overburden stress. The acid fracture conductivities measured did not agree with the predictions of the Nierode-Kruk correlation. The newly developed correlation predicts conductivity much closer as it includes the effect of rock strength and surface etching pattern on resulting conductivity.

DEDICATION

Dedicated to my mom, dad, sister and brother and most importantly my wife.

ACKNOWLEDGEMENTS

I would like to express my deepest gratitude and appreciation to my advisor and committee chair, Dr. A. Daniel Hill, for his continuous encouragement, guidance, and support. Also, I would like to give special thanks to Dr. Ding Zhu for her support and motivation during the course of this research. I would also like to extend my appreciation to Dr. Peter Valko and Dr. Hisham Nasr-El-Din for their advice, guidance, and encouragement.

Appreciation is extended to the other member of my committee, Dr. Zhengdong Cheng, for his help and time serving on my committee.

Many thanks are due to all my colleagues who helped me during the course of this research. Special thanks to my research group team: Luis Antelo, Camilo Malagon, Gina Melendez, and Chunlei Zou. Outside my own research group, Manabu Nozaki and Weibo Sui provided me with a lot of support through out my time at Texas A&M University.

Finally, I would like to acknowledge financial support from the Acid Fracturing JIP at Texas A&M University. The facilities and resources provided by the Harold Vance Department of Petroleum Engineering of Texas A&M University are gratefully acknowledged.

NOMENCLATURE

k_f	equivalent fracture permeability (L^2)
k_fw	fracture conductivity (L^3)
$(k_fw)_0$	initial fracture conductivity under no load (L^3)
q_f	fracture flow rate (L^3/T)
q_l	leak off flow rate (L^3/T)
u_f	fracture flow velocity or flux (L/T)
u_l	leak off flow velocity or flux (L/T)
w_f	fracture width (L)
w_i	ideal fracture width (L)
w_h	hydraulic width (L)
X	volumetric dissolving power of acid (L^3 rock /L^3 acid)
V	volume (L^3)
h_f	fracture height (L)
x_f	fracture length (L)
P	pressure (M/LT^2)
L	length of core (L)
k	core permeability (L^2)
S_{RE}	rock embedment strength (M/LT^2)
DREC	dissolved rock equivalent conductivity (L^3)
a	constants

K	kurtosis (L)
c	stress correction factor
$N_{Re,f}$	fracture flow Reynolds number
$N_{Re,l}$	leak off flow Reynolds number
$N_{Pe,l}$	leak off flow Peclet number
D_{eff}	effective diffusion coefficient (L^2/T)
D	diffusion coefficient (L^2/T)
D_o	reference diffusion coefficient (L^2/T)
n’	flow behaviour index
k’	flow consistency index (M/LT)
A	cross sectional area of flow
E_f	reaction rate constant
E_f^0	reference reaction rate constant
R	ideal gas constant
T	temperature
h	asperity height (L)
n	constant for power of width
m	constant
E	Young’s modulus
M	Effective modulus of asperity

ΔE	activation energy
β	inertial flow coefficient
σ_c	closure stress (M/LT^2)
σ_0	initial closure stress (M/LT^2)
σ_y	rock yield stress (M/LT^2)
σ_w	standard deviation of width (L)
σ_h	standard deviation of asperity height (L)
Δ	Differential change in a parameter
μ	viscosity (M/LT)
φ	porosity
ρ	density (M/L^3)
γ	shear rate (T^{-1})
γ_w	shear rate at the wall or fracture face (T^{-1})
α	contact ratio

TABLE OF CONTENTS

Page

Page

LIST OF FIGURES

FIGURE Page

FIGURE Page

FIGURE Page

FIGURE Page

FIGURE Page

FIGURE Page

FIGURE Page

FIGURE Page

LIST OF TABLES

TABLE Page

1. INTRODUCTION

1.1. Introduction

Acid fracturing is a standard practice to increase production rate and improve ultimate recovery in carbonate reservoirs. This technique was initially applied in oilfield in 1960s. It has been proven to be an effective stimulation technique through extensive field applications in carbonate reservoirs all around the world.

Acid fracturing is a stimulation technique in which a fluid (usually a viscous pad) is injected in a carbonate formation at pressures above the fracturing pressures to create a hydraulic fracture or to open existing natural fractures. After the fracture is created, acid is injected into fracture, which reacts and dissolves formation materials on fracture face. After acid injection is completed, process is complete and well is placed on production. As injection pressure is taken off, closure pressure increases on fracture

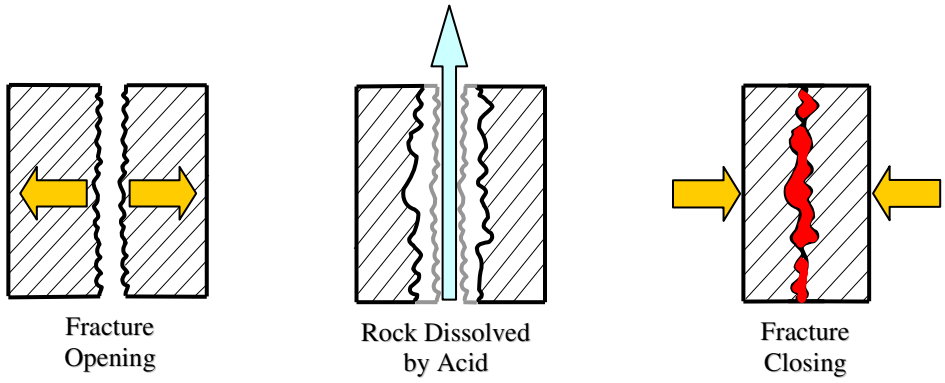

Fig. 1.1—The acid fracturing process.

This dissertation follows the style and format of *SPE Production & Operations*.

faces, tending to close the fracture. Uneven etching along the face of the fracture by acid dissolution is required to create lasting conductivity after fracture closure (**Fig. 1.1**).

Success of acid fracturing depends greatly on the created conductivity which must be retained under closure stress. Acid fracture conductivity is a measure of the capacity for fluid flow through an acidized fracture. The resulting conductivity is influenced by the amount of rock dissolved, the pattern in which the rock is dissolved, the strength of pillars that prop the fracture open, and the amount of closure stress on the fracture. Very little fracture conductivity will be obtained if only a small amount of fracture face is dissolved, resulting in a small fracture width for flow. Similarly, uniform etching does not provide a conductive pathway after fracture closure. When fracturing pressure is withdrawn, and the surrounding stress is applied to the fracture, it usually causes crushing of the fracture areas that hold the fracture open. If these pillars lack the strength to resist deformation, conductivity is greatly reduced.

In order to have sufficient conductivity after fracture closure, the fracture face must be non-uniformly etched with sufficient amount of dissolution of fracture faces by the acid, while the strength of the pillars on fracture faces propping the fracture open still maintained at high levels to withstand the closure stress. Therefore, there is an optimum amount of dissolution or reaction time which creates sufficient area for flow without weakening the supports that hold the fracture open under closure stress.

At low closure stress, amount of etching and the etched pattern of the fracture face should have a dominant influence on the resulting fracture conductivity as long as the strength of the rock can withstand the load. As the closure stress is increased,

surface features along the fracture faces may be crushed and the fracture conductivity is more dependent on the rock strength than on the initial etching pattern.

The primary objectives in designing an acid fracturing treatment are to optimize the penetration distance of acid and the conductivity created by acid in order to maximize productivity of well. The parameters that can be designed for are acid type and strength, injection rate of acid, and injection volume of acid. The design of the fracture geometry can be achieved by using the standard hydraulic fracturing theory including analytical or finite element calculations to determine the fracture geometry as a function of the fluid pumped. The rock dissolution stage is much more difficult to design since the dissolution of the fracture faces changes the fracture geometry and the leak-off behavior.

Acid fracturing treatment performance varies significantly with different formations, reservoir conditions like temperature and closure stress. While there has been significant amount of studies on acid fracturing process, most of these have emphasized on the acid penetration distance with only a few dealing with fracture conductivity. Currently, there is neither a definite design mechanism to optimize fracture conductivity nor an appropriate method to predict created conductivity.

1.2. Literature Review

While success of the acid fracturing process depends highly on the resulting fracture conductivity, the resulting conductivity is very difficult to predict as it inherently depends on a stochastic process and is affected by a wide range of parameters. There have been many experimental and theoretical studies to improve understanding of

acid fracture performance. There has been also extensive work on fluid flow in rough-walled natural fractures. However, very few studies have concentrated on fracture conductivity, especially on developing a correlation for prediction of conductivity. Even though, effect of variable conductivity on productivity of acid fractured wells has been shown to be significant, most studies on fracture conductivity have placed more emphasis on volume of rock removed and length of etched fracture rather than actual conductivity generated.

Clearly the conductivity of a rough-walled fracture under closure stress depends on aperture width, surface roughness pattern, rock strength, and closure stress. Most of these parameters are affected by treatment conditions. The final outcome of a treatment depends highly on the conductivity of the fracture created under different closure stresses.

1.2.1. Fracture Width and Roughness Pattern

One of the first studies on acid fracturing was conducted by Barron et al. (1962) which showed that both flow velocity and fracture width affect the overall acid reaction rate. While reaction rate increased with an increase in flow rate, increase in fracture width caused a decrease in reaction rate. This concurs with theoretical understanding as the reaction between HCl and limestone is diffusion controlled, which means reaction rate is affected by the shear rate (velocity gradient) of the acid near the fracture face. However at shear rates below about 100 s^{-1}, changes in acid velocity or fracture width have no appreciable effect on reaction rate. They postulated that surface roughness alters

the diffusion layer and results in an increase in reaction rate. It was mentioned that non-uniform dissolution of fracture face was observed on samples exposed to acid.

Realizing the lack of work on study of acid-etched fracture conductivity and how it is related to reservoir rock characteristics, Anderson and Fredrickson (1989) developed a laboratory technique to determine fracture conductivity created by acid, which they utilized to optimize treatment design. They recognized that fracture conductivity depends on two primary factors, which are quantity of rock removed and pattern of rock removal. While amount of etching was believed to depend on kinetic parameters (such as acid type and strength, reaction time and temperature, formation reactivity, and flow regime), pattern of removal was postulated to depend on formation characteristics.

Etching tests were also performed by Van Domelen (1992), which confirmed that heterogeneity of fracture face affects resulting etching pattern and conductivity. Acid etching of a core with streaks of high and low solubility materials resulted in significantly better differential etching compared to a core with uniform distribution of insoluble materials treated under the same conditions. Fracture conductivity measurements under closure stress also confirmed previous findings that greater etched volume does not always result in higher retained acid fracture conductivity.

Etching tests at different contact times with the same acid confirmed that increasing contact time with acid which results in more surface dissolution always does not always result in higher retained conductivity (Van Domelen et al. (1994)). Similar results were obtained by a systematic experimental study on acid fracture conductivity conducted by Beg et al. (1996). Their experimental work also showed that increasing

contact time does not always increase fracture conductivity. Reduced conductivity with longer exposure to acid was related to increased rock structure weakening with more acid which was more prone to crushing under closure pressure. They also observed that experiments at different leak-off rates exhibited different etching patterns and resulting fracture conductivity.

Fracture conductivity measurements were performed by Navarrete et al. (1998) in a lab carefully scaled to represent field conditions which resulted in injection rates of 1,000 ml/min in the laboratory. It was observed that more etched volume did not always result in higher conductivities. As they did not measure etching pattern or rock strength, the results could not be explained.

1.2.2. Rock Strength and Closure Stress

Even though Anderson and Fredrickson (1989) realized the importance of differential etching, they recognized also that once differential etching is achieved, formation hardness and ratio of supporting area to etched area control the amount of reduction in created conductivity under closure stress.

Similarly, Van Domelen et al (1994) showed that pattern of rock etching and hardness of fracture rather than actual amount of rock removed control the resulting conductivity as closure stress is increased. Abass et al. (2006) performed experimental studies to investigate the effect of creeping on acid fracture conductivity. They recognized that acid weakens the contact points, causing a susceptible surface to creeping. From their findings, they suggested that the presence of strong contact points

that transfer the creeping force would favor to retain conductivity under high closure stresses.

More recently, Nasr-El-Din et al. (2006) studied the effect of rock strength reduction due to acid etching on production. Their work included experimental analysis for limestone and dolomite with different acid systems, suggesting that the effects of strength reduction are more significant on limestone than on dolomite. Their work showed that that acid weakens rock strength to a considerable degree, with the amount of softening depending on acid and formation type.

1.2.3. Effect of Treatment Parameters

The first actual study on acid fracture conductivity was conducted by Broaddus et al. (1968). They did dynamic acid etching experiments with different formation rocks and measured resulting fracture conductivity under closure stresses of reservoirs. They concluded that acid fracture conductivity is a function of acid type, acid concentration, acid-rock contact time, formation type and temperature. While at low temperatures (less than 150 ^{o}F), regular HCl produced higher fracture conductivity, retarded acid sometimes resulted in larger conductivity at higher temperatures. Based on etching tests, they suggest that there is probably an optimum contact time which produces maximum conductivity while still maintaining adequate rock strength. They recommend using etching tests to determine the optimum acid type and contact time for each specific formation based on adequate created fracture conductivity.

Experiments conducted by Anderson and Fredrickson (1989) provided important information about the effect of treatment and formation parameters on acid etching and

conductivity. Acid fracture conductivity of low temperature formations (less than 100 ^{o}F) at bottom hole closure stress increased as injected acid temperature was increased for all formation types and contact times tested. Acid etching of most chalk samples resulted in rapid conductivity decline with increasing closure stress. Resulting fracture conductivities of formations with low solubility in HCl acid were relatively small, with an average of about 1,500 md-ft. Great differential etching of low-solubility cores that contained patches of anhydride was observed, which resulted in high conductivities. While in most experiments, longer acid contact times resulted in higher conductivities, two tests had conductivity decrease with increasing contact time. Experimental results clearly showed that retained acid fracture conductivity depends on closure stress, formation strength, contact time, acid type, and temperature of acid in addition to formation type. They conclude from their experimental results that formation characteristics have dominant effect on fracture conductivity created by acid etching.

Bartko et al. (1992) conducted acid fracture conductivity experiments on both limestone and dolomite samples from Wahoo formation of Prudhoe Bay to evaluate the effect of various acid systems on etching pattern and resulting conductivity. Core flow experiments resulted in a single, small wormhole formation in all core types acidized with various strengths of HCl and gelled acid. However, 10% emulsified acid generated many small wormholes and showed uneven etching across fractured core when core was split in half. Cores etched with 15% emulsified acid had lower conductivity than those etched with 10% emulsified acid, which was related to greater weakening of rock by 15% emulsified acid. Rock strength measurement showed that the core lost about 60%

of its strength after pumping of 15% emulsified acid (embedment strength was reduced from 100,000 psi to 33,000 psi). Both limestone and dolomite had similar initial conductivities at no closure stress. However dolomite samples lost most of their conductivity at closure stress of 2,000 psi, while limestone cores retained appreciable conductivities up to 4,000 psi closure stress.

Etching tests were also performed for emulsified acids with three different acid/oil ratios of 70:30, 60:40, and 80:20. While a textured etching pattern was observed with 70:30 emulsion and a similar trend but with less etching with 60:40, 80:20 emulsion etched a relatively smooth pattern. Results showed the importance of having the correct ratio of acid to crude and final viscosity of mixture. Also experiments confirmed that two steps are critical in the mixing of emulsified acid. Addition of emulsifier to crude must be metered to have a consistent viscosity through the batch, while it is also crucial to add crude to acid system in a proper manner to obtain a good oil external emulsion.

Van Domelen (1992) performed dissolution rate experiments which showed that different formations display diverse reaction characteristics, and simulator runs confirmed the importance of using formation specific reactivity data in order to determine acid spending profile and etched width profile.

Etching tests conducted by Van Domelen et al. (1994) also confirmed the importance of fracture face heterogeneity on resulting conductivity as etching of two core samples taken from different depths from the same formation with similar properties resulted in different fracture conductivity under same treatment conditions. While gelled acid etching of one core resulted in higher conductivity than straight HCl

acid of same strength, the other core retained higher conductivity when etched with straight HCl.

1.2.4. Conductivity Prediction

Williams and Nierode (1972) mention that there are several models for prediction of fracture geometry and etched fracture length while acid fracture conductivity cannot be predicted with certainly. As conductivity cannot be predicted with certainly, they recommend pumping about 1.5 and 3 times fracture volume for 28% and 15% HCl, respectively, to achieve adequate fracture conductivity. Similarly, they assume the ratio of fracture conductivity to formation permeability to be in the range of 10^3 to 10^5 md-in / md in order to calculate stimulation ratios. Importance of accurately predicting fracture conductivity is admitted as they state that "*shortcoming of this or any design procedure for acid treatments is our inability to predict accurately the fracture conductivity to be created by acid etching*."

One simple estimate of acid fracture conductivity was developed, based on assumption of uniform dissolution of fracture face by Williams et al. (1979). Uniform dissolution of fracture face forms a channel of uniform width, w_i, called the ideal fracture width. This ideal width is determined by dividing the total volume of rock dissolved by fracture area:

$$w_i = \frac{\text{volume of rock dissolved}}{\text{Fracture area}} = \frac{XV}{2(1-\phi)h_f x_f}, \quad \text{..... (1.1)}$$

where X is the volumetric dissolving power of acid, V is the volume of acid injected, h_f is the fracture height, x_f is the fracture half-length, and ϕ is the porosity of matrix. Laminar

flow through a smooth fracture is assumed to be analogous to flow between two perfectly smooth and parallel plates, which is described by the so-called "cubic law":

$$q = h_f \frac{w^3}{12\mu}\frac{\Delta P}{L}, \quad \text{..... (1.2)}$$

where q is the flow rate, h_f is the fracture height, w is the fracture width or aperture, ΔP is the pressure drop across fracture length, L, and μ is the fluid viscosity. From comparison of cubic law with Darcy's law, we obtain:

$$q = h_f w \frac{k_f}{\mu}\frac{\Delta P}{L}, \quad \text{..... (1.3)}$$

where the equivalent fracture permeability, k_f is defined as:

$$k_f = \frac{w^2}{12}. \quad \text{..... (1.4)}$$

As fracture conductivity, $k_f w$, is defined as product of fracture permeability and fracture aperture, we obtain:

$$k_f w = \frac{w^3}{12}. \quad \text{..... (1.5)}$$

Similarly, ideal fracture conductivity, $(k_f w)_i$, is defined based on ideal width (w_i) as:

$$\left(k_f w\right)_i = \frac{w_i^{\,3}}{12}. \quad \text{..... (1.6)}$$

While this is a simple estimate of fracture conductivity under no closure stress, ideal fracture conductivity never exists in reality due to uneven etching of fracture faces.

The current correlation for fracture conductivity that is used in industry was developed by Nierode and Kruk (1973). The correlation is based on experimental study

conducted on different formation samples acidized with HCl acid. The conductivity estimation depends on amount of rock dissolved, rock strength and closure stress:

$$k_f w = C_1 \exp(-C_2 \sigma_c), \quad \text{..... (1.7)}$$

where

$$C_1 = 1.47 \times 10^7 w_i^{2.47}, \quad \text{..... (1.8)}$$

$$C_2 x 10^3 = 13.9 - 1.3 \ln(S_{RE}), \ for: 0 < S_{RE} < 20{,}000 psi, \quad \text{..... (1.9)}$$

$$C_2 x 10^3 = 3.8 - 0.28 \ln(S_{RE}), \ for: 20{,}000 < S_{RE} < 500{,}000 psi, \quad \text{..... (1.10)}$$

where σ_c is the closure stress (in psi), S_{RE} is the rock embedment strength (in psi), fracture width is in inches, and conductivity calculated is in md-ft. [Note: In the original publication, there was a typographical error in the equation presented here as Eq. 1.9. The original publication has the constant 19.9 instead of 13.9.] There is no consideration of the effect of etched pattern and rock weakening from acid dissolution of rock on resulting conductivity. The correlation also does not include the effect of acid leak-off on resulting conductivity as the experiments did not allow leak-off from fracture faces. The authors state that the correlation shows the lower bound of attainable conductivity as heterogeneities and fingering leads to channels development along the fracture in field applications.

Analysis of the correlation reveals that conductivity is dependent on amount of rock dissolved (C_1), rock embedment strength (C_2), and closure stress. The correlation states that ideal fracture width raised to power of 2.47 determines the initial fracture conductivity under zero closure stress. This suggests that increasing the amount of rock

dissolution (i.e. increasing acid contact time), which results in higher etched ideal width, will greatly increase the conductivity at all different closure stresses (**Fig. 1.2**). The second coefficient, C_2, accounts for the effect of the un-acidized strength of the rock (S_{RE}). However, there are only two very broad categories considering very soft rocks or hard rocks. The correlation also indicates that the rate of decline of conductivity is determined by the initial rock strength and the closure stress (**Fig. 1.3**).

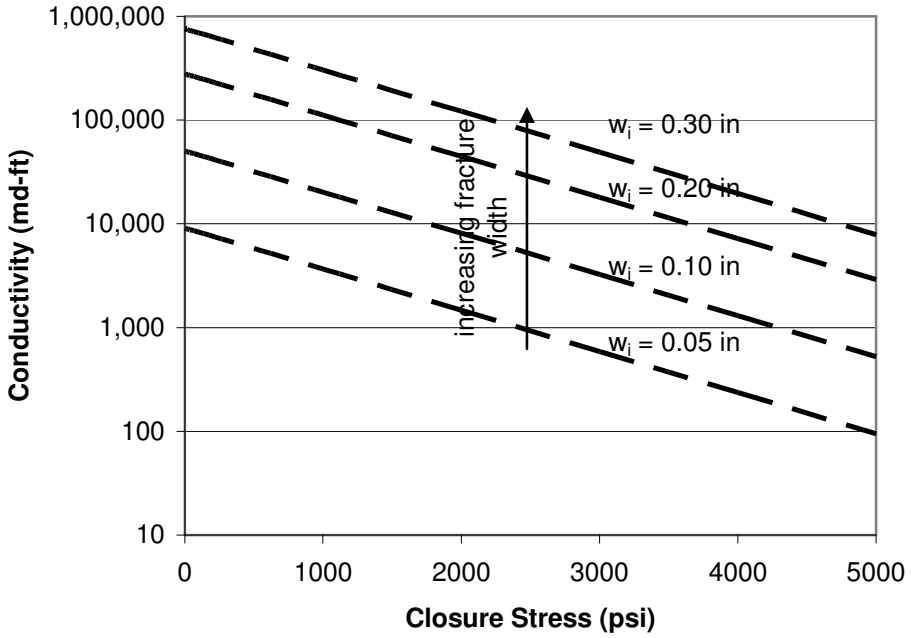

Fig. 1.2—Effect of fracture width on conductivity based on Nierode and Kruk model.

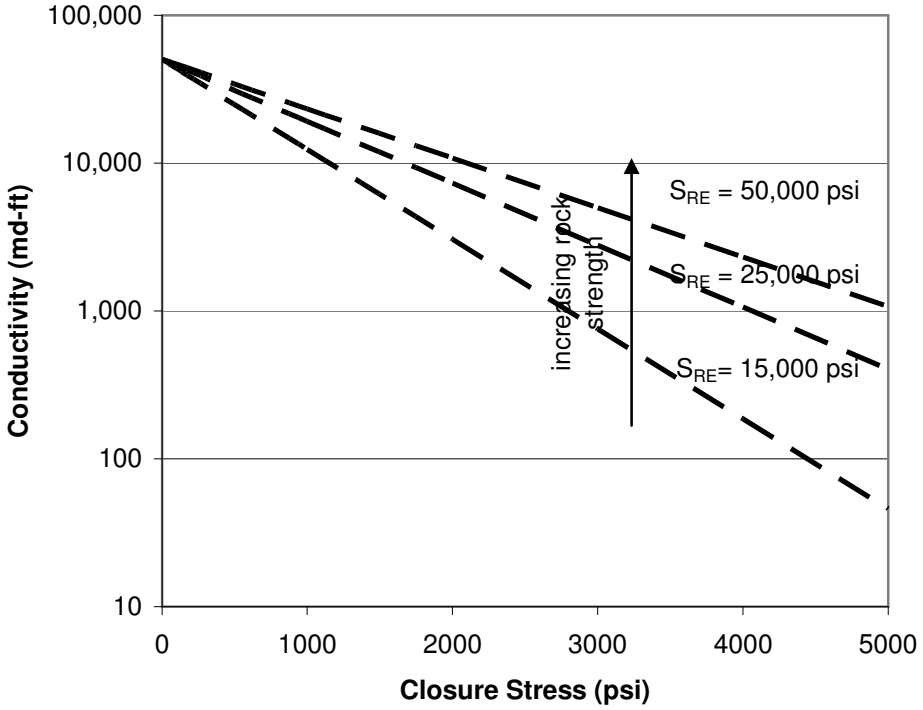

Fig. 1.3—Effect of rock strength on conductivity based on Nierode and Kruk model.

Due to lack of an appropriate conductivity prediction model and dependence of conductivity on many parameters, Anderson and Fredrickson (1989) suggest conducting a series of etching tests to determine the optimum acid system for a given formation based on etched conductivity and use the experimental value of acid fracture conductivity as input in an acid fracturing design program. Their experimental work clearly shows the importance of having a comprehensive acid fracture conductivity predictive model which accounts for effect of etched pattern and formation hardness in addition to amount of rock removed.

Following experimental work which showed the importance of formation heterogeneity on resulting etching pattern and conductivity, Van Domelen (1992) showed the importance of using correct value of fracture conductivity in a fracture acidizing simulator in order to correctly optimize treatment design and predict well response to treatment. The simulator was run for a specific treatment condition using once average conductivity data from experiments and another time using Nierode and Kruk (1973) correlation. While Nierode and Kruk (1973) model predicted conductivity under 100 md-ft, etching tests predicted conductivity over 50,000 md-ft, which compares more closely with the actual treatment as production rate was increased about three folds.

Gong et al. (1998) developed a correlation for fracture conductivity accounting for effect of etching pattern and rock strength reduction from acidizing. The conductivity prediction depends on initial fracture conductivity, fracture face roughness characteristic, rock yield stress, and closure stress as shown below:

$$k_f w = (k_f w)_0 \left[1 - \left(\frac{4+K}{5+K} \right) \left(\frac{2\sigma_c}{c\sigma_y} \right)^{1/(K+4)} \right]^6, \quad \text{..... (1.11)}$$

where $(k_f w)_0$ is the initial fracture conductivity under no closure stress, K is the kurtosis of asperity height distribution, c is a stress correction factor, and σ_y is the rock yield stress. The model predicts increasing conductivity with longer acid-rock contact time as initial fracture conductivity will increase with more etched surface (**Fig. 1.4**), which is not in accordance with the several experimental results mentioned above. Furthermore, while they measured Brinell hardness and rock embedment strength to determine rock

weakening due to acid, the model uses rock yield stress as measure of rock strength under load. The surface etching was not characterized in detail and some parameters in the model (stress correction factor and yield stress) were assumed to match experimental data. The model can not be used to predict conductivity in field conditions as there is no relationship between acidizing conditions and input parameters for the model like surface roughness and rock yield stress after acidizing.

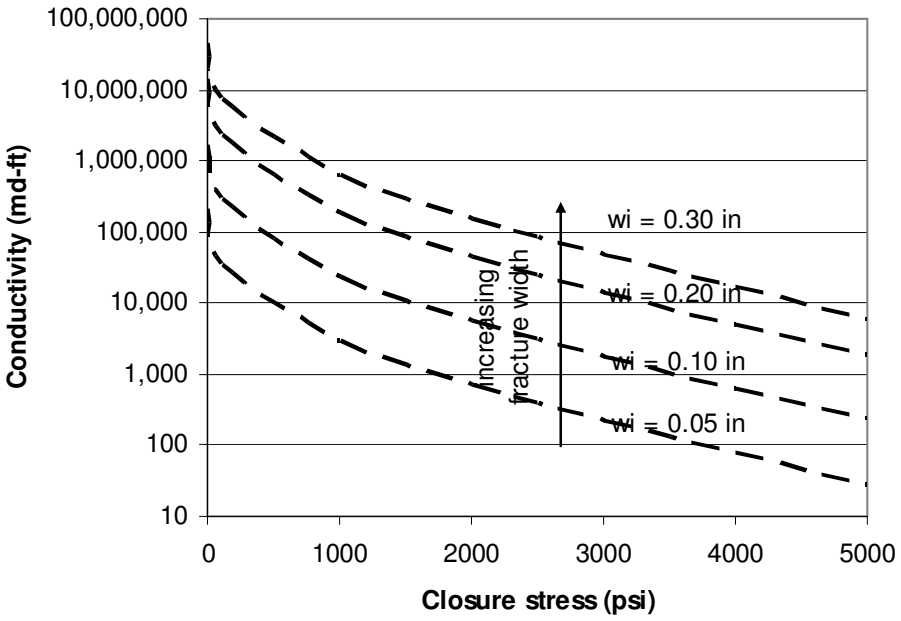

Fig. 1.4. Effect of fracture width on conductivity based on Gong et al. (1998) model.

1.3. Problem Description

The resulting fracture conductivity is one of the measures upon which engineers base their decision when selecting a particular stimulation treatment or making a design

assessment. If conductivity is not properly predicted, it leads to inappropriate evaluation of treatment design, prediction of production, and economic evaluation. Therefore, accurate acid fracture conductivity prediction is a key aspect for design and outcome of acid fracturing process. Currently, failure in designing effective acid fracture treatments with predictable outcomes are due to limited knowledge of the parameters that influence the resulting conductivity.

While fracture conductivity created and retained under closure stress by acid etching of fracture faces during acid fracturing process is essential for success of process and prediction of productivity enhancement outcome, the mechanism of acid fracture conductivity creation is not well understood. There have been only few publications addressing fracture conductivity created by acid, with only two of these leading to correlation for prediction of acid fracture conductivity. While the current correlation used in industry has failed to predict correctly the resulting conductivity, the other correlation has not been able to be easily applied to field operations. Most of the experimental works including the ones that lead to correlation development were conducted at conditions that did not scale to field conditions. Furthermore, many of these works did not consider effect of rock weakening and etching pattern on resulting conductivity and conducted experiments with limited number of rock types, acid types and contact times.

In order to improve success and prediction of acid fracturing treatments, a thorough understanding of the influence of treatment variables and formation properties on resulting conductivity is required. Understanding and predicting the created fracture

conductivity requires extensive laboratory experiments to be conducted. These experiments must be conducted at conditions that properly scale to field conditions to ensure validity of these experiments in field applications. Furthermore, these experiments must focus on all the treatment parameters that are important to the industry with emphasis on testing at conditions faced in field operations. All appropriate and significant parameters that influence resulting conductivity must be measured and quantified to enable the development of a predictive model for acid fracture conductivity.

1.4. Objectives of Research

The main objective of this research study is to design and conduct appropriate experimental work on acid fracture conductivity in order to develop a new correlation for conductivity prediction, which can be readily used by industry. In order to achieve our goal, the following tasks must be performed:

1) Scale experimental conditions to mimic field
2) Design and setup experimental apparatus
3) Develop experimental procedure
4) Plan a systematic experimental study
5) Conduct experiments
6) Analyze effects of parameters on resulting conductivity
7) Buildup a design procedure for acid fracture treatments
8) Develop a correlation for conductivity prediction

In order ensure laboratory experiments represent field conditions, the different phenomena that occur in the process of acid fracturing must be properly scaled. Once the conditions for testing are determined from scaling of experiments, the design and set up of lab facility is undertaken. The experimental apparatus can be divided into four different areas: rock strength measurement, acid etching, surface characterization, and fracture conductivity measurement. As experimental work must cover all the important parameters that effect resulting conductivity, a systematic set of experiments must be planned. The important parameters that influence conductivity will be determined and a complete set of experiments planned to study effect of these parameters. Section 2 describes in detail the experimental scaling, design, procedure and planning.

As one of the main objectives is to determine the effect of treatment conditions on etching, rock weakening, and resulting fracture conductivity, experimental results will be used to analyze the effect of each treatment factor, which will be used to develop effective designing criteria for acid fracture treatments. The outcomes of experiments with emphasis on effect of treatment parameters on etching pattern, rock strength, and resulting conductivity are summarized in Section 3.

Our main objective is to use our experimental work to develop a correlation for conductivity prediction. Experimental results will be used to determine the parameters that significantly and consistently influence the resulting conductivity. These parameters will be ones that characterize etching pattern, fracture width, and rock strength. Once important parameters are determined from results, statistical methods will be used to develop a correlation for conductivity. Available theoretical models will also be used to

determine if we can develop a theoretical correlation for conductivity prediction. The development of conductivity correlation is described in detail in Section 4.

The validation of our correlation is also covered in Section 4, where the two developed correlations will be used together to predict our experimental results and compared to other available conductivity models. Section 5 summarizes the conclusions drawn from this systematic experimental study on acid fracture conductivity and also the recommendations for future work.

.

2. EXPERIMENTAL STUDY

2.1. Previous Experimental Work

There have been several major experimental studies on how the resulting fracture conductivity from acid fracturing process depends on treatment parameters. While there are some similarities between studies, there are several major differences in both testing conditions and results obtained. The experimental works from three major studies are summarized. The results from these studies have not been sufficient and adequate enough to explain the effect of treatment parameters on resulting conductivity which would enable a more accurate correlation of fracture conductivity.

2.1.1. Experimental Conditions

There have been three major different studies of resulting acid fracture conductivity. The experimental conditions were significantly different in each study. Figure 2.1 shows the size and shape of core samples used in the three different studies. In the original study of Nierode and Kruk (1973), cylindrical cores of approximately 1 inch in diameter and 3 inches in thickness were used with no leak off allowed (**Fig. 2.1 a**), while the more recent studies of Gong (1997) (**Fig. 2.1 b**) and Navarrete et al. (1998) (**Fig. 2.1 c**) used rectangular shaped cores with larger fracture face dimensions and allowed leak off rates similar to field. The fracture faces of the Navarrete et al. (1998) cores have the largest exposed surface area to acid enabling more realistic etching patterns to develop and also greater depth in leak off direction, which allows improved leak off control. While there was no leak off allowed in Nierode and Kruk (1973) work,

Gong (1997) varied leak off rate from 0 to 40% of total flow rate and Navarrete et al. (1998) fixed the leak off rate with a differential pressure across leak off of 100 psi.

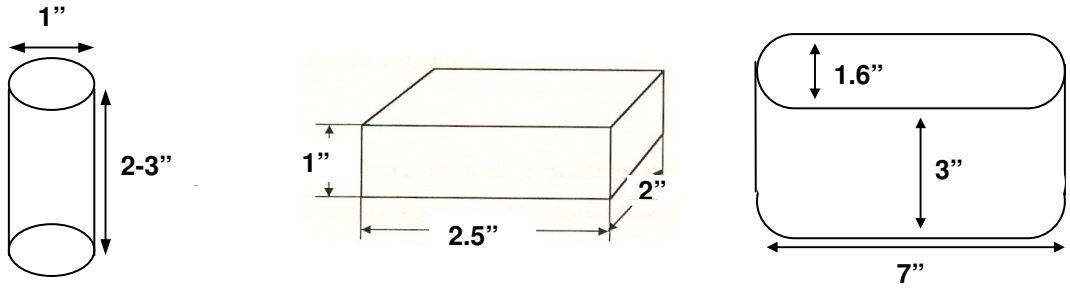

a) Nierode and Kruk **b) Gong** **c) Navarrete et al.**

Fig. 2.1—Core sample size and shape compared between three studies.

Another major difference among the experiments was the scaling of laboratory testing to field conditions. While Nierode and Kruk (1973) do not specify the injection rate used, Gong (1997) used an injection rate of 10 ml/min which is similar to majority of experiments conducted on acid fracturing. However, Navarrete et al. (1998) were the first to inject at high injection rates of about 1,000 ml/min as they believed it was required to inject at these rates in order to scale to field conditions. Another difference among studies that is also related to injection rate is the volume of acid injected, which depends on injection rate in addition to injection rate. While there is no mention of injection time in the Nierode and Kruk (1973) work, Gong (1997) used several different injection times ranging from about 10 to 50 minute and Navarrete et al. (1998) injected for about 20 minutes in their experiments. As a result, while Gong (1997) injected a

maximum volume of 500 ml, Navarrete et al. (1998) injected about 20,000 ml, which is 40 times more than maximum injected volume of Gong (1997).

Two main parameters that influence the acid fracturing process but can not be designed are temperature and formation properties. They both have significant influence on the resulting etching and conductivity of fracture. While Nierode and Kruk (1973) conducted experiments with about 8 different formation types, Gong (1997) and Navarrete et al. (1998) fracture acidized only two types of formations. It seems that Nierode and Kruk (1973) conducted experiments at only one temperature which is the same case as Gong (1997), however Navarrete et al. (1998) conducted experiments with each rock type at two temperatures.

One of the main parameter that can be controlled in acid fracturing process is the acid type. There are now several different acid systems used in industry that allow controlled leak off and reaction rate, enabling better use of acid in creating longer and more conductive fractures. However these three major experimental studies have not studied the effect of acid type. The correlation developed by Nierode and Kruk (1973) was based on only straight HCl acidized samples (assumed based on available information). While Gong (1997) used also only straight HCl acid system, Navarrete et al. (1998) used one type of modern acid system in addition to using straight HCl system. It was an emulsified acid system with a 70:30 HCl acid-to-oil ratio stabilized with an emulsifier with three different concentration of HCl: 15%, 20%, and 28%.

2.1.2. Experimental Results

While the main objective of experiments is to determine the resulting conductivity after fracture acidizing, the resulting etching pattern of fracture face is very important as it influences final conductivity. The resulting conductivity depends highly on non-uniform etching of fracture face in order for unetched sections to act as pillars to keep fracture open for flow. **Fig. 2.2** compares the etching patterns between the tests conducted by Gong (1997) and Navarrete et al. (1998) under the most similar possible condition. There are no etching patterns available from Nierode and Kruk (1973). While there seems to be a lot of surface roughness on Gong's acidized core, there is more eddy etching with channeling on acidized core of Navarrete et al. (1998). The main difference that caused such a variation in etching pattern between these two experimental studies is the injection rate. Similar results were observed in our laboratory which will be discussed in Section 3.

a) Gong **b) Navarrete et al.**

Fig. 2.2—Etched surface profile comparison.

Another important parameter that influences the resulting conductivity is the strength of the fracture face as it must withstand the closure stress on it. There are many different methods and parameters that represent the strength of formation. However, in acid fracturing, rock embedment strength (S_{RE}) has been the main parameter used to define the rock strength. Nierode and Kruk (1973) seem to have measured rock embedment strength for cores before and after acidizing, while Gong (1997) measured S_{RE} only before acidizing. However Gong (1997) did measure brinell hardness of cores before and after acidizing. There are no rock strength measurements in Navarrete et al. (1998) work. While S_{RE} measurements of Gong (1997) for Indiana limestone samples ranged from 30,000 to 182,000 psi with an average of 64,000 psi, Nierode and Kruk (1973) measured S_{RE} of about 45,000 psi for unacidized Indiana limestone. Nierode and Kruk (1973) do not mention such a large variation among the rock embedment strength of Indiana limestone samples. The acidized S_{RE} of Indiana limestone samples ranged from 14,000 to 23,000 psi.

The main outcome of the experiments was fracture conductivity under different closure stresses. There were large differences in the final conductivity, both at low and high closures stress. At low closure stress of 1,000 psi, the range of conductivity values were from 12,500 to 165,000, 300 to 85,000, and 2,000 to 8,000 md-ft for Nierode and Kruk (1973), Gong (1997), and Navarrete et al. (1998), respectively. However it must be mentioned that the tests were not at the exactly same condition. There were more similarities at high closure stress of 5,000 psi where the resulting conductivities ranged from 120 to 850, 2 to 8,000, and 200 to 800 md-ft for Nierode and Kruk (1973), Gong

(1997), and Navarrete et al. (1998), respectively. However it is interesting to note that majority of conductivity results showed an exponential decline with closure stress for all the three different studies.

2.1.3. Experimental Conclusions

It is very interesting that there were some contradicting conclusions among the three studies on the effect of treatment parameters on resulting conductivity. Both Nierode and Kruk (1973) and Gong (1997) results show that there is general trend of increasing conductivity at zero closure stress with increasing dissolved rock volume or contact time. However Gong (1997) results suggest that there might be faster rate of conductivity decline with closure stress for cores with larger dissolved rock volume or longer contact times, while Nierode and Kruk (1973) results show little or no effect of dissolved rock volume on decline rate of conductivity. On the contrary, Navarrete et al. (1998) results indicate that fracture conductivity at low closure stress actually declines with increasing temperature even though increased temperature should result in more dissolved rock volume. Also conductivity depends on acid type from Navarrete et al. (1998) results. Surface etching analysis of Gong (1997) revealed that the etching pattern has a significant influence on fracture conductivity with much difference in conductivity between channel etched pattern versus rough etched pattern.

2.1.4. Shortcomings and Recommendations for Future Work

Most of the studies have not considered the need to scale experiments to represent field conditions. Results from Navarrete et al. (1998) study where scaling to field conditions was taken into consideration during experimental work revealed

different conclusions in terms of resulting conductivity. The results showed different etching pattern compared to previous results and also showed that there might be a decrease in conductivity even at low closure stress with increased dissolved rock volume. In addition to the importance of scaling, studies have shown the importance of etching pattern on resulting conductivity, however little emphasis has been given to characterize surface pattern in order to relate it to resulting conductivity. Furthermore, while importance of rock strength has been shown in experiments, the effect of acidizing on rock weakening and the impact on final conductivity has not been appropriately accounted. While results have shown that treatment parameters like acid type and injected volume and actual reservoir conditions like temperature and rock type influence resulting conductivity, the precise pattern of influence of these parameters on resulting conductivity has not been determined from detailed experimental studies.

2.2. Experimental Scaling

2.2.1. Importance of Scaling

One of the major short comings of most previous experimental studies has been the lack of scaling experiments to field conditions. As a result, most experimental findings have not reflected actual field results. The different phenomena that occur in fracture acidizing process must be scaled properly to ensure experiments represent field conditions. In order to achieve proper scaling, the different dimensionless groups that represent all the phenomena that occur must be identified and matched.

2.2.2. Scaling Procedure

The main phenomena that occur in acid fracturing process are acid transport along the fracture, acid leak off, and acid reaction at the fracture wall. One of the main dimensionless numbers in fluid dynamics that provides a criterion to ensure dynamic similitude is Reynolds number, N_{Re}. The hydrodynamics of fluid flow in experiments must match field applications. Reynolds number is the ratio of inertial forces to viscous forces and quantifies the relative importance of these two types of forces for a given flow condition. Reynolds number for flow through a fracture, $N_{Re,f}$ is expressed as:

$$N_{\mathrm{Re},f} = \frac{w v_f \rho}{\mu}, \quad \text{..... (2.1)}$$

where w is the fracture width or aperture, v_f is velocity along the fracture, ρ is the fluid density, and μ is fluid viscosity. As there are two symmetrical fractures in a field fracturing case, the injection rate, q is expressed as:

$$q = v_f \times (2 w h_f), \quad \text{..... (2.2)}$$

where h_f is the fracture height. Hence, Reynolds number in terms of injection rate is expressed as:

$$N_{\mathrm{Re},f} = \frac{q\rho}{2 h_f \mu}. \quad \text{..... (2.3)}$$

Similarly, there is flow of acid through the fracture face defined as leak off acid. The hydrodynamics of flow in leak off direction must also be matched to field conditions. Similar to above, Reynolds number for flow in leak off direction, $N_{Re,l}$ is defined as:

$$N_{\mathrm{Re},l} = \frac{w v_l \rho}{\mu}, \quad \text{..... (2.4)}$$

where v_l is the leak off velocity. Another parameter that accounts for acid transport phenomena (diffusion and convection) and leak off effect is the leak off Peclet number, $N_{Pe,l,}$ which represents ratio of convective transport due to leak off over diffusion transport toward the fracture wall expressed as:

$$N_{Pe,l} = \frac{v_l w}{2D_{eff}}, \quad \text{..... (2.5)}$$

where v_l is the leak off velocity, and D_{eff} is the effective diffusion coefficient. Since

$$q_l = v_l \times 2h_f \times 2x_f = 4v_l h_f x_f, \quad \text{..... (2.6)}$$

then

$$N_{Pe,l} = \frac{q_l w}{8h_f x_f D_{eff}}. \quad \text{..... (2.7)}$$

While there are still some more scaling parameters, however these scaling parameters account for all the major processes that occur during acid fracturing and enable relatively accurate similitude between field and experiments.

2.2.3. Fluid Properties Scaling

Scaling experiments to field for the different phenomena that occur during treatment requires that fluid properties are matched between field and experiments. It is clear from above parameters that fluid properties play an important role in the process of scaling. It is important to ensure fluid properties are properly scaled. Fluid properties are affected by several different parameters depending on the fluid type. Many different fluid systems are used in acid fracturing ranging from straight, plain HCl to more complicated HCl mixtures containing surfactants, polymers and acid-in-oil emulsions.

While straight acid is characterized as Newtonian fluid with viscosity independent of shear rate, most of the other acid systems like emulsified, viscoelastic and gelled acids are non-Newtonian fluids with changing viscosity with shear rate. Most fluids also exhibit a change in density, viscosity, diffusion coefficient, and reaction rate constant with changing temperature.

In order to ensure similar fluid properties as in the field, the operating temperature of experiments must be maintained at same levels as field conditions. As long as temperatures are similar, most of the fluid properties will be the same between the field and experiment. However for non-Newtonian fluids, the shear rate (γ) which is function of injection rate and fracture dimension must also be matched to field in order to ensure fluid properties like viscosity are similar. Most of the non-Newtonian acid systems follow the power law model where viscosity is given by:

$$\mu = k'\gamma^{n'-1}, \quad \text{..... (2.8)}$$

where *k'* is the flow consistency index, and *n'* is the flow behaviour index. The shear rate for flow of power law fluid in slot geometry is given by (Navarrete et al., 1998):

$$\gamma = \frac{2(1+2n')}{n'}\frac{q}{w^2 h}. \quad \text{..... (2.9)}$$

Then Reynolds numbers for power law fluid can be defined using the viscosity and shear rate function, leading to the following equations:

$$N_{\mathrm{Re},f} = \frac{w^{2(1-n')} q_f^{2-n'} \rho}{2h_f^{2-n'}\left(k' \frac{2(1+2n')}{n'}\right)^{n'-1}}. \quad \text{..... (2.10)}$$

$$N_{\mathrm{Re},l} = \frac{w^{2-n'} u_f^{1-n'} u_l \rho}{\left(k' \frac{2(1+2n')}{n'} \right)^{n'-1}} . \quad \text{..... (2.11)}$$

2.2.4. Calculation of Required Values

The scaling parameters which have been recognized from the acid fracturing process must be matched between the field and experiment. In order to achieve this, the required field information must be obtained. In the field acid fracturing treatments, the acid injection rate varies a lot from 10 to 50 bbl/min due to different target zones depth, treatment intervals height and field location logistics. The reported fracture widths are about 0.1 to 0.2 inch during acid injection and the fracture height ranges from 50 ft to 200 ft. **Table 2.1** summarizes typical values of parameters for a field acid fracturing job (Navarrete et al., 1998; Bartko et al., 2003). Acid properties differ for each acid system and depend highly on temperature of formation. Fluid properties for four typical acid systems used in industry at the temperature of 175 ^{o}F are given in **Table 2.2** (de Rozieres et al., 1994; Conway et al., 1999; Nasr-El-Din et al., 2008).

TABLE 2.1—TYPICAL FIELD ACID FRACTURING TREATMENT

Acid pumping rate, q	20	*bbl/min*
Formation height, h_f	100	*ft*
Fracture width, w	0.15	*inch*

TABLE 2.2—FLUID PROPERTIES OF FOUR ACID TYPES AT 175 °F

Parameters	HCl	Gelled	Viscoelastic	Emulsified
ρ (g/cm^3)	1.06	1.07	1.1	1.02
n'	1	0.5	0.36	0.73
k' (lbf-s/ft2)	0.0000155	0.0137	0.0411	0.0033
D_{eff} (cm^2/sec)	$1x10^{-4}$	$5x10^{-5}$	$6x10^{-5}$	$6x10^{-6}$

Based on above given data, the values of shear rate, corresponding viscosity and dimensionless numbers are calculated and summarized in **Table 2.3**. It is important to state that the injection rate given in Table 2.1 is for both wings of a fracture; hence injection rate used in shear rate calculation is based on injection rate into one wing since it is based on flow in a single slot.

TABLE 2.3—TYPICAL SHEAR RATE, VISCOSITY, AND DIMENSIONLESS NUMBERS FOR FIELD CONDITIONS

	HCl	Gelled	Viscoelastic	Emulsified
Shear rate (s^{-1})	269	359	429	303
Viscosity (cp)	0.74	35	41	34
$N_{Re,f}$	934	20.2	17.6	19.5
$N_{Re,l}$	0.033	0.00072	0.00063	0.00069
$N_{Pe,l}$	1.45	2.90	2.42	24.2

In order to scale experiments to field conditions, the above parameters calculated in Table 2.3 must be matched in experiments. There are certain limitations on parameters that can be modified and designed for in the laboratory due to equipment and space. In

order to have consistent and comparable results, the conductivity cell used for performing the experiments must be designed based on specifications of API standards. The API conductivity cell limits the extent of fracture length and height, however the length in the leak off direction can be modified in order to allow better leak off control. Based on API cell standard, the fracture length and height are limited to 7.25" and 1.75", respectively. The main parameters that can be designed for in the experiment are fracture width, injection rate, and leak off flux. As there are certain restrictions on fracture width based on API cell design, a fracture width of 0.12" is set for all experiments. This allows fracture width to be consistent to field results and comparable to other experimental studies. Matching of fracture Reynolds number sets the injection rate that must be used based on given fluid properties. Then shear rate can be calculated to determine if correct fluid properties were used in Reynolds number calculation. As the fracture width has been set, leak off Peclet and Reynolds numbers determine the leak off flux. The values of parameters obtained by matching scaling parameters are shown in **Table 2.4**.

TABLE 2.4—EXPERIMENTAL PARAMETERS FROM SCALING

	HCl	**Gelled**	**Viscoelastic**	**Emulsified**
Injection rate (l/min)	1.74			
Shear rate (s^{-1})	421	561	671	473
Viscosity (cp)	0.74	28	31	30
$N_{Re,f}$	934	25	23	22
Leak off rate (ft/min)	0.0019			

Calculations clearly show that while Reynolds numbers are well matched to field data, the shear rate and viscosity are not as well matched. An injection rate of 1.74 L/min is required in the laboratory to match field application which is much higher than the usual 10 ml/min injection rate used in experiments. The best available pump to inject at high rates with high outlet pressures without corrosion could only pump at about 1.04 L/min with a maximum discharge pressure of 2,200 psi. Based on the available injection rate of 1.04 L/min, scaling parameters and viscosity of fluids were calculated and summarized in **Table 2.5**. All scaling parameters are very similar to field data and experiments are well scaled to field conditions. The leak off flux can be controlled at the specified rate based on scaling which allows similar Peclet numbers between experiments and field.

TABLE 2.5—EXPERIMENTAL VALUES OF SCALING PARAMETERS

	HCl	Gelled	Viscoelastic	Emulsified
Shear rate (s^{-1})	242	323	386	272
Viscosity (cp)	0.74	37	44	35
$N_{Re,f}$	537	19.1	16.5	18.9

2.2.5. Limitations of Scaling Experimental Work

While great emphasis has been placed on scaling experiments to field conditions, laboratory conductivity tests cannot completely represent field conductivity due to several major differences that can not be scaled properly. Obviously the size of core samples and conductivity cell are limited and cannot be representative of a real fracture.

As the length of the cell is much shorter than a real fracture, mainly fresh acid is reacting with fracture faces and should be more representative of the entrance of a fracture in field treatment. The size of core is too small to be able to capture some of the heterogeneous nature of real formation. The composition and physical properties of a real fracture surface may vary significantly both in horizontal and vertical direction, resulting in a much more differential etching than observed in laboratory scale. There are also some rock mechanics effects, such as spalling, which results in relative displacement of etched surfaces, which can not be captured in laboratory (Navarrette et al., 1998). Furthermore, there are certain effects in the laboratory like entrance effect and core preparation that are not observed in field applications.

2.3. Experimental Planning

2.3.1. Parameters Fixed

Scaling experiments to match field applications sets certain limits on experimental conditions. Temperature, injection rate, leak off flux, and fracture width must be kept at specified values to ensure experiments are scaled appropriately to field conditions. Another limitation on parameters is due to size and capacity of apparatus. The API conductivity cell limits the fracture dimensions.

In order to ensure single phase flow during acidizing process, the pressure inside the fracture must be kept at a level to ensure any CO_2 gas produced from reaction is kept in solution and does not flow as gas in a separate phase. While there is detailed information on the solubility of CO_2 in water, there is very limited data on solubility in unspent and spend HCl acid solutions. Detailed data of CO_2 solubility in water can be

used to determine solubility at any temperature and pressure. The available solubility data of CO_2 in HCl solutions are limited to few pressures and temperatures. Solubility of CO_2 in totally spent 5% and 15% HCl acid solutions at temperatures of 25 and 76 ^oC for pressures up to 1,500 psi are available (Shaughnessy & Kunze, 1981). Solubility of CO_2 in unspent HCl solution of 1% to 4% concentration is also available at ambient pressure and temperatures up to 25 ^oC (Wong et al., 2005). While these data are very limited, they provide insight on the possibility of presence of CO_2-rich gas phase during experiments.

Solubility data at 25 ^oC clearly show CO_2 solubility in unspent HCl acid solutions of 1% and 4% concentrations are about double that of water and fully spent 5% HCl and almost four times the solubility in fully spent 15% HCl at pressure of 1,000 psi (**Fig. 2.3**).

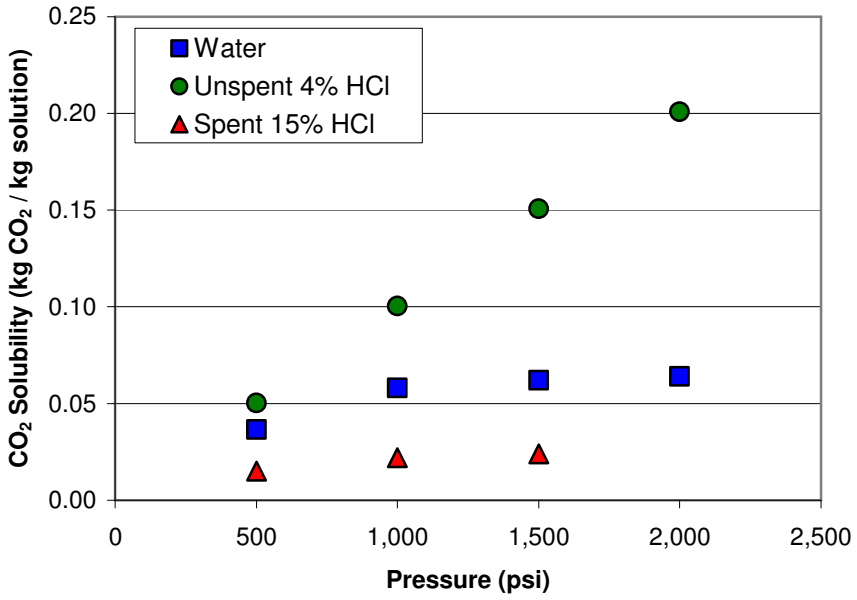

Fig. 2.3—Solubility curve of CO_2 in water and HCl acid at 25 ^oC.

Since most experiments were conducted at temperature of 175 ^{o}F, CO_2 solubility are compared at this temperature with amount of CO_2 produced from acidizing process (**Fig. 2.4**). Data on solubility of CO_2 in unspent acid at 175 ^{o}F was not available, however from above results, it might be accurate to assume that solubility of CO_2 in unspent acid is higher than that of water. While there should be no free CO_2 gas phase in fully spent 15% HCl acid solution as long as only up to about 15% of acid has been reacted to produce CO_2, CO_2 produced from 15% HCl reacted up to 30% of its capacity can be dissolved in water and fully spent 5% HCl. Figure 2.3 results indicate that probably more CO_2 can be dissolved in acid solution that is only partially spent that can be dissolved in water.

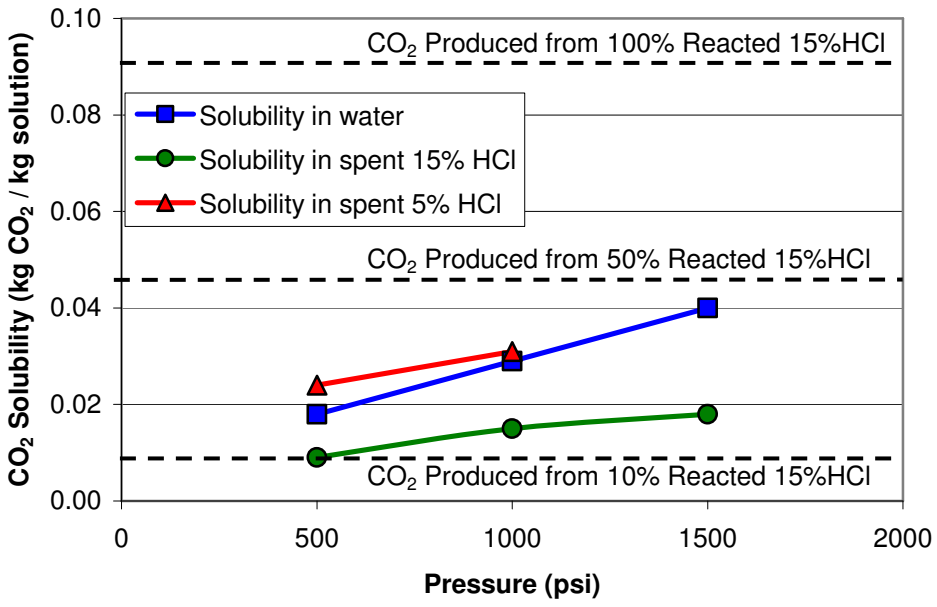

Fig. 2.4—Solubility curve of CO_2 in water and HCl acid at 175 ^{o}F.

As our experimental results clearly show that only about 9% of the acid reacts with formation (section 3.2.1)**,** there should be no free CO_2 gas phase formed and there should be no concern of two phase flow. There should be more acid reacted with fracture face as the residence time of acid in fracture increases which occurs with decreasing injection rate of acid. Results from other experimental works conducted at 10 ml/min injection rate indicate that only about one third (33%) of acid was reacted based on measured HCl concentration of waste acid in effluent (Gong, 1997).

2.3.2. Parameters Set for Planning

The parameters that have not been limited due to scaling or apparatus can be selected to provide best set of experimental data that enable understanding of factors that have great influence on acid fracturing process and aid in the development of conductivity correlation.

Previous experimental studies have clearly shown several parameters to have significant influence on the resulting fracture conductivity. These parameters have been contact time of acid with fracture, acid type, and formation type. Experiments are planned such that the effect of each of these parameters on the resulting conductivity can be determined and used in correlation development.

2.3.3. Parameters to Be Measured and Studied

As the main objective was to determine a correlation for conductivity, a wide range of parameters that believed to influence resulting conductivity were measured. One of the main parameter that influences resulting conductivity is the etching pattern of fracture face, including parameters like average fracture width, distribution of asperities,

interaction of two etched faces, and other statistical parameters that describe the etching pattern characteristics that might influence conductivity. Another similarly influential parameter is the strength of fracture faces that must withstand the closure stress. However there are many parameters that relate to strength of core like rock embedment strength (S_{RE}), Young's modulus, Poisson ratio, and yield stress and other less well known parameters. Based on previous work in the area of acid fracturing (Nierode and Kruk, 1973) that had related conductivity to SRE, rock embedment strength was chosen as the method to measure strength of fracture faces.

2.4. Experimental Apparatus

As detailed information on the experimental apparatus is given in Zou (2006) and Melendez (2007), some major components are explained briefly. The test cell is a modified API RP-61 conductivity cell made of Hastelloy C-276 material which is corrosion resistant to most acid systems, especially 15% HCl. The core samples used in this study have a rectangular shape with rounded edges to provide the best fit of the core inside the cell. Cores are about 7.25" long, 1.75" wide and 3" in thickness in the leak off direction. The cores are covered with a sealant material to provide a perfect fit inside the cell. The cell with pistons and flow inserts and the cores covered with silicone material that fit inside the cell are shown in **Fig. 2.5**.

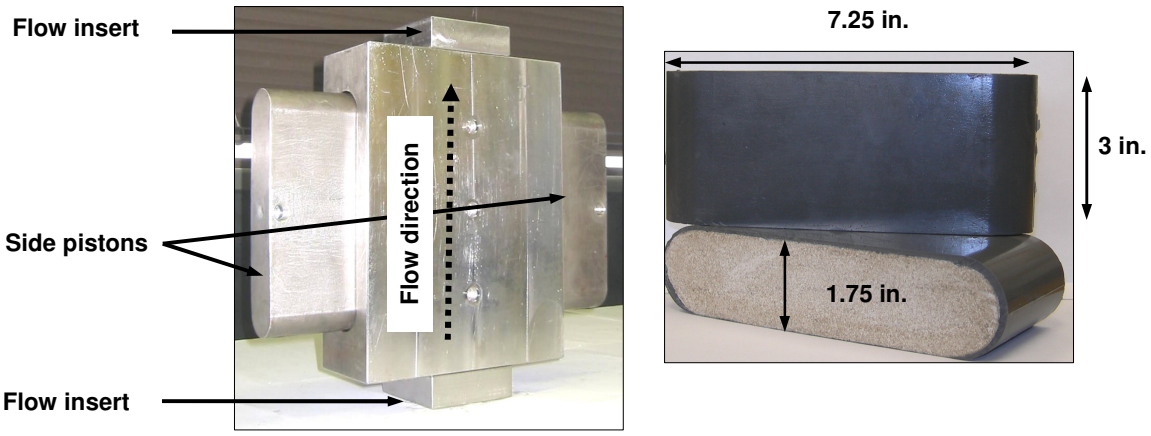

Fig. 2.5—Test cell and core sample used in this study.

The schematic of the experimental apparatus for the acid etching procedure is shown in **Fig. 2.6**. Acid is injected through the cell in a vertically upward flow in order to avoid gravity effects. Ceramic heaters are used to heat the fluids to the desired experimental condition with maximum temperature of about 300°F feasible. The leak off fluid is controlled through the use of a backpressure regulator in the leak off line. Three different pressure transducers are used to monitor the conditions throughout each test. One monitors cell pressure, another reads the pressure drop across the fracture, and the other measures pressure differential across the leak off flow direction.

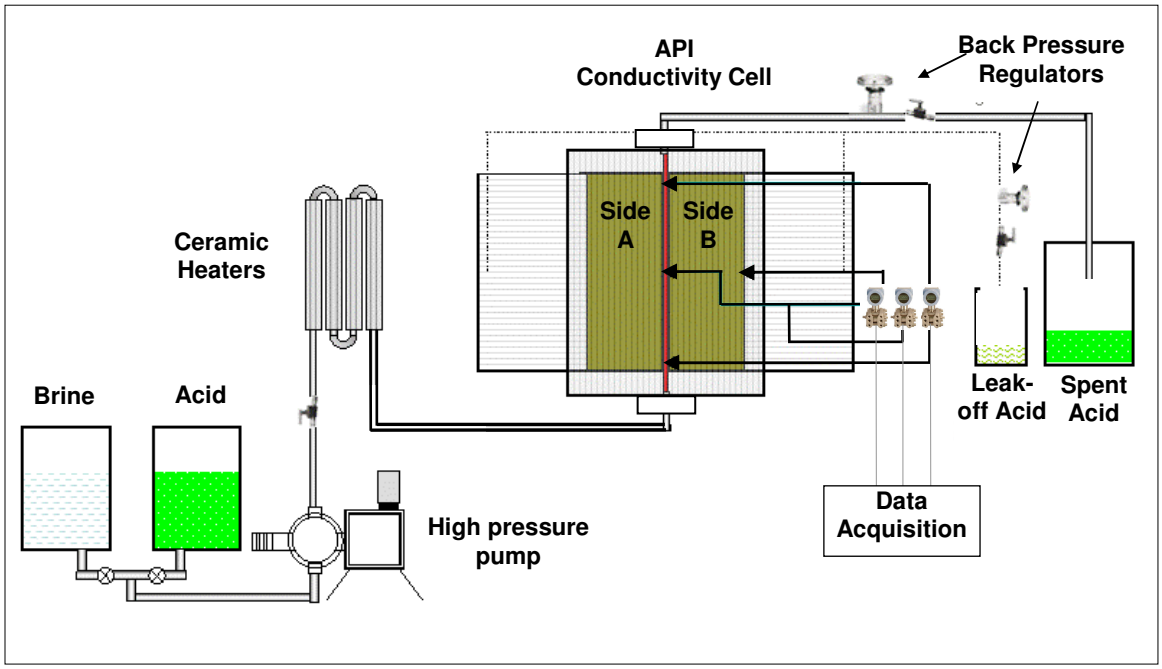

Fig. 2.6—Schematic of acid etching laboratory set up.

Conductivity is measured by flowing nitrogen through the closed acidized fracture, and measuring the pressure drop across the fracture under different closure stresses. The conductivity apparatus is made of two main components, a conductivity cell and a load frame. In **Fig. 2.7**, a schematic of the conductivity set up is shown. The conductivity cell has the same dimensions as the acidizing cell, but is made of stainless steel as it does not need to be resistant to acid. The cell is placed horizontally in the load frame. The load frame is a compression tester that can apply up to 10,000 psi closure stress on the fracture faces. The pressure drop across the fracture is measured by pressure transducers: one measures front section pressure drop while other measures the back section pressure drop. Actual cell pressure is monitored by the transducer in the middle. The flow rate of nitrogen is measured and controlled with a mass flow regulator.

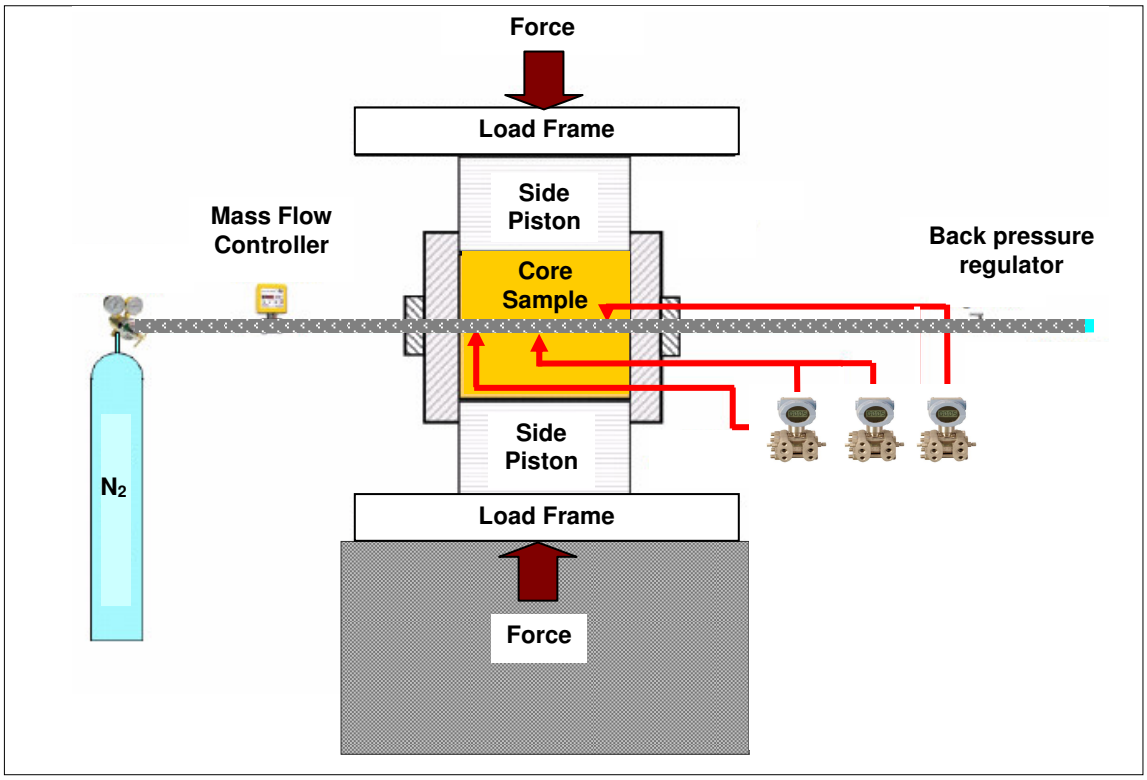

Fig. 2.7—Conductivity schematic.

2.5. Experimental Procedure

The experimental procedure is comprised of six consecutive steps (**Fig. 2.8**):

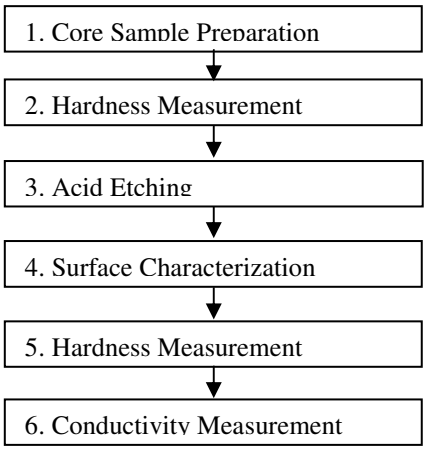

Fig. 2.8—Experimental process for acid fracturing conductivity.

As there are detailed procedure in Zou (2006) and Melendez (2007), a brief description is given below. Cores are cut in half into two 3" thick samples and then covered with a silicone-based sealant to allow perfect fit intocell and also prevent acid loss from the sides. Detailed information on surface characterization procedure can be found in Malagon (2007). A profilometer (**Fig. 2.9**) is used to characterize the surface of the fracture faces both before and after acidizing. 3D images are generated by the profilometer from the scanned surfaces as shown in **Fig. 2.10**. Additionally, it can quantify the amount of rock dissolved based on comparison of scans before and after.

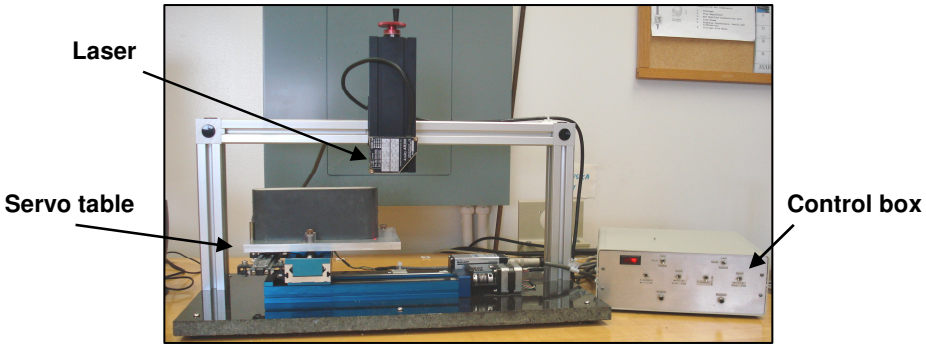

Fig. 2.9—The profilometer device used for surface characterization.

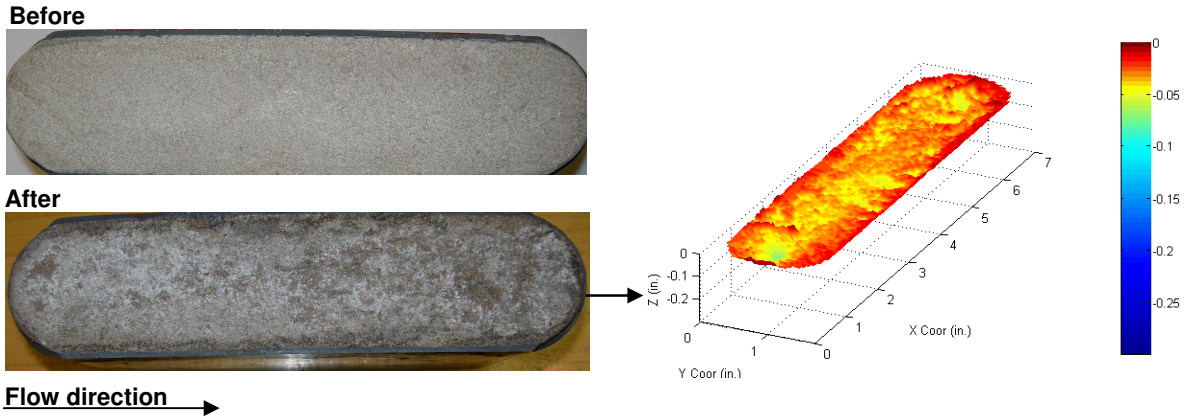

Fig. 2.10—Photographs before and after with 3D Surface image after acidizing.

Rock embedment strength of cores before and after acidizing are measured using the method described by Howard and Fast (1970). **Fig. 2.11** shows the rock embedment strength measurement apparatus. While initially there was no set up for rock embedment strength, SRE was measured at about 9 different scattered locations across the fracture face before and after acidizing. Later on, SRE measurements were conducted more precisely across 28 specific locations on the fracture faces as shown in **Fig. 2.12**.

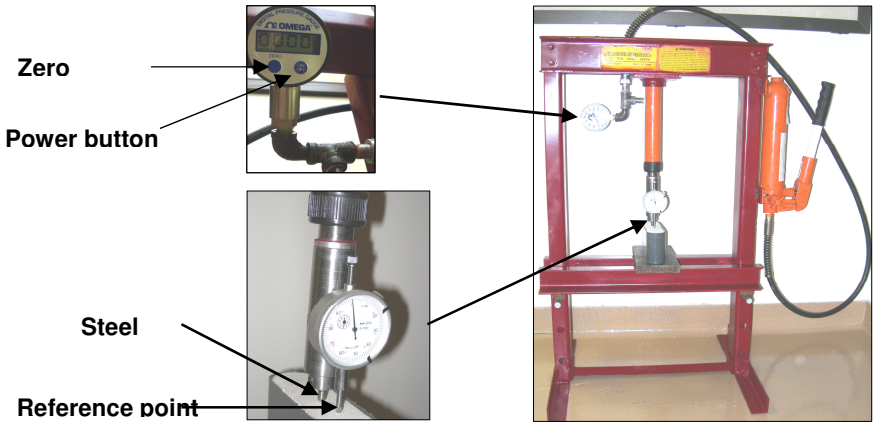

Fig. 2.11—Rock embedment strength machine.

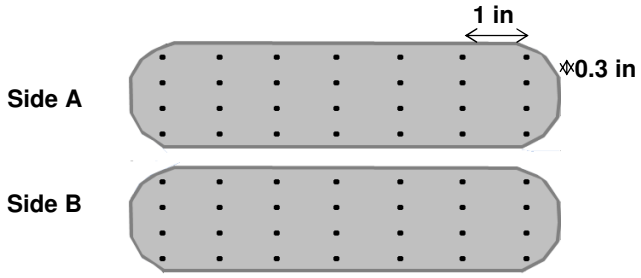

Fig. 2.12—Core faces with the points of strength measurements.

The acid etching process involves many different steps including core saturation in brine, core placement in cell with shims setting the fracture gap, preheating the system to desired temperature by flowing water through fracture, preparation of acid system, and finally acid injection followed by a post flush of water to clean the system.

The conductivity measurement step also involves placing the cores in the cell, applying the desired closure stress, and flowing nitrogen at required rates to determine conductivity. Closure stress at each load is maintained for about 60 minutes before reading of pressure drops are taken at several different nitrogen flow rates and then load increased to the next closure stress.

Conductivity is determined from pressure drop measurements at different flow rates using the Forcheimer equation which can be rearranged to (Pursell, 1987):

$$\frac{\left(p_1^{\,2}-p_2^{\,2}\right)Mh}{2ZRTL\mu\rho q}=\frac{1}{k_f w}+\frac{\beta\rho q}{w^2\mu h}, \quad \text{..... (2.11)}$$

where p_1 is the inlet or upstream pressure, p_2 is outlet or downstream pressure, M is molecular weight, Z is compressibility factor, R is universal gas constant, h is height across the fracture face, L is length along pressure drop, and β is the inertial flow coefficient. Eq. 2.11 is in a form of straight line equation with the intercept as the inverse

of the conductivity and slope proportional to the inertial flow coefficient. The values for all the fixed parameters are presented in **Table 2.6.** The properties of nitrogen like density and viscosity are taken at standard condition.

TABLE 2.6—DATA USED FOR CONDUCTIVITY CALCULATIONS

M	kg/kg-mol	0.028
h	in	1.61
Z	Dimensionless	1.00
R	J/mol K	8.32
L	in	5.25
μ	Pa.s	1.747E-05
ρ	kg/m^3	1.16085

In order to determine the conductivity of a completely closed fracture where flow occurs mainly through the porous matrix, Darcy's law for gas flow is applied:

$$q_{sc} = \frac{kA}{2\mu p_{sc}} \frac{\left(p_1^{\,2} - p_2^{\,2}\right)}{L}, \quad \text{..... (2.12)}$$

where q_{sc} is flow rate at standard condition, k is core permeability, A is cross sectional area of flow, p_{sc} is the pressure at standard condition. Eq. 2.12 is used to determine the pressure squared difference (p_1^2-p_2^2) at several different injection rates of nitrogen. Values for average core permeability (k) were 4 md for Indiana limestone, 10.7 md for San Andres dolomite and 7 md for the cream chalk, which were measured using a Probe Permeameter. With the above pressure squared differences and injection rates, Forcheimer's equation is applied to calculate the matrix flow conductivity. The

calculations yielded the following values for matrix flow conductivity: 41.5 md-ft for limestone, 111 md-ft for dolomite, and 72.7 md-ft for chalk.

2.6. Experimental Conditions

In this study, the experimental variables were acid type, formation type, contact time, and temperature. There were about 4 different acid types used: straight HCl, gelled, viscoelastic, and emulsified acid. Similarly, there were about 5 different formations tested which were Indiana limestone, Macae limestone, Bryozoan Limestone, Texas cream chalk, and San Andres dolomite. The contact times ranged from 5 up to 60 minutes. Contact time was the parameter that was tested the most with several different combinations. There was only one set of experiments conducted at two different temperatures of 200 and 275 ^{o}F. Most of the other tests were conducted at about 175 ^{o}F. The summary of all experiments conducted is shown in **Table 2.7**. There are total of 65 experiments. It should be noted that some tests were repeated twice or more at the same conditions.

TABLE 2.7—SUMMARY OF EXPERIMENTAL CONDITIONS

Set No.	Rock Type	Acid Type	Contact Time (min)	Temp. (°F)	Count	Note
1	Indiana Limestone	Viscoelastic, Emulsified A, Gelled A	15, 30, 60	200 & 275	17	
2	Bryozoan Limestone	15% HCl	2.5, 5, 7.5	100	3	
3	Bryozoan Limestone	15% HCl , 15% HCl/1% HF, Gelled A	10 & 15	175	3	
4	Indiana Limestone	15% HCl	5, 10, 15	175	9	
5	Indiana Limestone	Gelled A	5, 10, 15, 20, 30	175	8	
6	San Andres Dolomite	Gelled A	10, 20, 30	175	5	
7	Texas cream Chalk	Gelled A	5, 10, 15, 20, 30	175	7	
8	Indiana Limestone	15% HCl	20	175	3	3 Injection rates
9	Macae Limestone	Viscoelastic, Emulsified B, Gelled B, 15% HCl	20, 30	185	10	3 Different permeabilities

3. EXPERIMENTAL RESULTS AND DISCUSSION

3.1. General Observations

Many interesting findings were discovered while experiments were conducted which are worth to mention as they help in explanation of results and also might aid in future improvements of experimental testing.

3.1.1. Hydrodynamic Effects on Etching

After conducting many acidizing experiments at different conditions, a deeper etching pattern was observed at the inlet of many fracture faces. The depth and length of this deeper etched pattern were different for each experiment. The cause of this inlet etching pattern is believed to be hydrodynamics effects as a result of change in flow geometry from a circular pipe to rectangular flow geometry of fracture. The change in flow pattern is depicted in **Fig. 3.1**. As it can be seen, the change in flow pattern from circular to rectangular pattern actually occurs almost about 1.5 inches before fluid enters the fracture.

3-D images of two core samples with this inlet etching pattern are shown in **Fig. 3.2** with a cross-section profile of fracture in **Fig. 3.3**. While one sample showed almost 4 times more etching at the inlet side compared to the other sections of the core, the other sample shows only about twice as much etching at inlet. Similarly, the inlet effect seems to penetrate on the fracture face for about 1 inch for one core and up to 2 inches for the other core which had also deeper etched depth. Most experiments with inlet effect showed only about 1 inch of penetration. Inlet effects can not be completely removed from experiments even with use of some inlet spacers.

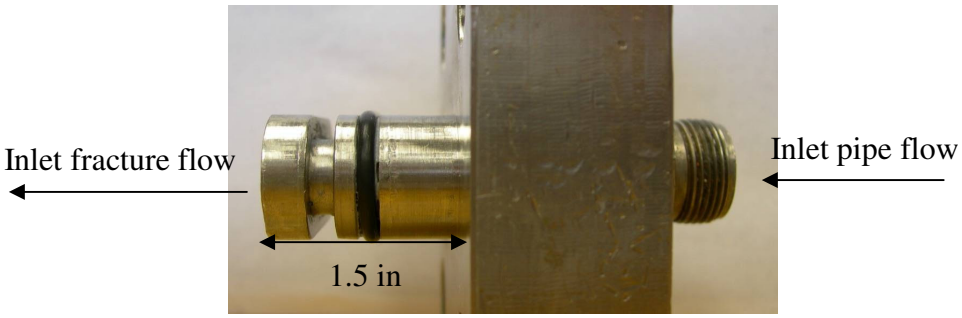

Fig. 3.1—Change in flow pattern in the cell.

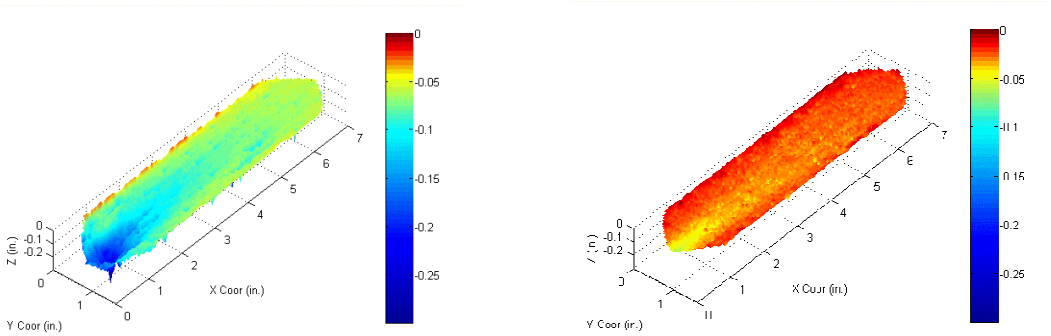

Fig 3.2—3-D images of two cores showing inlet effect.

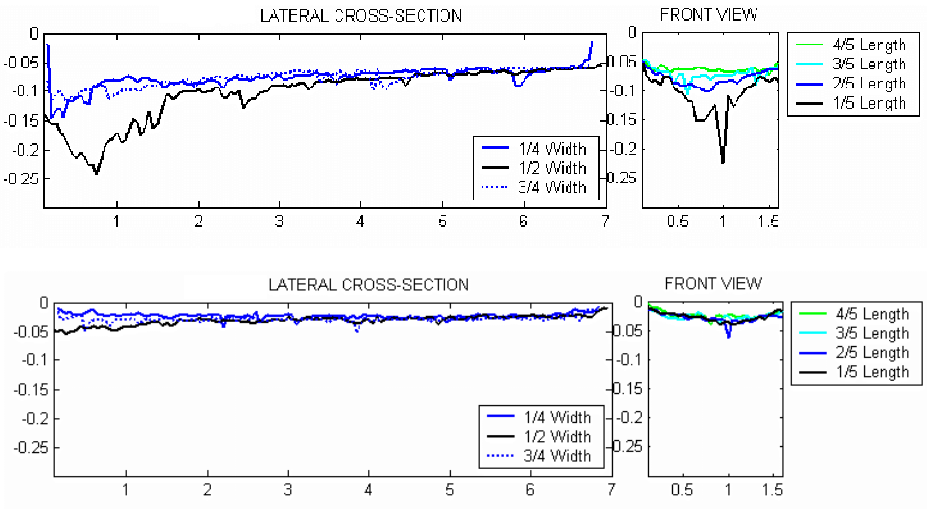

Fig. 3.3—Longitudinal and transversal cross-section profiles.

This kind of inlet effect might also be occurring in the field as there is also a change in flow pattern as acid flows from drill pipe into the fracture. However the field inlet effect may have no observable influence on resulting conductivity as the fracture is relatively long in length and inlet effect length is very limited. On the other hand, the inlet effect in experiments may have a substantial effect on resulting conductivity as it is a significant part of the actual fracture length. However as conductivity in experiments are measured only after about 1 inch from the inlet face (**Fig. 3.4**), this additional etching at the inlet does not cause any significant error on conductivity measurements.

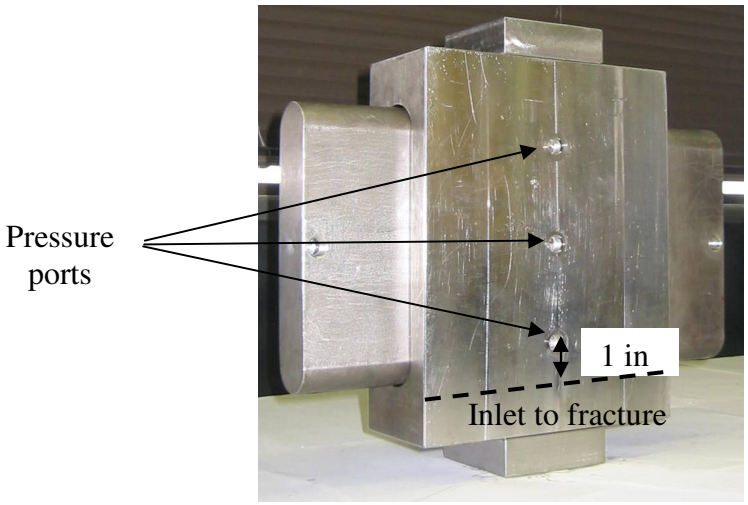

Fig. 3.4—Picture of cell with three pressure ports.

In addition to the inlet effect, there was also substantial difference in etching pattern across the width of the fracture face in some experiments. The sides of fracture faces are etched less than the middle of the fracture width as can be seen in Figs. 3.2 and 3.3. This side effect seems to be due to the geometry of API cell. There is a velocity

profile across the fracture face with a zero velocity at the core side. In addition, the invasion of silicone rubber that has been place around the core sides into the core might also be another reason for this differential etching.

Similar effects may also be occurring in field as there is also a velocity gradient across the width direction due to flow boundary on the sides. Regardless, the effect of this differential etching is removed in analysis of results as the unetched sides are removed by sanding the sides to be the same depth as the rest of fracture face before measuring conductivity. In this manner, the differential etching at the core sides does not influence conductivity. Also the etching profiles of the sides are removed in the analysis of the effect of etching pattern on conductivity as surface parameters are based on surface profiles that ignores 0.3 inches from the core sides.

3.1.2. Invasion of Silicone Epoxy Coating into Cores

We performed CT scans on some core samples in order to analyze the wormholing pattern in the leak off direction. While performing these scans, it was observed that the silicone epoxy coating that covers the core had invaded into the core sample especially on the sides for about 0.15 to 0.25 inches as can be seen from **Fig. 3.5** with the silicone invaded zone darker in color than the rest. The effect of the invaded zone on acid etching process is not known and could not be determined. However as the unetched sides were removed before conductivity measurement, the invasion should not influence resulting conductivity.

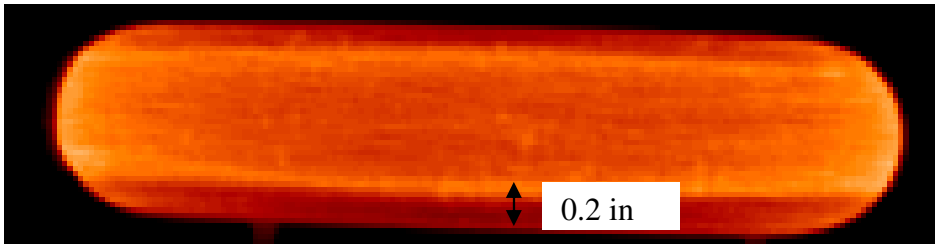

Fig. 3.5—CT scan of fracture face before acidizing.

3.1.3. Reaction Products Covering Surface of Cores

In some experiments, a certain sticky material seemed to cover the fracture face as shown in **Fig. 3.6**. Only about 8 experiments showed this behavior which occurred after the apparatus was not used for over a month in January and February of 2007. The extent of the formation of sticky material varied between the tests; however the thickness was no noticeable under the profilometer so it must have been less than 0.005 inches. The effect of sticky material on etching amount revealed a reduction of etched width with increasing thickness of film for a few experiments. This was taken into consideration during analysis of results.

Fig. 3.6—Pictures of two different acidized cores showing different amount of surface coating (ACC 11 (left) with more coating compared to ACC 12 (right)).

The sticky material from the core face was analyzed using XRD analysis (**Fig. 3.7**). The analysis revealed that most of the materials were undissolved materials from the core samples. Potassium chloride with dominant silica were identified. The silica was fine grained and was most probably left behind after dissolution of calcite. Presence of potassium suggests that there might be some feldspar, clay or something similar in the core. The calcium chloride and potassium chloride present might be acting as cementing material keeping other materials in place, which also explains the sticky texture.

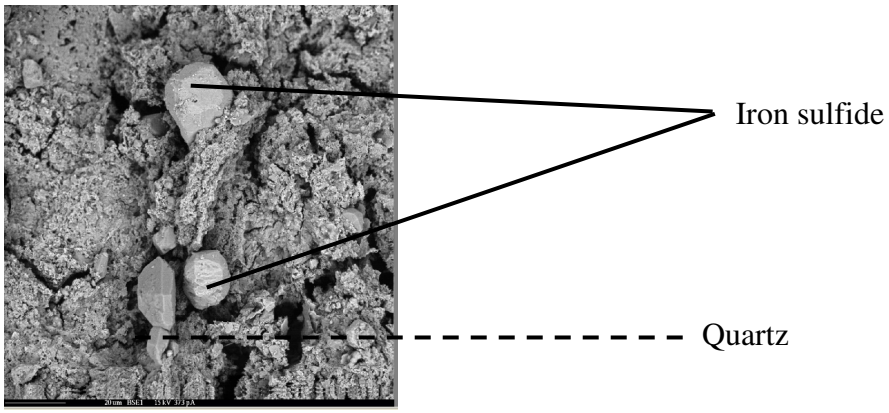

Fig. 3.7—Image of surface coating under XRD analysis.

3.2. Acidizing Process

The main mechanism that controls fracture conductivity is the acidizing process. There are many different factors which are affected by the acidizing process.

3.2.1. Types of Etching Patterns

After conducting 65 experiments with about five different types of formations, five distinctly different etching patterns were observed. The patterns observed are named as: channeling, roughness, uniform, turbulence, and cavity.

In about nine tests, a channel developed in the middle of the fracture face with minimal etching of the other parts of fracture face. The depth and length of the channel down the fracture differed among the experiments. Two samples with channeling pattern are shown in **Fig. 3.8**. The resulting conductivity should be highly dependent upon the dimensions of the channel rather than roughness of the overall fracture face. Once a channel forms, flow will be down the channel and the roughness of other parts does not influence flow behavior. Most samples acidized with gelled acid for longer times than 30 minutes and those acidized with VES acid for short contact times less than 15 minutes showed channeling behavior.

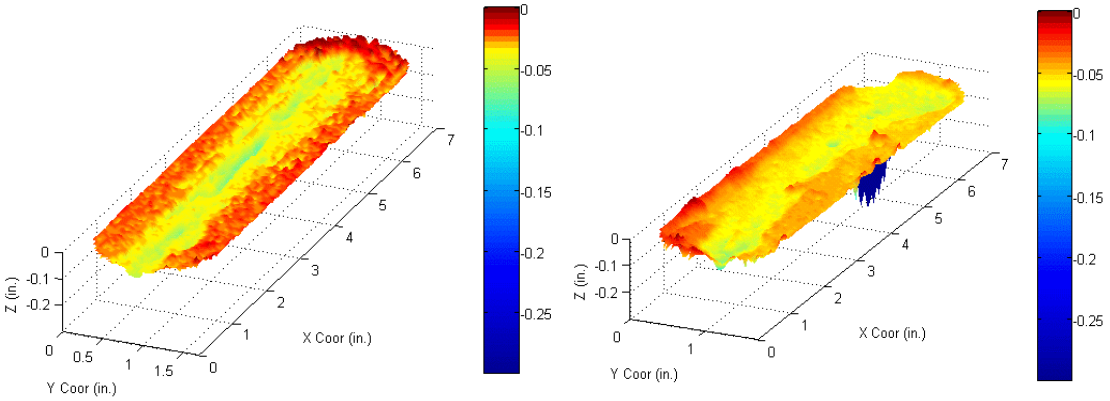

Fig. 3.8—3D images of two core samples with channeling behavior: IL 3 is an Indiana limestone sample while ACC 12 is a Texas cream chalk sample.

Most experiments (about 50) resulted in etching across most of the fracture face, however with three distinctly different etching patterns. Some experiments showed a rather rough etching pattern with randomly distributed areas open for flow of varying width and also a scattered distribution of asperities of different heights. This kind of etching was called roughness etching and two examples of this type of roughness etching are shown in **Fig. 3.9**. The resulting fracture conductivity should be mainly dependent on the distribution and dimension of asperities in addition to fracture width.

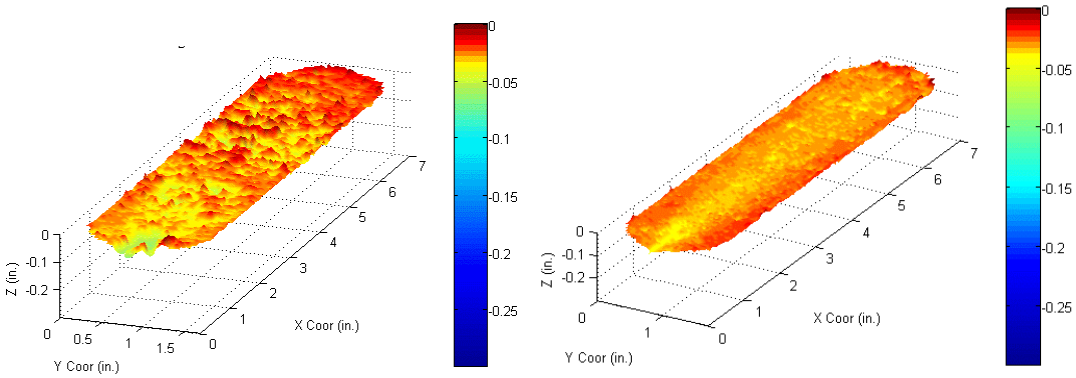

Fig. 3.9—3D images of two core samples with roughness behavior: CD 5 is a San Andres dolomite sample while ACC 13 is a Texas cream chalk sample.

Several experiments showed etching across the entire face, however a rather uniform etching with similar fracture widths across the face. The whole fracture was dissolved about the same amount across the face and consequently, there were not a lot of larger asperities to hold the fracture open. Two examples of such uniform etching, with one showing significant etching while the other shows minimal etching, are shown

in **Fig. 3.10**. The conductivity of such pattern is very low as there is no roughness to keep fracture open. The conductivity of such uniformly etched pattern highly depends on amount and strength of the few possible asperities that are holding the fracture open in addition to width.

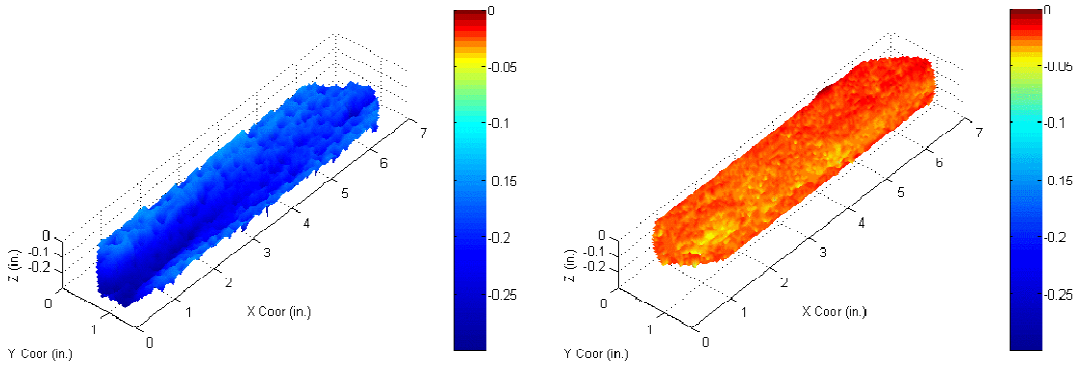

Fig. 3.10—3D images of two core samples with uniform etching behavior: Both are Indiana limestone samples: IL 6 acidized with VES while IL 10 was acidized with gelled acid.

The other kind of etching which was seen for many of the samples acidized with straight HCl was a kind of turbulence etching with areas of valleys and peaks (downs and ups) following each other. The etching pattern is very similar to effect of turbulence seen in fluid flow. One example of such turbulence etching pattern is shown in **Fig. 3.11**. This pattern mainly occurred with HCl acidized samples as the HCl flow has Reynolds numbers of almost two orders of magnitude larger than other acid types, resulting in much more turbulence flow (see Table 2.5). While the conductivity of this type of turbulence etching should also depend on distribution of these asperities and the

widths of valleys, it should also depend on connectivity between the valleys in order to have a complete path for flow.

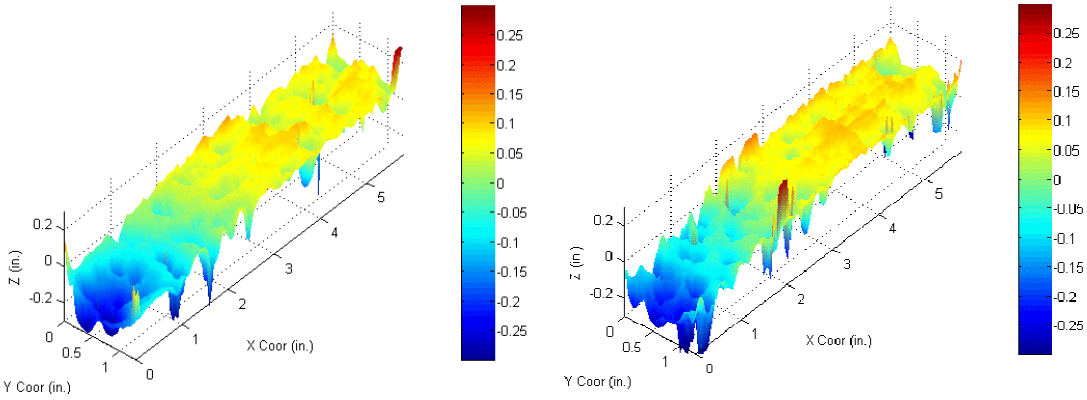

Fig. 3.11—3D images of one core sample with turbulence etching behavior: Indiana limestone acidized with HCl for 15 minutes.

Almost all samples of the Bryozoan limestone from the North Sea showed a very different etching pattern with formation of large, pockets of cavities across the fracture face (**Fig. 3.12**). It is clearly evident that these cavities are relatively deep with no noticeable roughness etching. As these cavities are separate from each other with no real connection, resulting conductivity should be minimal.

Fig. 3.12—Photos of two Bryozoan limestone samples with cavity etching.

Experimental results clearly show that the etching pattern is greatly influenced by acid type, contact time and rock type. While acid type has the greatest influence on etching pattern, rock type has the least effect. Experiments are grouped into 5 different groups based on their etching pattern as shown in **Table 3.1**. It is clear that acid type influences etching pattern greatly with the amount of acid injected in terms of contact time sometimes resulting in a change in etching pattern for the same acid type.

TABLE 3.1—CLASSIFICATION OF EXPERIMENTS BASED ON ETCHING PATTERN OBSERVED

Etching Pattern	Rock type	Acid Type	Contact time (min)
Channeling	Indiana limestone	VES	15, 30
		Emulsified	30, 60 at 200 °F
Roughness	Indiana limestone	Emulsified	15 at 200 °F
		Gelled	All
	San Andres dolomite	Gelled	All
	Texas cream chalk	Gelled	All
	Macae limestone	Gelled	All
		VES	All
Uniform	Indiana limestone	VES	60
		Emulsified	30, 60 at 275 °F
Turbulence	Indiana limestone Texas cream chalk Macae limestone	HCl	All
Cavity	Bryozoan limestone	All	All

Analysis of etched fracture faces has shown that there are five distinctly different etching patterns. Each etching pattern requires a unique method for relating surface parameters to conductivity as the method of fracture opening is different. Focus on correlating surface roughness parameters to conductivity will be placed only on tests that show roughness etching patterns as the surface roughness plays a major role on the resulting conductivity, while it does not have much influence on conductivity of samples with channel pattern or cavity behavior.

3.2.2. Residence Time in Cell

The dissolution of fracture face with acid is affected by amount of time that the acid has to react with the formation. In our experiments, as the acid flows relatively fast at 1 L/min, the residence time of acid with fracture face is very short. Since the fracture volume is about 22.5 cm^3 with a width of 0.12 inch, the residence time of acid across the fracture face is only about 1.35 seconds. As a result, the acid does not have much time to react with the formation and most of it flows out from the fracture without reacting with the fracture face.

The volume of rock that can be dissolved from injected acid volume was calculated using the concept of dissolving power of acid for straight 15wt% HCl acid system. The calculated dissolved volumes ($V_{dissolved}$) were compared to actual dissolved volumes based on profilometer data only for tests conducted with straight HCl acid system. The percentage of the total calculated dissolved volume that actually dissolved was calculated, which is the same as percentage of acid consumed during surface dissolution. The calculations are summarized in **Table 3.2**.

The results clearly show that only a small proportion of acid reacts with fracture face. While an average of about 8.5% of acid reacted with fracture face of Indiana limestone and Texas cream chalk samples, only about 0.7% of acid reacted with Macae limestone formations. There were two main reasons for much lower dissolution of Macae limestone. The main reason was the fact that the cores were oil saturated while other formation types were brine saturated. Also Macae limestone samples have significant presence of quartz (up to 5%), resulting in lower reaction rate with acid. The percentage of acid reacted were very similar between experiments. The consistency among experiments shows that similar amount of injected acid reacted with fracture face among the experiments conducted with the same acid system and rock type.

TABLE 3.2—COMPARISON OF CALCULATED AND MEASURED ETCHED VOLUMES

Label	Rock Type	Temp (^{o}F)	Time (min)	Measured		Calculated	
				w (in)	$V_{dissolved}$ (in^3)	$V_{dissolved}$ (in^3)	Percentage Reacted (%)
ALC 4	Indiana Limestone	175	5	0.201	2.301	25.02	9.2
ALC 7			5	0.174	1.997	25.02	8.0
ALC 2			10	0.376	4.309	50.04	8.6
ALC 5			10	0.423	4.840	50.04	9.7
ALC 1			15	0.525	6.014	75.06	8.0
ALC 6			15	0.498	5.705	75.06	7.6
ILS9			20	0.743	8.502	100.08	8.5
ACC 7	Texas cream Chalk	175	5	0.192	2.193	25.02	8.8
ACC 6			10	0.399	4.569	50.04	9.1
ACC 1			15	0.495	5.669	75.06	7.6
PBC 3	Macae Limestone	185	30	0.077	0.882	150.12	0.6
PBC 7			20	0.070	0.798	100.08	0.8
PBC 17			20	0.053	0.603	100.08	0.6

3.2.3. Effect of Injection Rate

One set of experiment with Indiana limestone was carried out at three different injection rates, 10, 225, and 1,000 ml/min in order to study the effect of injection rate on acid fracturing process. The experiments were conducted under identical conditions using 15 wt% HCl acid at 175 ^{o}F and 20 minutes of contact time. While the contact time was kept the same among the three different injection rates, the volume of acid injected was different. The slower injection rate allows acid to have more time to react with fracture face, however there was much less acid injected at the lower rate. The residence time of acid in the API cell in fracture volume was calculated to be 135, 6, and 1 seconds for injection rates of 10, 225, and 1,000 ml/min, respectively. Simple calculation of the percentage of acid reacted with fracture face based on dissolution power of acid and measured dissolved surface volume indicated that about 69%, 20%, and 8% of acid reacted with fracture face for injection rates of 10, 225, and 1,000 ml/min, respectively.

Calculation of fracture flow Reynolds number shows that while injection rate of 225 and 1000 ml/min are most probably in turbulent flow regime with Reynolds numbers of 121 and 537, respectively, flow is definitely laminar at the low injection rate of 10 ml/min as Reynolds number is only 5. The effect of differences in flow regimes clearly shows on the etching pattern as shown in **Fig. 3.13**. There is clearly turbulence etching with lots of valleys and peaks for the higher injection rates of 225 and 1,000 ml/min, while no such turbulence effect is seen for sample acidized at 10 ml/min. Repeated experiments under different injection rates clearly shows the need to ensure

injection rates are properly scaled to field conditions as it has a significant influence on etching pattern during the acid fracturing process

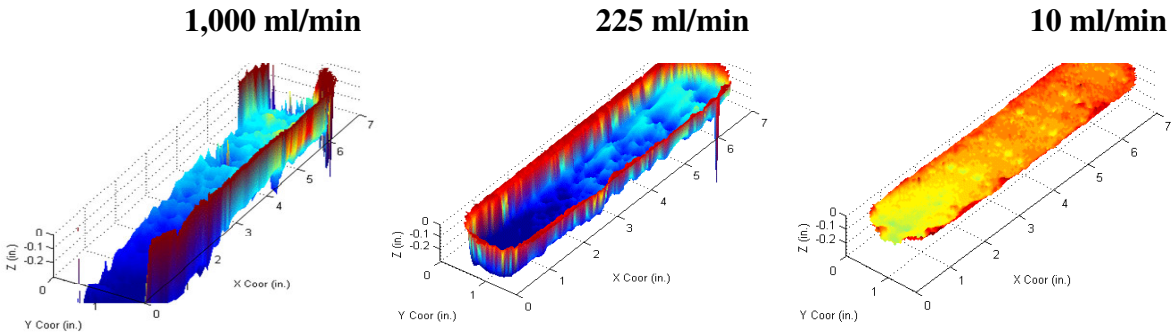

Fig. 3.13—3D images of three experiments conducted at different injection rates.

3.2.4. Fracture Width

The main parameter controlling fracture conductivity is the fracture width, the gap between two surfaces. The fracture width is defined in our study as the average width of fracture obtained from distribution of widths once the two fracture faces are put together. In order to obtain fracture width, the two surfaces of the fracture are superimposed on each other to obtain a global distribution of etched gap or local width at each location which is the averaged arithmetically.

3.2.4.1. Contact Time Effect

With increasing contact time, more acid will contact the fracture face and hence more fracture face volume should be dissolved with increasing acid volume. There is no theoretical reason for reduction in surface etching with increasing contact time for the

same formation. However, the rate of change in surface etching with contact time might be different for different acids and formation types as it depends on overall reaction rate and leak-off behavior.

There were 8 different set of experiments that were conducted at same conditions except at different contact times. The fracture widths for Indiana limestone acidized under different contact times are shown in **Fig. 3.14**. All the experiments show an increase in width with contact time; however the rate of change of width with contact time differs for each acid type. While straight HCl acid shows the fastest rate of increase in width with contact time, gelled acid shows very little increase in fracture width with contact time. Similar results were observed on Texas cream chalk samples acidized under different contact times as shown in **Fig. 3.15**.

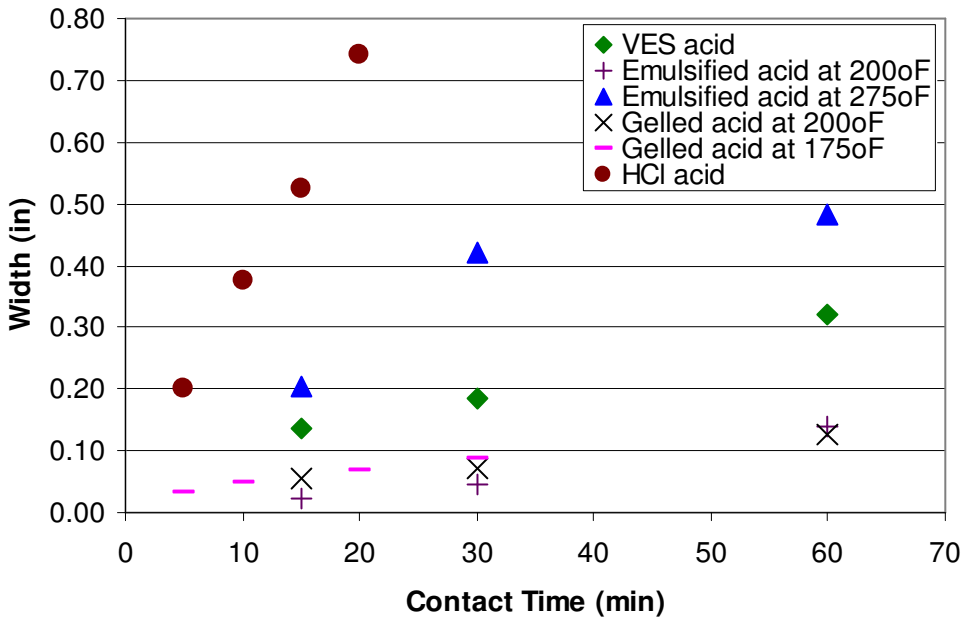

Fig. 3.14—Fracture width of Indiana limestone samples at different times.

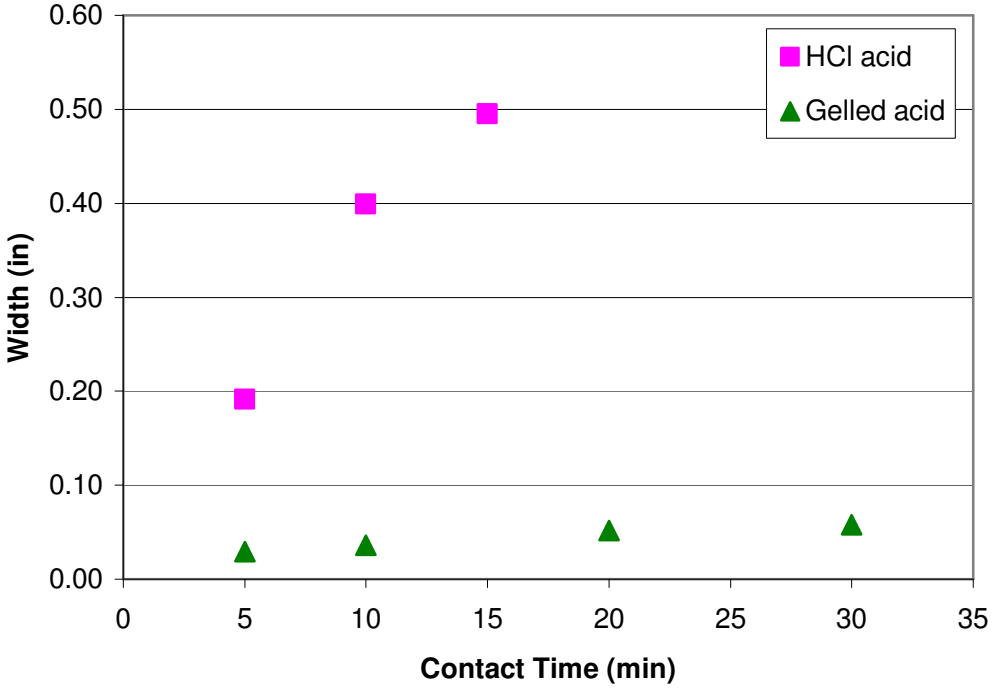

Fig. 3.15—Fracture widths of Texas cream chalk samples at different times.

3.2.4.2. Temperature Effect

There should be an increase in etched width with temperature as reaction rate of acids, with the exception of VES acid system (Nasr-El-Din et al., 2008), with formation increases based on Arrhenius equation which shows an increase in reaction rate constant, E_f, with temperature in the following form:

$$E_f = E_f^0 \exp\left(-\frac{\Delta E}{RT}\right), \quad \text{..... (3.1)}$$

where E_f^o is reference reaction rate constant, ΔE is activation energy, R is universal gas constant, and T is temperature. For reactions of straight HCl with calcite, an increase in temperature from 200 ^{o}F to 275 ^{o}F results in an eight fold increase in reaction rate due to

the exponential dependence of reaction rate on temperature, based on data from Economides et al. (1994). Similarly, diffusion coefficient, D, increases with temperature following a similar pattern as the Arrhenius equation (Conway et al., 1999):

$$D = D_0 \exp\left(-\frac{\Delta E}{RT}\right), \quad \text{..... (3.2)}$$

where D_o is reference diffusion coefficient. The same increase of temperature from 200 to 275 ^{o}F results in about four times increase in diffusion coefficient of straight HCl based on approximate dependence of diffusivity on temperature (Conway et al., 1999). Increased reaction rate and diffusion rate at higher temperatures will result in more etching of fracture face and hence larger widths. There is no reason for a decrease in width with increasing temperature as long as all the conditions including core properties are the same. There was only one set of experiment conducted at two widely different temperatures which shows the effect of temperature on fracture width as shown in **Fig. 3.16**.

There is a clear trend of increasing fracture width with temperature for all the three experiments; however the rate of increase in fracture width was different for each experiment. Results also clearly show that there is more difference in widths between tests conducted at different contact times with increasing temperature. While all the widths for the 3 experiments from 15 min to 60 min contact time had similar values at 200 ^{o}F, the widths varied more than two times at the higher temperature of 275 ^{o}F.

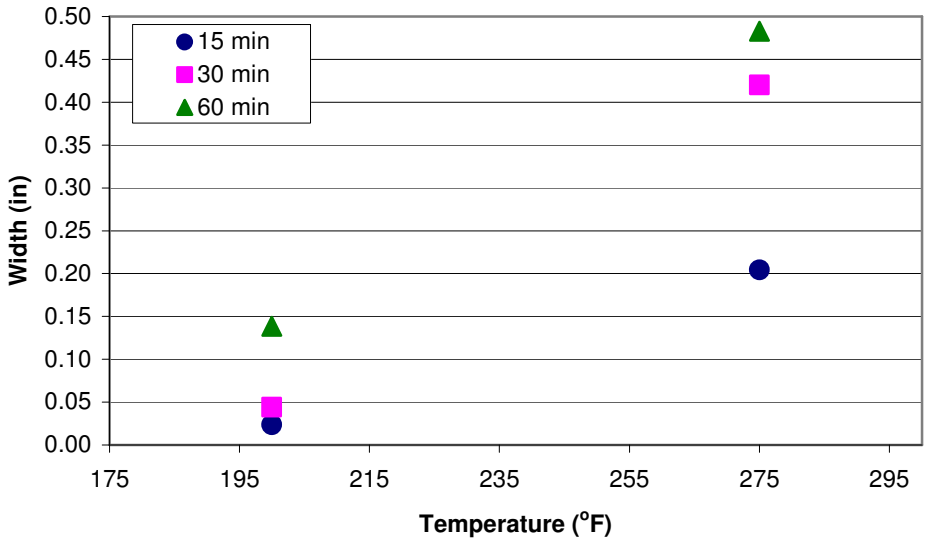

Fig. 3.16—Fracture widths at two different temperatures for Indiana limestone samples acidized with emulsified acid.

3.2.4.3. Formation Type Effect

There are many properties of the formation that affect the etching process. The permeability, porosity and chemical composition of the formation affect the overall reaction rate and leak-off behavior of acid during acid fracturing process, which in turn affects amount of surface etching. For example, it is well known that limestone reacts much faster than dolomite with HCl. Simple calculation of reaction rates for straight HCl with limestone and dolomite indicate reaction rate is over 2 orders of magnitudes larger for limestone formations (Economides et al., 1994). At most reservoir conditions with majority of acid types, diffusion rate is much less than reaction rate for limestone formations, however actually higher than dolomite reaction rates. As a result, limestone

dissolution process is mass transfer limited (Lund et al., 1975), while dolomite dissolution is surface reaction rate limited (Lund et al., 1973).

Experiments under similar conditions were performed on three different types of formations: Indiana limestone, Texas cream chalk, and San Andres dolomite. The experiments were conducted with gelled acid at 175 ^{o}F for contact times of 20 and 30 minutes. The resulting fracture widths at different contact times are compared for these three formations in **Fig. 3.17**. There is a clear difference in the fracture width among the formation types with the greatest amount of etching usually for limestone sample and the least amount of etching for the dolomite formation. This is expected as dolomite has much lower reaction rate while chalk and limestone have similar reaction rates due to similar mineralogy.

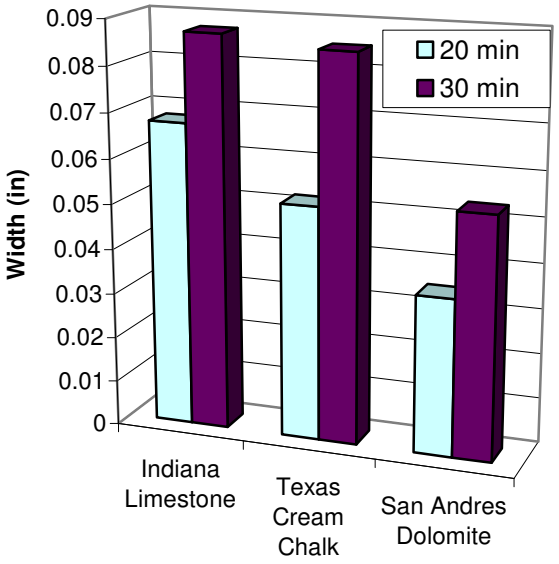

Fig. 3.17—Fracture widths of three different formation types acidized with gelled acid at 175 ^{o}F at two contact times.

3.2.4.4. Acid Type Effect

One of the main treatment parameters that can be adjusted to best suit the field situation is the acid type. There have been many different types of acid formulations developed with wide variety of physical and chemical properties. Some of the most important properties are diffusivity, viscosity and reaction rate. While reaction rates are not well known for the different acid systems, diffusivity and viscosity are available as shown in **Table 3.3** (Navarrete et al., 1998; Conway et al., 1999).

TABLE 3.3—VISCOSITY AND DIFFUISON COEFFICIENT OF THE FOUR ACID FORMULATIONS TESTED (VALUES ARE AT TEMPERATURE OF 175°F AND SHEAR RATES OBSERVED IN EXPERIMENTS)

Acid Type	Viscosity (cp)	Diffusion Coefficient (cm^2/s)
15% HCl	0.74	1.0E-04
Gelled acid	37	6.0E-05
VES acid	44	6.0E-05
Emulsified acid	35	6.0E-06

There are wide variations among the acid systems in terms of their properties which significantly affects acid etching and leak off behavior. There were 3 different set of experiments conducted with different acid formulations under the same conditions. The resulting fracture widths of the sets are shown in **Figs. 3.18 to 3.20**.

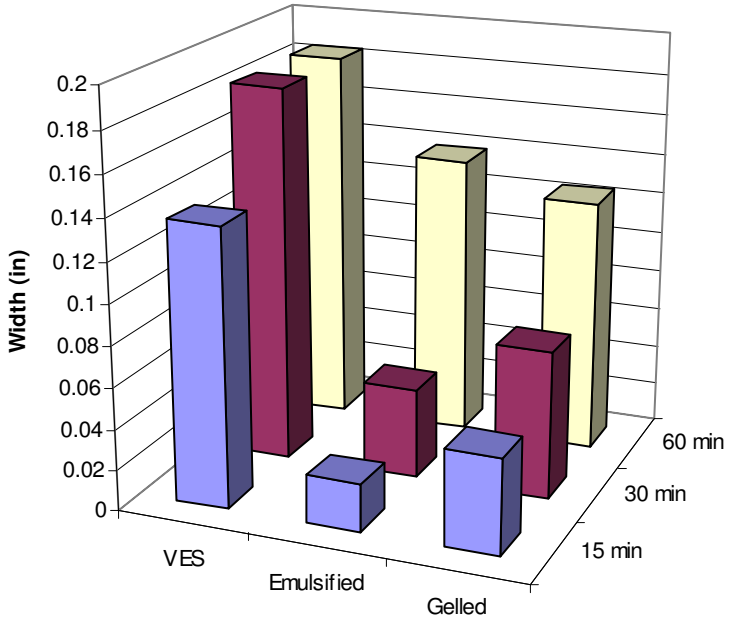

Fig. 3.18—Fracture width of Indiana limestone samples acidized at 200 °F with three different acid types at three contact times.

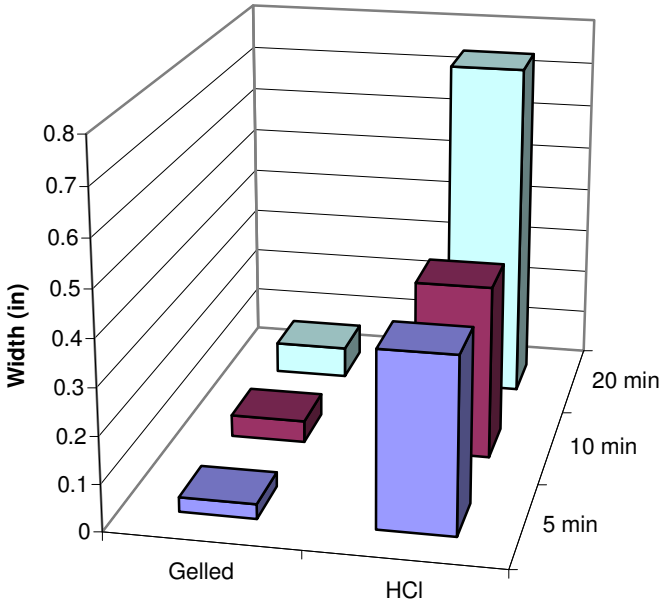

Fig. 3.19—Fracture width of Indiana limestone samples acidized at 175 °F with two different acid types at four contact times.

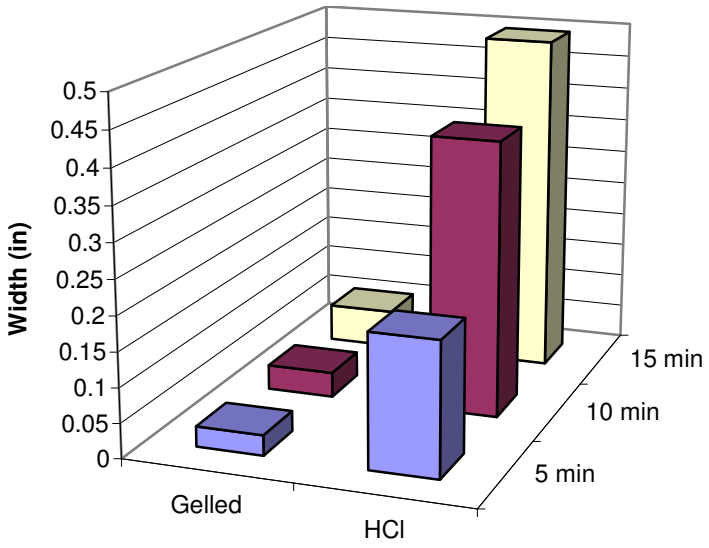

Fig. 3.20—Fracture width of Texas cream chalk samples acidized at 175 °F with two different acid types at three contact times.

The results clearly show that the acid type has a significant influence on fracture width. VES acid system results in the highest fracture width at all different contact times compared to the other acid systems as shown in Fig. 3.18. While VES acid system has high diffusion coefficient compared to emulsified acid but similar to gelled acid, it has much higher initial viscosity compared to the other two acid systems. Gelled acid and emulsified acid resulted in similar amount of fracture width even though gelled acid has higher diffusion coefficient with little higher viscosity than emulsified acid. Straight HCl acid created much higher widths as compared to gelled acid for all different contact times for both Indiana limestone and Texas cream chalk formations as shown in Fig. 3.19 and Fig. 3.20, respectively. Straight HCl acid has higher diffusion coefficient than gelled acid, however it has also lower viscosity than gelled acid. While results suggest

that fracture widths depend on acid type, there is no clear indication of how the fracture widths depend on acid properties like diffusion coefficient and viscosity.

3.2.4.5. Repeatability

Repeated tests conducted on the same formation under the same conditions should result in similar values of fracture widths as long as the process is not stochastic and is repeatable. There were about four main sets of experiments that were repeated under the same conditions and the resulting fracture widths are shown in **Figs. 3.21 to 3.24**. While majority of repeated tests show similar fracture widths, there are a few repeated tests with large differences in measured widths. One of the experiments with large difference in fracture width was the Indiana limestone sample acidized for 30 minutes with gelled acid at 200 ^{o}F (Fig. 3.21). The fracture width differed about two times (0.07 inches compared to 0.14 inches). The main reason for the difference was that the sample with higher width had almost twice the leak off rate as the other (0.01 compared to 0.005 ft/min). The experimental set that was repeated five times shows also that fracture width for two experiments were much lower than the other three experiments with about half the fracture width (see Fig. 3.22). Also the Texas cream chalk sample acidized with gelled acid for 20 minutes (Fig. 3.24) showed differences in fracture width as one repeat test had half the leak off rate as the other.

The main reason for differences between fracture width of repeated tests are due to differences in leak off rates as leak off rate could not be controlled very precisely. However there are also inherent differences in terms of permeability distribution across fracture face between the core samples that were used to compare repeated experiments.

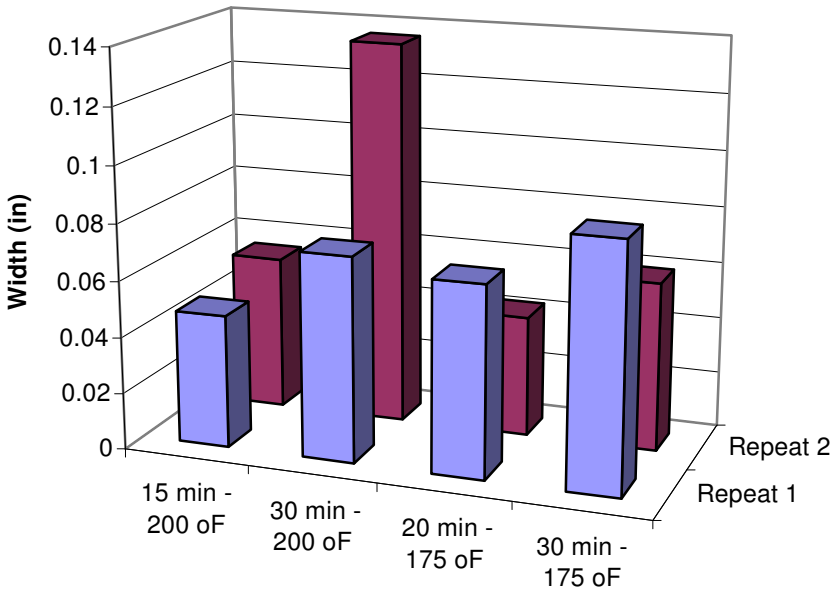

Fig. 3.21—Fracture width of four sets of experiments repeated twice each with Indiana limestone samples acidized with gelled acid.

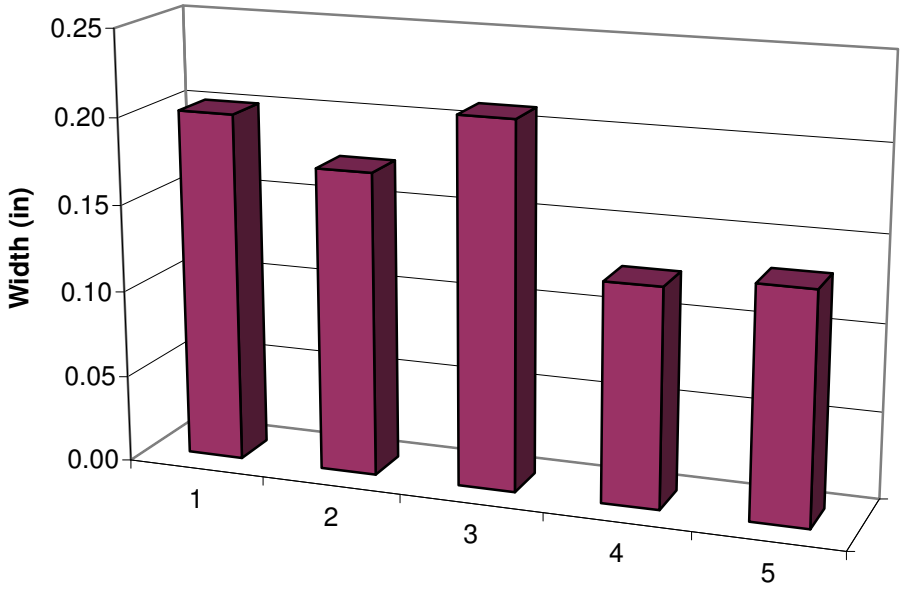

Fig. 3.22—Fracture width of one set of experiments repeated five times with Indiana limestone samples acidized with HCl acid at contact time of 5 minutes.

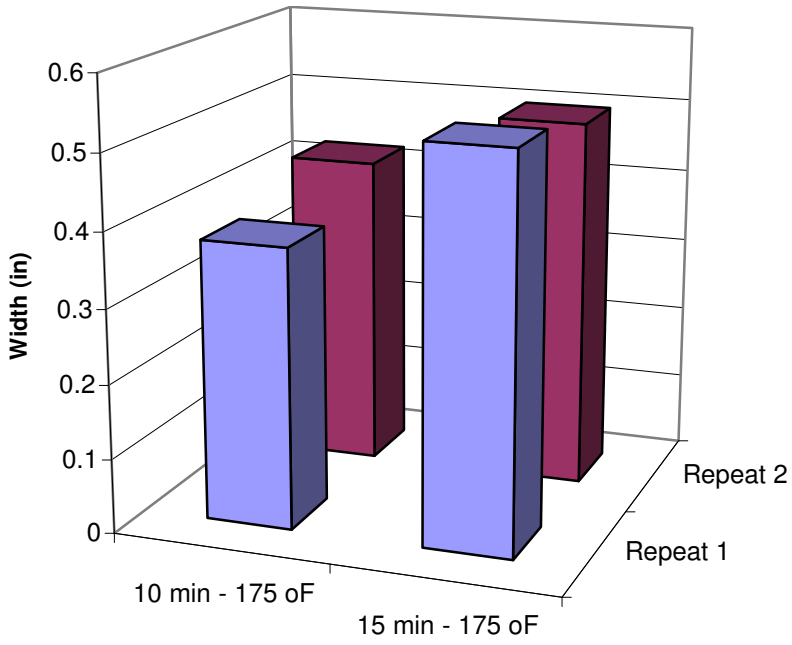

Fig. 3.23—Fracture width of two sets of experiments repeated twice each with Indiana limestone samples acidized with HCl acid.

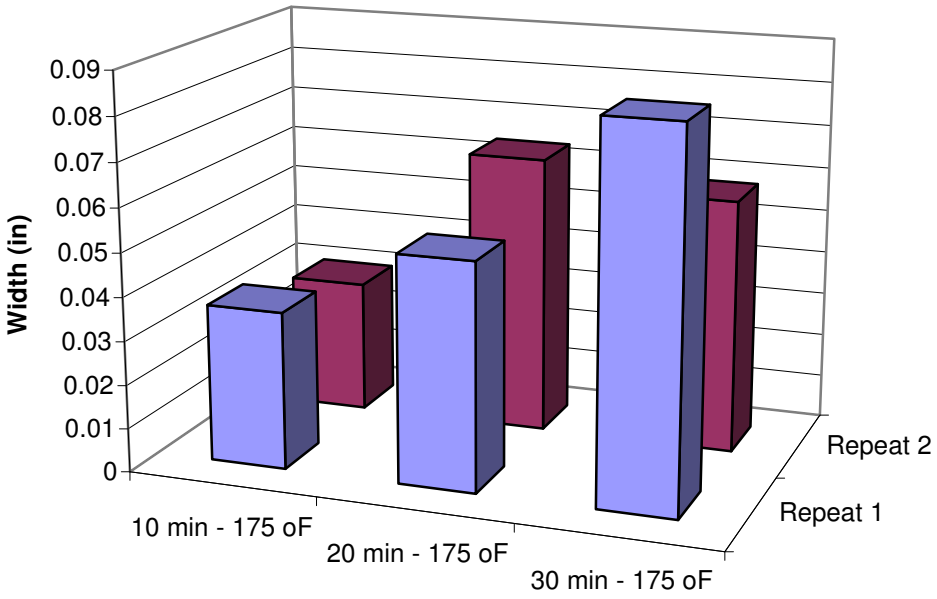

Fig. 3.24—Fracture width of three sets of experiments repeated twice each with Texas cream chalk samples acidized with gelled acid.

3.2.5. Pressure Analysis

The pressure measurements during the acidizing process were comprised of absolute cell pressure, fracture differential pressure, and leak off differential pressure. The absolute cell pressure was maintained at about 1,000 psi. Cell pressure profile showed that the pressure was well maintained at 1,000 psi (**Fig. 3.25**). The fracture differential pressure profile showed that since the fracture gap was set at 0.12 inches, there was almost no pressure drop across the fracture and the acidizing process did not change it much as it was already small (**Fig. 3.26**).

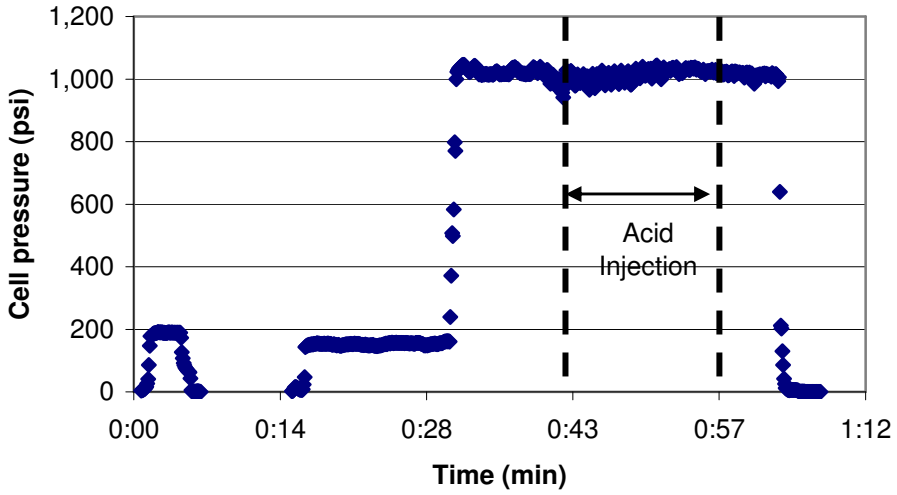

Fig. 3.25—Cell pressure with time during preflush, acid injection and postflush.

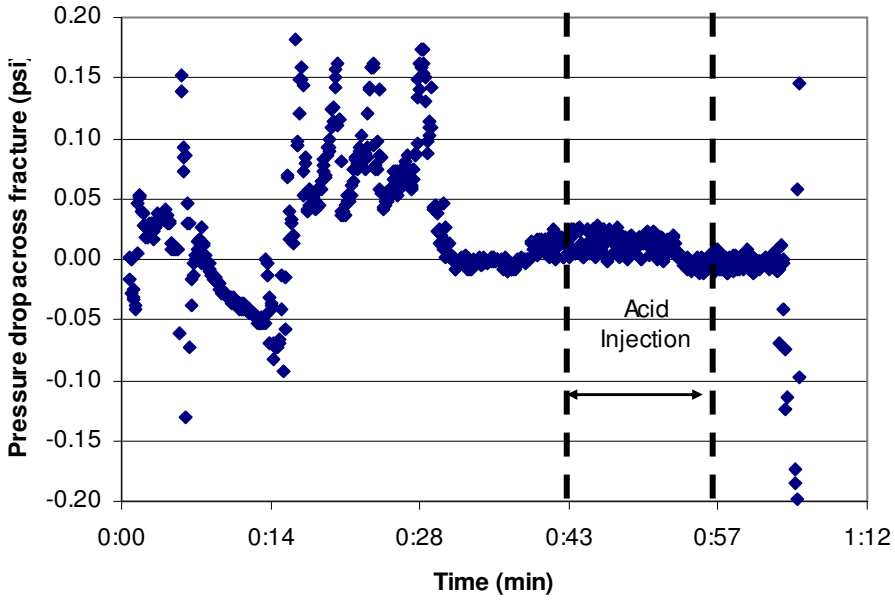

Fig. 3.26—Pressure drop across the fracture length with time during preflush, acid injection and postflush.

3.2.6. Leak-off Behavior

Even though differential pressure across the leak off line was controlled with the aid of a back pressure regulator, the leak off flux varied during the experiment. Sometimes there was a substantial leak off rate initially and then pressure across leak off controlled more, causing a reduction in leak off flow. This fluctuation in leak off flow can be clearly seen in **Fig. 3.27** which shows the differential pressure drop across the leak off line. The effect of fluctuation in leak off rate on etching pattern and resulting conductivity is not substantial as it is such small change in leak off rate. The change in leak off flux is a natural result of wormholing and etching pattern as acidizing process progresses with time.

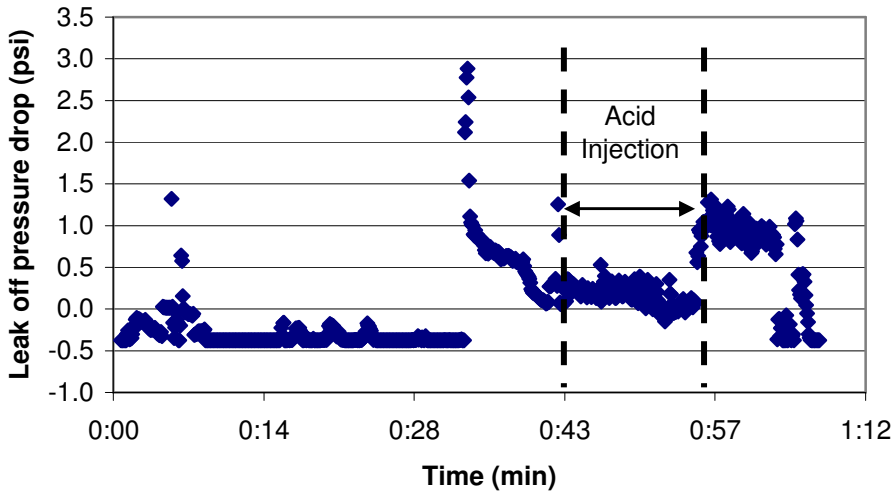

Fig. 3.27—Pressure drop across leak off direction with time during preflush, acid injection and postflush.

3.2.7. Acidizing Experimental Errors

There were several issues with the acidizing process which might have been sources of some errors, however these have minimal impact on final results. One of the major concerns was with the pump, which is a hydraulic displacement pump resulting in flow rate fluctuations. A pulsation dampener was added to the line after the pump to stabilize the flow rate, however the flow rate still showed some fluctuations but less than before the installation. The comparison of experiments without and with pulsation dampener did not show any noticeable differences in terms of etching pattern and fracture widths on rock surface.

Another concern was the fluctuation in temperature which was controlled with a temperature control relay. While the controller was set at a specified temperature, the

controller works by turning on and off the heater depending on whether the temperature is below or above the set point, respectively. As a result of this turning on and off of the heater, the temperature fluctuated about 20 ^{o}F below and 10 ^{o}F above the set point during the experiments. However, the temperature reached the set point after falling below or above the set point in about 3 minutes.

3.3. Surface Etching Characteristics

The main feature that controls the resulting acid fracture conductivity is the etched fracture face pattern as it determines the amount and distribution of fracture width open for flow. As the fracture surface after acidizing was analyzed in detail with the aid of the profilometer, different aspects of the etching pattern are discussed.

Several different parameters, which were believed to influence resulting conductivity, were calculated from the surface asperity distribution. These parameters were selected based on previous studies on effect of roughness on flow (Tsang, 1984; Brown, 1987; Zimmerman and Bodvarsson, 1996) and previous acid fracture conductivity model by Gong (1997). The main parameters were kurtosis, contact ratio, mean height of asperities, and standard deviation of asperity heights and fracture widths.

3.3.1. Distribution of Asperities – Kurtosis

In addition to fracture width, the distribution of the asperities that are holding the fracture open has a substantial influence on the resulting conductivity. While a rough surface with evenly distributed asperities can keep fracture open along the entire length of fracture, a distribution of asperities with most asperities gathered in one location can not keep fracture open along the entire length. One statistical parameter that describes

the distribution of asperities that relate to fracture conductivity is kurtosis of asperities. Kurtosis of asperities is a measure of the "peakedness" of the probability distribution of asperity heights. A higher kurtosis means more of the variance is due to infrequent extreme deviations, as opposed to frequent modestly-sized deviations. Conductivity model of Gong (1997) indicates that kurtosis influences resulting fracture conductivity, with a decrease in conductivity with increasing kurtosis.

3.3.2. Contact Ratio

When two rough surfaces are placed together, the interaction between the surface asperities of the two surfaces has significant influence on the resulting conductivity. One parameter that explains the interaction between two surface asperities is the contact ratio which is ratio of the surface area of asperities that touch each other compared to the total fracture surface area. Several theoretical models have accounted for the effect of contact ratio on flow through rough fractures (Walsh, 1981; Zimmerman and Bodvarsson, 1996).

To calculate the contact ratio, the method described by Greenwood and Williamson (1966) is used. The model states that the contact between two rough surfaces can be considered as an effective surface in contact with a flat surface. The two surfaces come together until their reference planes are separated by a fixed distance, in our case 95% of the maximum asperity height of the sample. The surfaces will be in contact at any location where the asperity height is originally greater than 95% of maximum asperity height. The 95% of maximum asperity height is chosen as it is a typical value chosen for contact ratio estimation of rough surfaces.

3.3.3. Height and Standard Deviation of Asperities

The height of asperities and the standard deviation of them influences the flow path as longer asperities can intrude more into the fluid flow field. Also the standard deviation of the asperity heights affects the relative roughness parameter of fracture which shows how much there is unevenness compared to a flat surface. Both the height and standard deviation of asperity heights affect the so called tortousity factor, which has been shown to influence conductivity of rough-walled fractures (Walsh and Brace, 1984; Zimmerman and Bodvarsson, 1996; Ge, 1997).

3.3.4. Effect of Parameters on Etching

Once all the important surface etching parameters were obtained from surface profile, their relationship to treatment parameters was analyzed in order to determine which of the surface parameters seem to relate to fracturing treatment parameters.

3.3.4.1. Contact Time Effect

Previous section results clearly showed that contact time had a significant influence on fracture width as expected based on theoretical understanding. It follows that contact time should also have substantial influence on etched surface characteristics.

There is more etching with increasing contact time and hence more tendency for a larger distribution of asperities and hence larger kurtosis. The kurtosis values of experiments with Indiana limestone and other rock types are shown in **Fig. 3.28** and **Fig. 3.29,** respectively. The results do not show any clear trend with contact time. While about two experiments show an increase in kurtosis with contact time, the same numbers of experiments show a decrease in kurtosis.

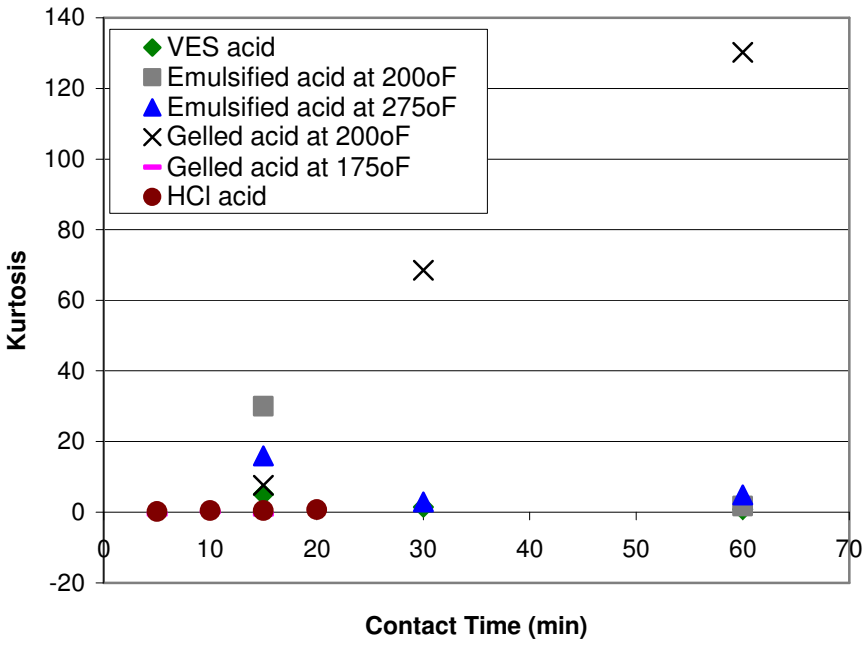

Fig. 3.28—Kurtosis at different contact times for Indiana limestone samples.

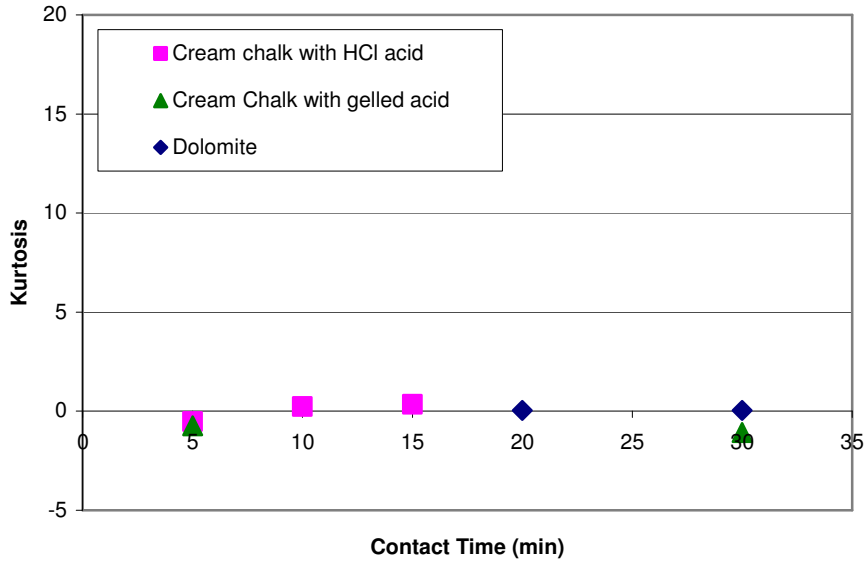

Fig. 3.29—Kurtosis at different contact times for Texas cream chalk and Sand Andres dolomite samples.

As there will be more etching of surface asperities with increasing contact time, fraction of total asperities touching each other should decrease with increasing contact time. Increased etching with time will result in more places along fracture face to be etched more uniformly also which will in turn reduce the amount of larger asperities holding fracture open. **Figs. 3.30 through 3.31** show the values of contact ratios at different contact times for Indiana limestone samples and other rock samples, respectively. Almost all of the experimental sets show a decrease in contact ratio with increasing contact time. Even the experiments that do not show a decreasing trend of contact ratio with contact time, most of them show almost no change with contact time rather than an opposite trend.

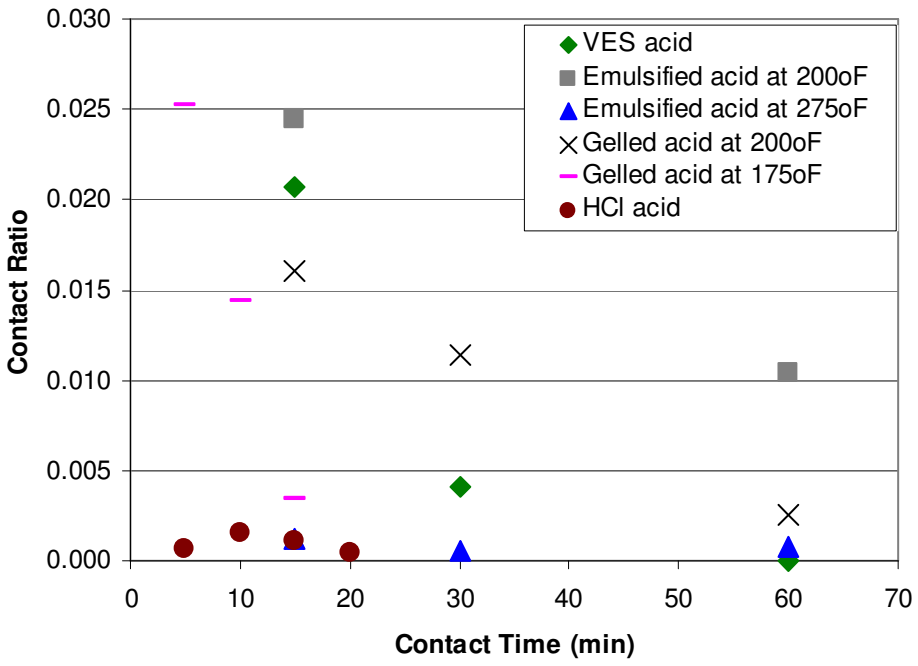

Fig. 3.30—Contact ratio at different contact times for Indiana limestone samples.

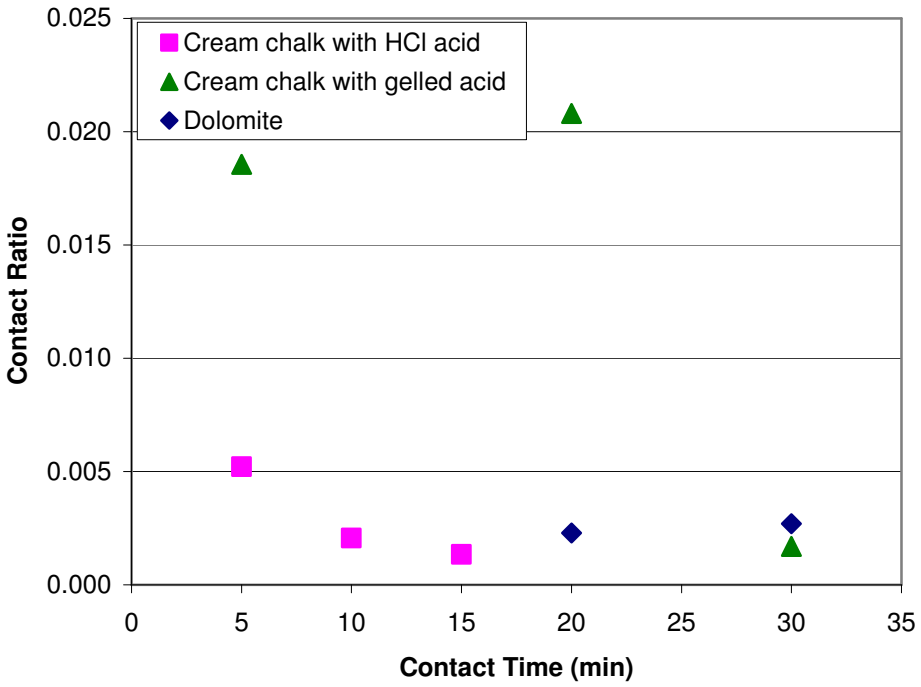

Fig. 3.31—Contact ratio at different contact times for Texas cream Chalk and San Andres dolomite samples.

3.3.4.2. Temperature Effect

The effect of temperature on surface characteristics should be similar to that of contact time as increasing temperature results in more etching of the surface. The expected pattern is of increasing kurtosis and decreasing contact ratio with temperature. The actual results of kurtosis and contact time with temperature are shown in **Fig. 3.32 and Fig. 3.33**, respectively.

Kurtosis does not show any trend with temperature as one experiment shows an increase while the other shows a decrease with temperature. However, contact ratio shows a clear and substantial decreasing trend with temperature as was the case with

increasing contact time. It must be noted that there are only two experimental sets showing the effect of temperature on surface parameters and hence it might be inappropriate and inaccurate to deduce a relationship from such limited data set.

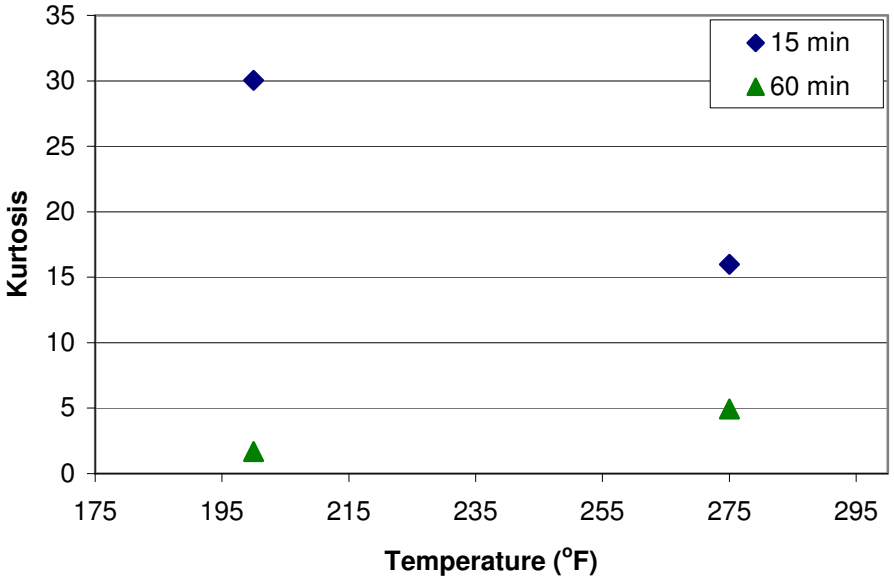

Fig. 3.32—Kurtosis at different temperatures for Indiana limestone.

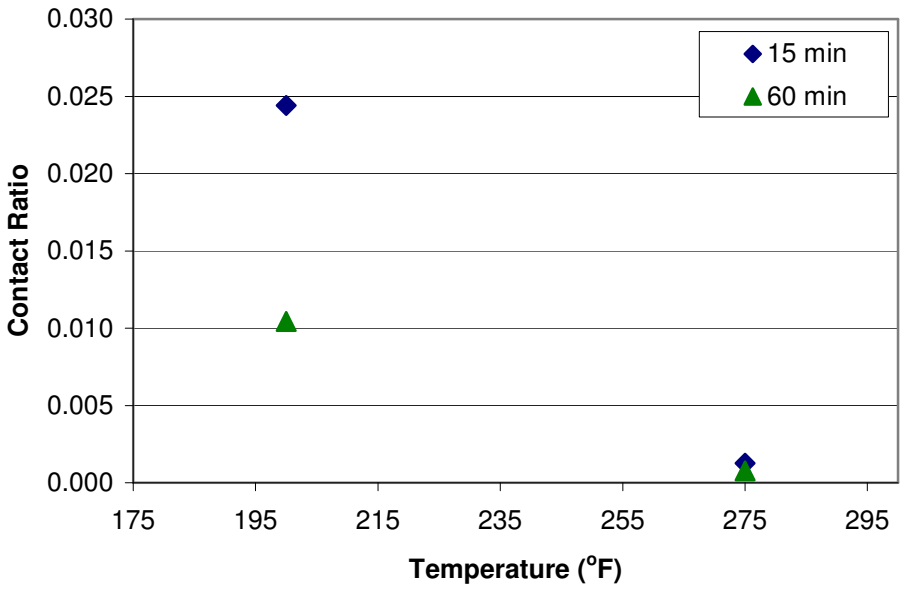

Fig. 3.33—Contact ratio at different temperatures for Indiana limestone.

3.3.4.3. Formation Type Effect

Theoretical understanding indicates that formation type has a great influence on etching pattern as it influences both the overall reaction rate and leak off pattern. Etched width results in the last section clearly showed that formation type has a great impact on amount of etching. Similar results should be expected on the effect of formation type on etching characteristics. The effect of formation type on kurtosis and contact ratio is shown in **Fig. 3.34** and **Fig. 3.35**, respectively. Results show great differences in the etching parameters among the formations at short contact time with no significant differences at longer contact time. While Texas cream chalk has the highest values of both kurtosis and contact ratio at contact time of 20 minutes, both formations have similar and very low values of surface characteristics at 30 minute contact time.

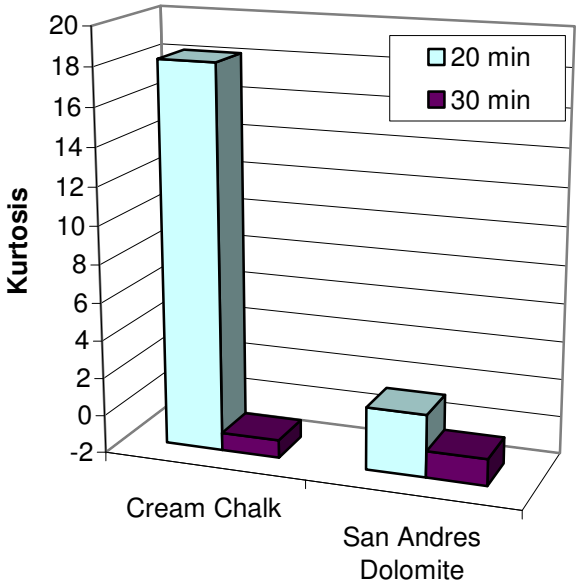

Fig. 3.34—Kurtosis for two different formations acidized with gelled acid at 175 °F at two contact times.

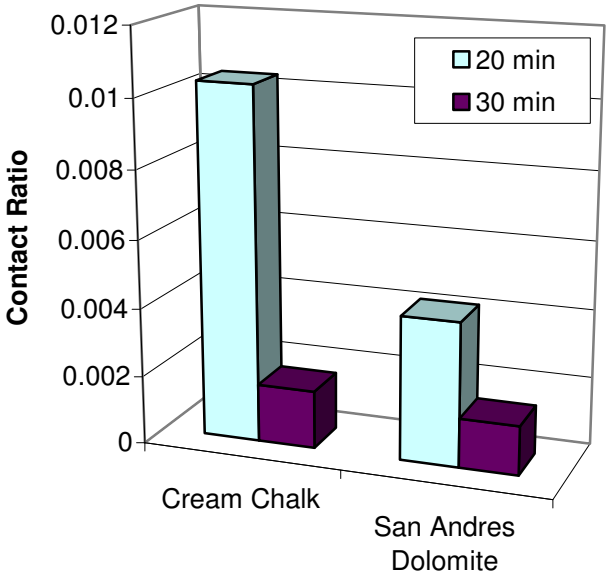

Fig. 3.35—Contact ratio for two different formations acidized with gelled acid at 175 °F at two contact times.

3.3.4.4. Acid Type Effect

Similar to the effect of formation, acid type affects etching characteristics through its effect on reaction rate, mass transfer rate, and leak off behavior. In the previous section, it was observed that acid type influenced fracture width. Kurtosis for three sets of experiments that show the effect of acid type are shown in **Figs. 3.36 through 3.38**. There are great differences in the kurtosis values among the acid types with some trends. While VES acid system results in the lowest values of kurtosis compared to other acid systems for majority of contact times, straight HCl followed by gelled acid result in highest values of kurtosis.

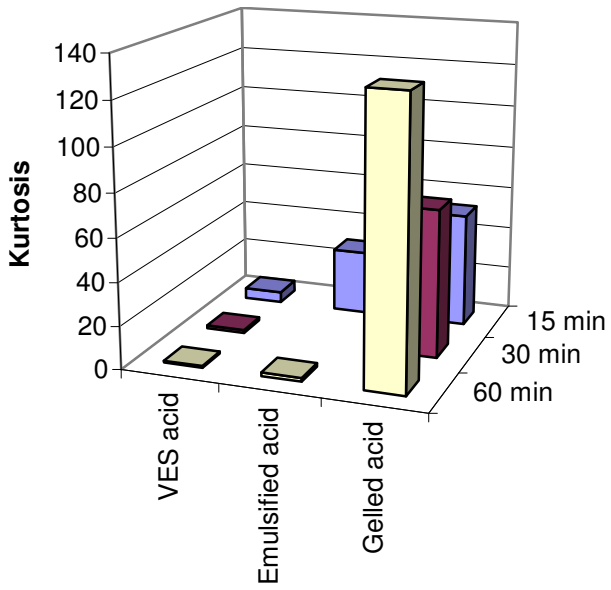

Fig. 3.36—Kurtosis of Indiana limestone samples acidized at 200 °F with three different acid types at three contact times.

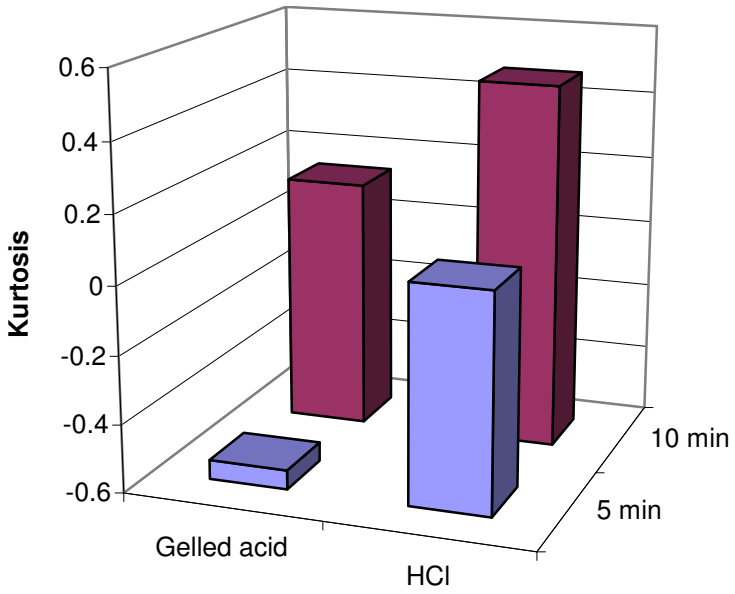

Fig. 3.37—Kurtosis of Indiana limestone samples acidized at 175 °F with two different acid types at two contact times.

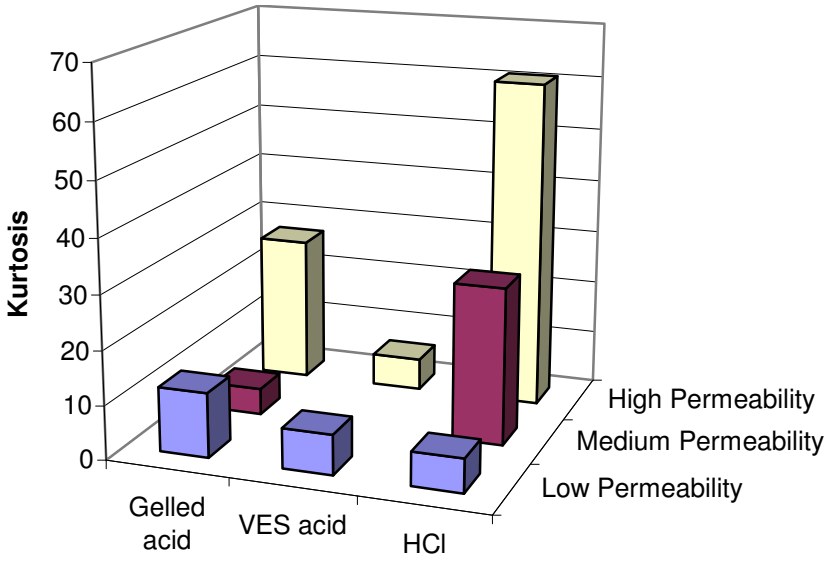

Fig. 3.38—Kurtosis of three different permeability ranges of Macae limestone samples acidized at 185 °F with three different acid types.

Similar to kurtosis, contact ratios for the three sets are shown in **Figs. 3.39 through 3.41**. There are great differences in the contact ratio values among the acid types. While there seems to be no clear pattern, the VES acid system results in the lowest values of contact ratio compared to other acid systems for majority of contact times (Figs. 3.38 and 3.40). While gelled acid results in higher contact ratio values than straight HCl on Indiana limestone (Fig. 3.39), straight HCl actually results usually in higher contact ratio values on the Macae limestone samples (Fig. 3.40).

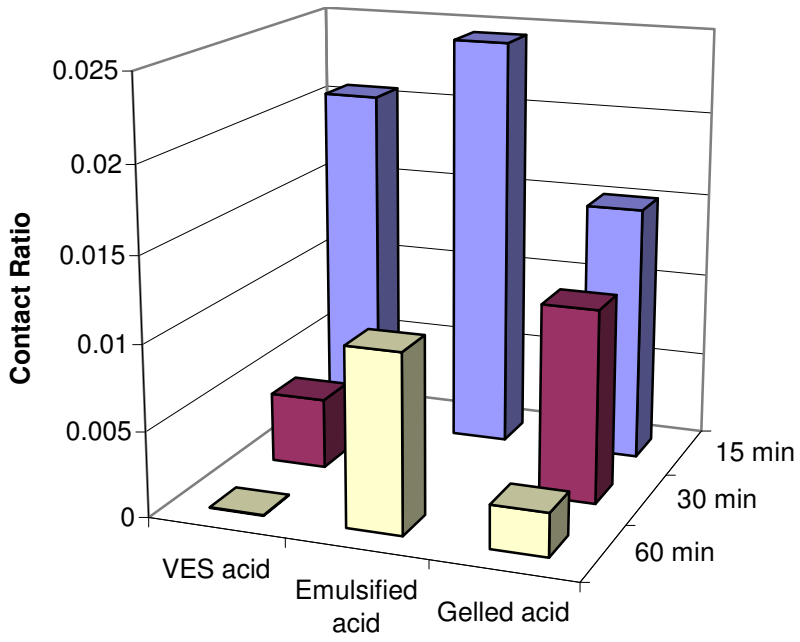

Fig. 3.39—Contact ratio of Indiana limestone samples acidized at 200 °F with three different acid types at three contact times.

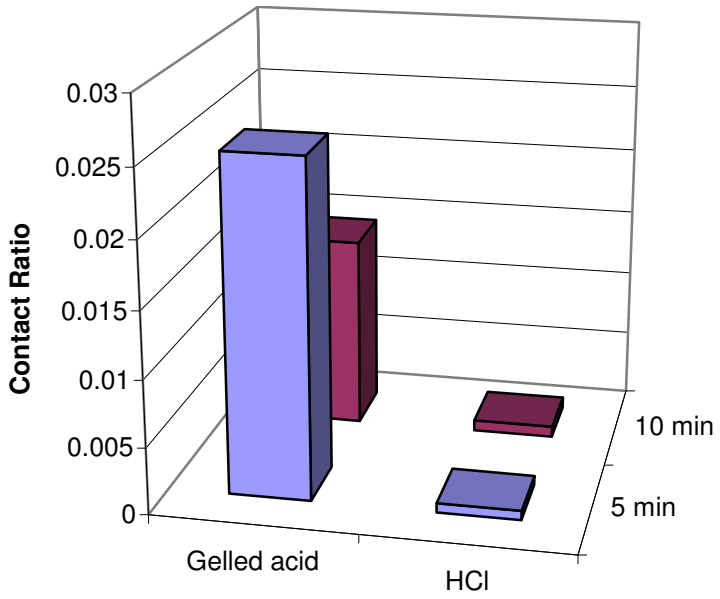

Fig. 3.40—Contact ratio of Indiana limestone samples acidized at 175 °F with two different acid types at two contact times.

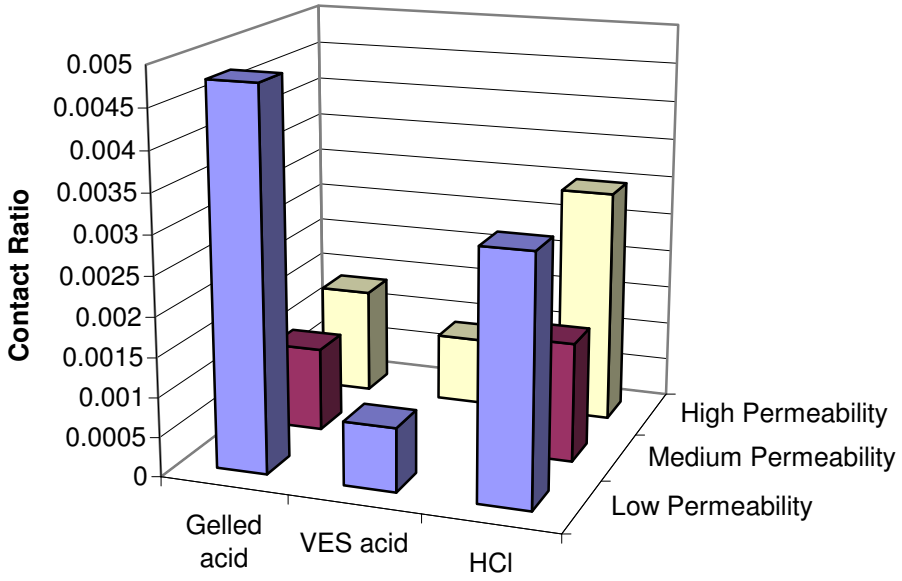

Fig. 3.41—Contact ratio of three different permeability ranges of Macae limestone samples acidized at 185 °F with three different acid types.

3.3.4.5. Repeatability

While repeated experiments should have similar values of etched characteristics, there could be differences due to core heterogeneities and also the stochastic nature of the etching process. **Fig. 3.42 and Fig. 3.43** show kurtosis values for six sets of repeated experiments. While majority of repeated experiments have similar values of kurtosis, some show significant differences in kurtosis. The major difference in kurtosis between repeated experiments occurs for tests conducted with gelled acid on Indiana limestone and Texas cream chalk samples. All except one of the five repeated tests in Fig. 3.42 show very similar values of kurtosis.

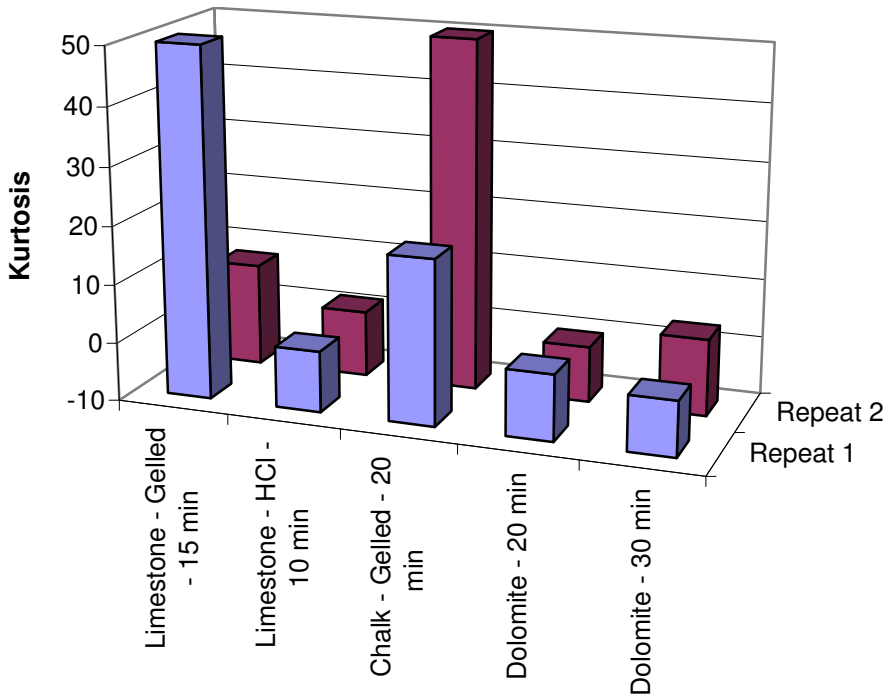

Fig. 3.42—Kurtosis of five sets of experiments repeated twice each.

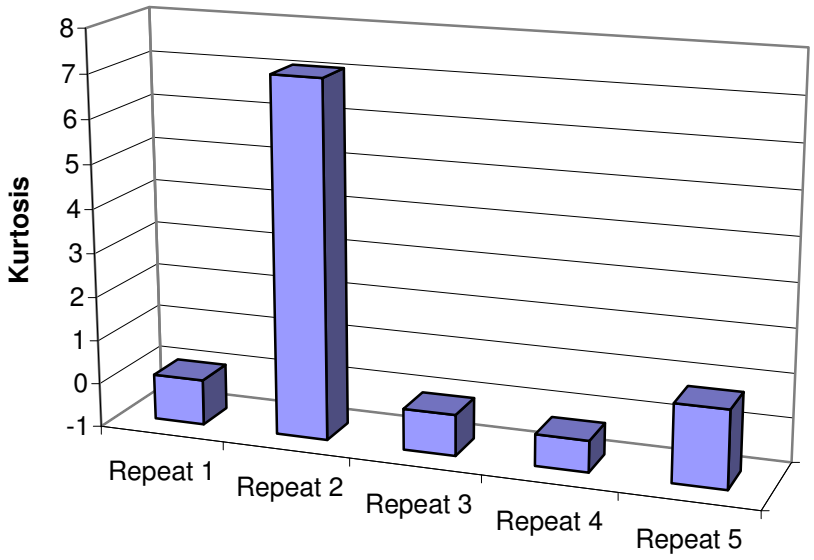

Fig. 3.43—Kurtosis for one set of experiment repeated five times with Indiana limestone samples acidized with HCl at 5 minutes.

Contact ratio comparison between repeated experiments for the six sets of experiments is shown in **Fig. 3.44 and Fig. 3.45**. Once again, majority of tests show similar values of contact ratio between repeated tests with two exceptions: one is chalk sample acidized with gelled acid and the other is one of the five repeated tests on Indiana limestone. It is interesting to note that the repeated tests that show differences in contact ratio are different from the repeated tests that showed differences in their kurtosis values.

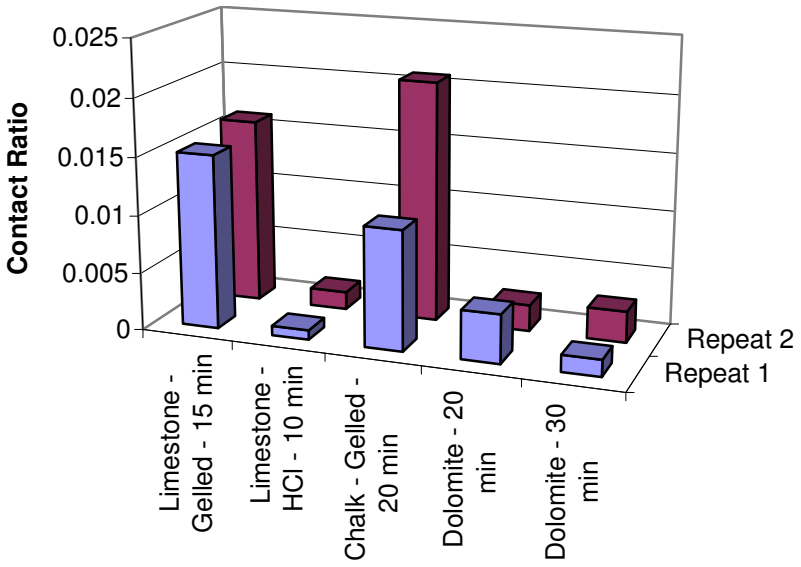

Fig. 3.44—Contact ratio of five sets of experiments repeated twice each.

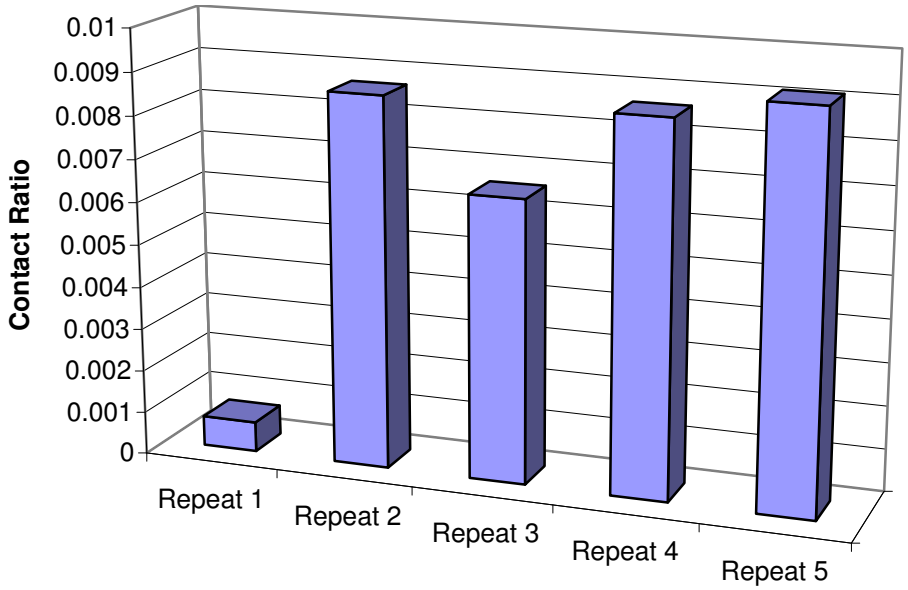

Fig. 3.45—Contact ratio for one set of experiment repeated five times with Indiana limestone samples acidized with HCl at 5 minutes.

3.4. Effect of Acid on Rock Strength

The strength of asperities on fracture face that hold the fracture open influences how much stress the fracture can withstand and how asperities are crushed and hence conductivity reduced with closure stress. Previous studies have shown that rock strength is affected by acid etching (Gong, 1997; Abbas et al., 2006; Nasr-El-Din et al., 2006).

3.4.1. Rock Strength Variation

Rock embedment strength (S_{RE}) was measured at about 28 points on each fracture face for most experiments. All these 28 data values were averaged to obtain the average S_{RE} for each fracture face. There was significant amount of variation among the S_{RE} values at the 28 different measurement points even before acidizing. The unacidized fracture face had commonly about two times difference between the minimum and the maximum value of S_{RE} across the core face (**Fig. 3.46**).

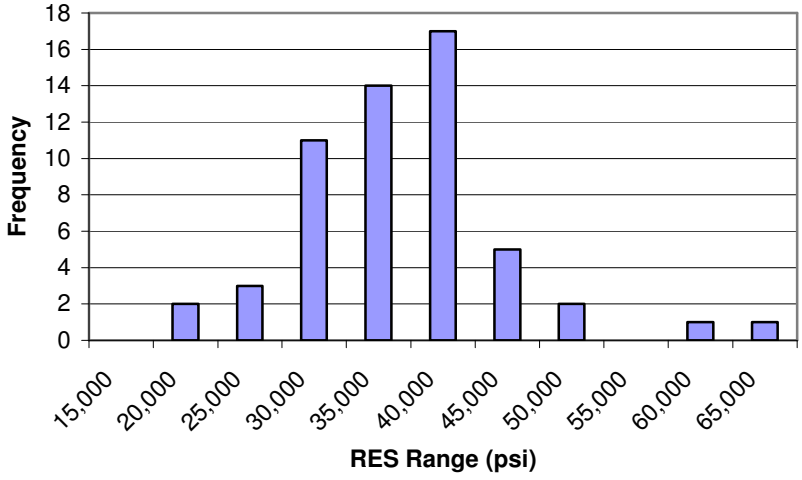

Fig. 3.46—Frequency distribution of S_{RE} measurements across the 56 different locations of the two fracture faces before acidizing (ILS 9).

S_{RE} values before acidizing for all experiments grouped based on rock type are plotted in **Fig. 3.47**, showing the scatter in S_{RE} values. Actually, there is good agreement among measurements for all the rock types except dolomite formation which shows a rather wider scatter of S_{RE} data. S_{RE} values before acidizing are 20,000 to 30,000 psi for Texas cream chalk, 25,000 to 35,000 psi for Macae limestone, 30,000 to 40,000 psi for Indiana limestone, and 50,000 to 70,000 for San Andres dolomite. The measured variations are much less than those reported in previous studies (Nierode and Kruk, 1973; Gong, 1997). The same plot of S_{RE} after acidizing for each rock type shows similar scattering with relatively good agreement between measurements (**Fig. 3.48**).

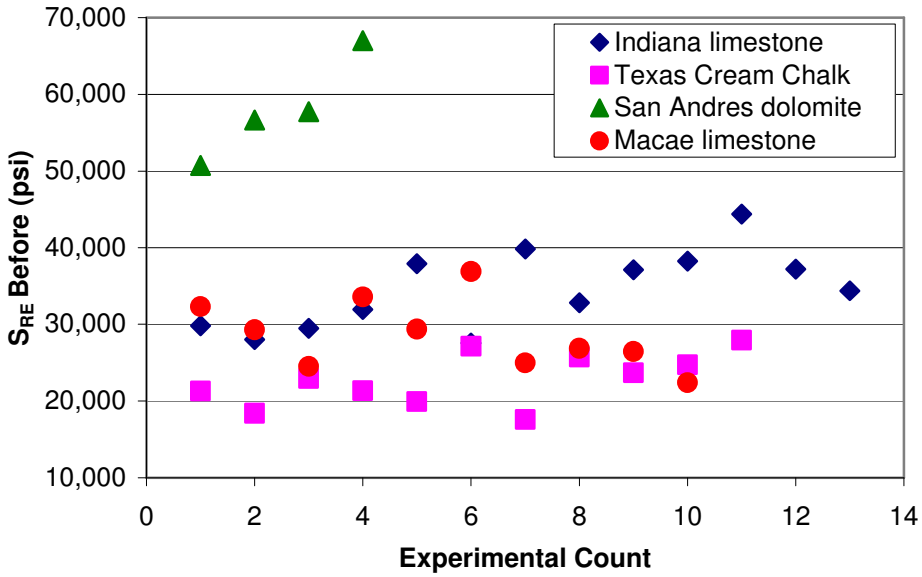

Fig. 3.47—S_{RE} values before acidizing for all experiments grouped based on rock type.

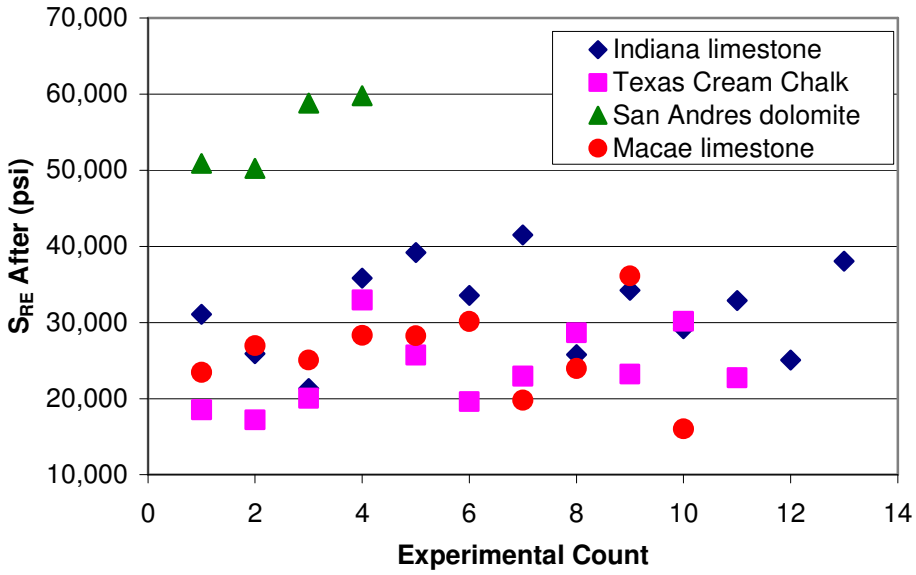

Fig. 3.48—S_{RE} values after acidizing for all experiments grouped based on rock type.

3.4.2. Rock Strength Change Due to Acidizing

The change in average rock embedment strength for all experiments after acidizing compared to unacidized samples are summarized in **Table 3.4**. The results plotted in **Fig. 3.49** clearly show that there is no general trend of decreasing rock strength with acidizing. About 39% of experiments show an increase in average S_{RE} after acidizing. The increase in S_{RE} after acidizing might be due to experimental error in measuring S_{RE} as the indentation might have been done on a surface with a deep valley, requiring larger force for indentation. Another reason for larger values of S_{RE} after acidizing might be due to the fact that acidizing removed the softer parts of the fracture face, revealing the harder materials under them. There is definitely no correlation between acidizing and rock weakening.

TABLE 3.4—SUMMARY OF AVERAGE S_{RE} MEASUREMENTS BEFORE AND AFTER ACIDIZING AND THE PERCENTAGE CHANGE IN SRE DUE TO ACIDIZING

Label	Rock	Acid	Time	SRE		
			min	Before (psi)	After (psi)	% Change
ALC 10	Indiana Limestone	Gelled	5	29,797	31,098	4
ALC 9		Gelled	10	28,028	25,878	-8
ALC 8		Gelled	15	29,461	21,315	-28
IL 4		Gelled	20	31,928	35,819	12
IL 2		Gelled	20	37,896	39,184	3
IL 3		Gelled	30	27,579	33,569	22
IL 1		Gelled	30	39,817	41,504	4
ALC 7		HCl	5	32,792	25,766	-21
ALC 2		HCl	10	37,108	34,238	-8
ALC 5		HCl	10	38,255	29,181	-24
ALC 1		HCl	15	44,363	32,871	-26
ALC 6		HCl	15	37,210	25,038	-33
ILS9		HCl	20	34,383	38,065	11
CD1	San Andres Dolomite	Gelled	20	50,739	50,903	0.3
CD2		Gelled	20	56,660	50,246	-11
CD3		Gelled	30	57,716	58,845	2
CD5		Gelled	30	67,029	59,811	-11
ACC 7	cream Chalk	HCl	5	21,315	18,544	-13
ACC 6		HCl	10	18,390	17,196	-6
ACC 1		HCl	15	22,939	20,042	-13
ACC 10		Gelled	5	21,357	32,960	54
ACC 9		Gelled	10	19,951	25,724	29
ACC 15		Gelled	10	27,161	19,620	-28
ACC 3		Gelled	15	17,592	22,953	30
ACC 11		Gelled	20	25,755	28,637	11
ACC 13		Gelled	20	23,694	23,217	-2
ACC 12		Gelled	30	24,728	30,172	22
ACC 14		Gelled	30	27,951	22,743	-19
PBC 1&2	Macae Limestone	Gelled	20	32,319	23,450	-27
PBC 11&12		Gelled	30	29,301	26,950	-8
PBC 15&16		Gelled	20	24,520	25,061	2
PBC 3&4		HCl	30	33,600	28,318	-16
PBC 7&8		HCl	20	29,380	28,260	-4
PBC 17&18		HCl	20	36,906	30,153	-18
PBC 9&10		VES	20	24,993	19,793	-21
PBC 5&6		VES	30	26,887	23,946	-11
PBC 19&20		VES	20	26,456	36,132	37
PBC 13&14		Emulsified	30	22,395	16,018	-28

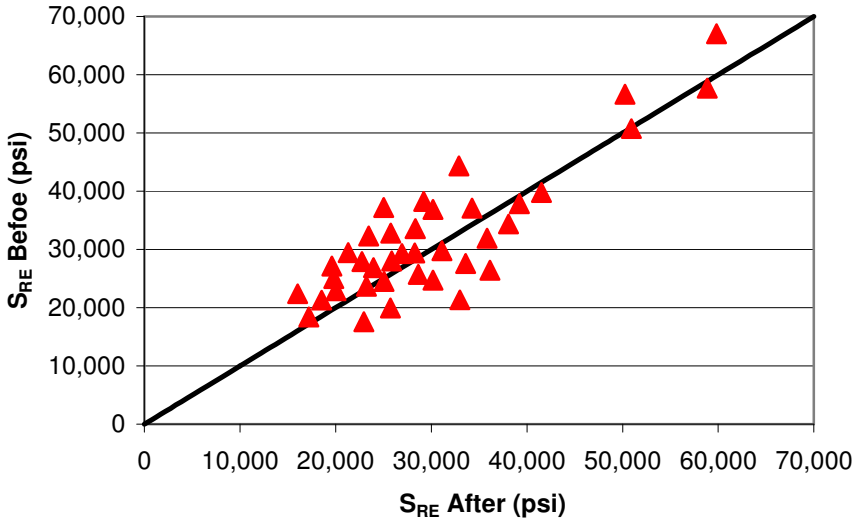

Fig. 3.49—The average S_{RE} values before and after acidizing.

3.4.3. Effect of Parameters on Rock Strength

The relationship between rock strength and treatment parameters was analyzed in order to determine if any of the treatment parameters correlate to S_{RE} values after acidizing or the amount of change in S_{RE}. However as there is such a large variation among S_{RE} measurements across an unacidized core and no general trend of decreasing rock strength with acidizing, there is little value in this analysis.

3.4.3.1. Contact Time Effect

The values of S_{RE} after acidizing for Indiana limestone and all other rock types with respect to changing contact time are shown in **Fig. 3.50 and Fig. 3.51**, respectively. Majority of experiments show a decreasing trend of S_{RE} with increasing contact time with a few exceptions. The trend is clear for all Indiana limestone samples except the ones acidized with HCl. Similarly, Texas cream chalk samples acidized with HCl show

almost no change in S_{RE} with contact time, while San Andres dolomite samples are the only experiments that show a clear trend of increasing S_{RE} with contact time.

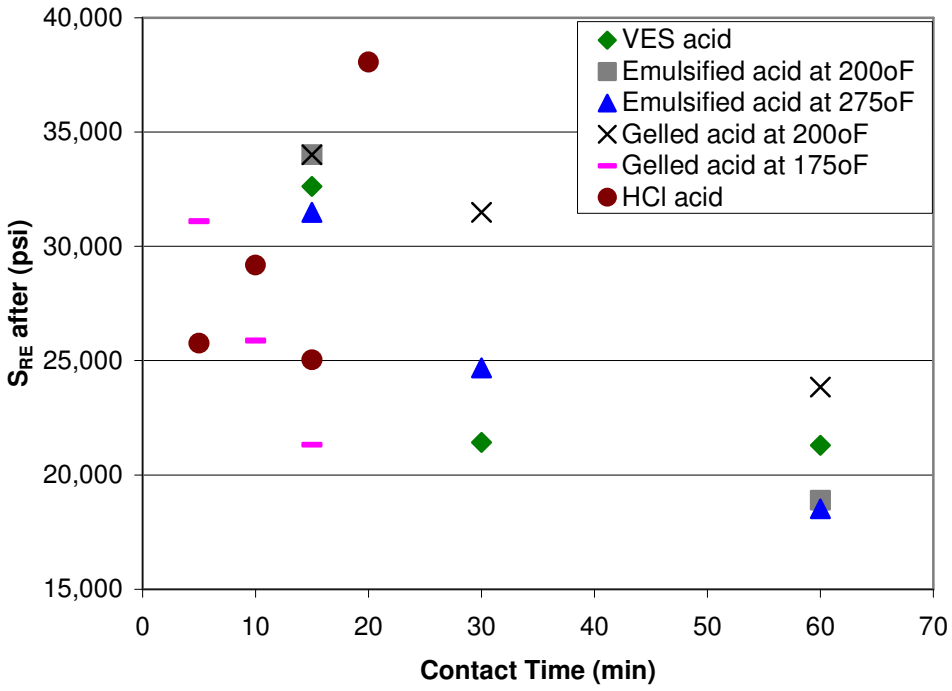

Fig. 3.50—S_{RE} after acidizing with contact time for Indiana limestone samples.

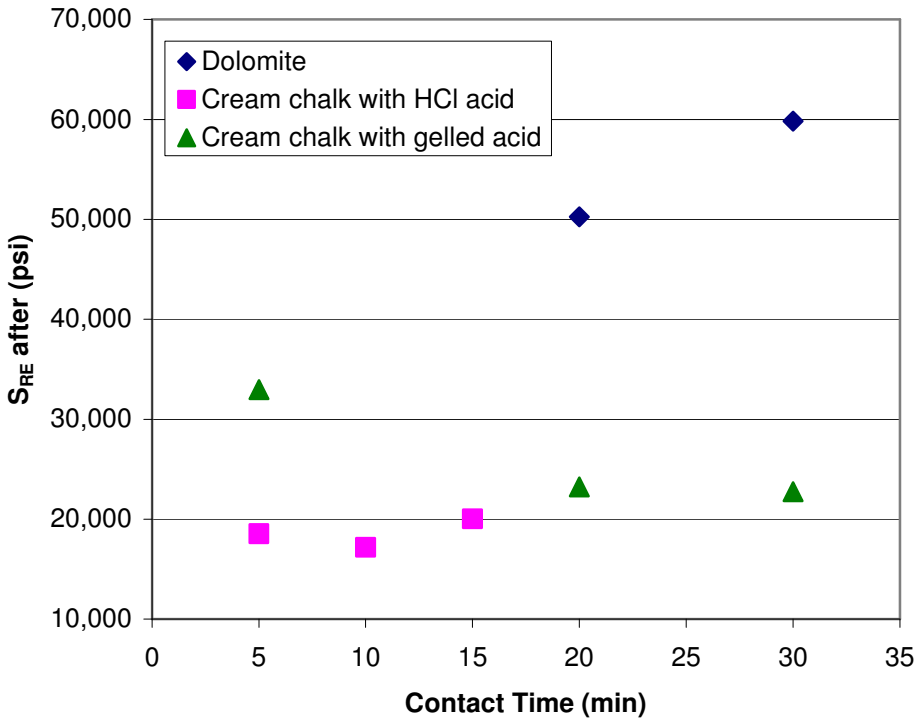

Fig. 3.51—S_{RE} after acidizing with contact time for cream chalk and dolomite.

3.4.3.2. Temperature Effect

The plot of S_{RE} after acidizing with changing temperature is shown in **Fig. 3.52**. There is not much change in S_{RE} values with increasing temperature even though there was a significant change in temperature with substantial change in fracture widths. However, it must be remembered that S_{RE} values after acidizing alone can not be used to determine the weakening of rocks as the initial S_{RE} values before acidizing for the rock samples could have been much different as was shown in Fig. 3.46.

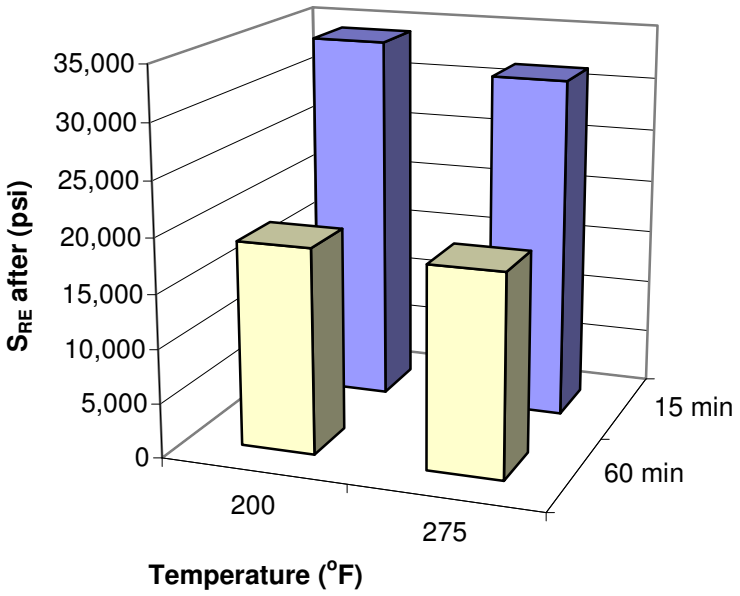

Fig. 3.52—S_{RE} after acidizing at two different temperatures for Indiana limestone samples acidized with emulsified acid at two contact times.

3.4.3.3. Formation Type Effect

Several studies have shown that rock strength is very much dependent on formation type with each formation having a certain range of S_{RE} values (Nierode and Kruk, 1973; Gong, 1997; Nasr-El-Din et al., 2006). In general, dolomite formations are stronger than limestone formations. Our results confirmed these findings as was shown in Fig. 3.46. Also recent study have shown that strength of limestone samples are much more effected by acidizing than dolomite samples (Nasr-El-Din et al., 2006). The percentage change in S_{RE} values between before and after acidizing for two sets of similar experiments for three different formations is shown in **Fig. 3.53**. There is much greater change in rock strength of limestone and chalk than dolomite due to acidizing with an average of 15% change in S_{RE} values for both limestone and chalk compared to

an average of only 2% for dolomite. The results are consistent with previous studies, showing that dolomite strength is much less affected by acidizing compared to limestone. However it must be noted that all testes showed an increase in S_{RE} with acidizing.

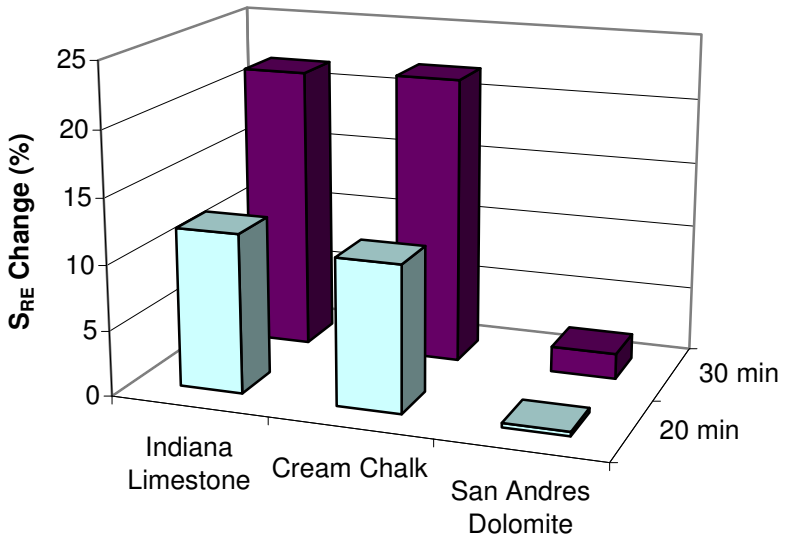

Fig. 3.53—Change in S_{RE} for three different formations tested at two contact times.

3.4.3.4. Acid Type Effect

Recent study has shown that acid type also affects the amount of rock weakening (Nasr-El-Din et al., 2006). The resulting change in S_{RE} values for three sets of experiments that show effect of acid type on rock strength are shown in **Figs. 3.54 through 3.56**. Each acid type has a different effect on rock strength for most experiments. While HCl and gelled acid both resulted in similar rock strength changes

on Indiana limestone samples (Fig. 3.53), gelled acid resulted in much more rock strength change than HCl for Texas cream chalk samples, however HCl caused a weakening of rock strength as opposed to an increase in rock strength with gelled acid (Fig. 3.54). Similarly, HCl acid resulted in usually more rock weakening than gelled acid on Macae limestone samples; however VES acid resulted in the greatest amount of change in S_{RE} as compared to other acid systems (Fig. 3.55)

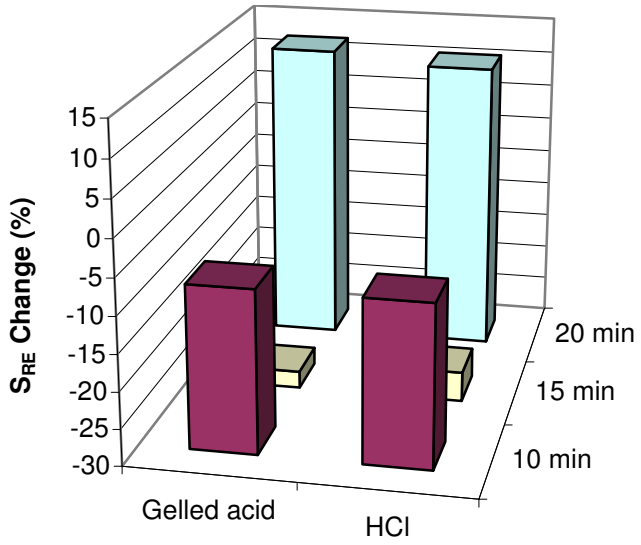

Fig. 3.54—Change in S_{RE} of Indiana limestone samples acidized at 175 °F with two different acid types at three contact times.

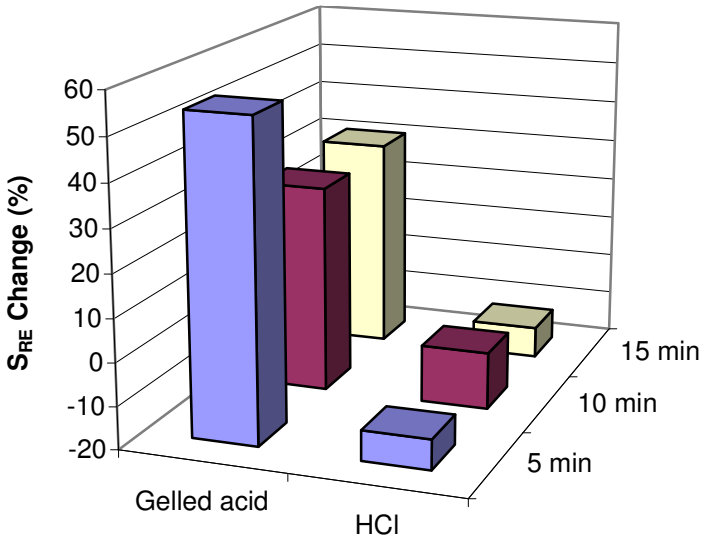

Fig. 3.55—Change in S_{RE} of Texas cream chalk samples acidized at 175 °F with two different acid types at three contact times.

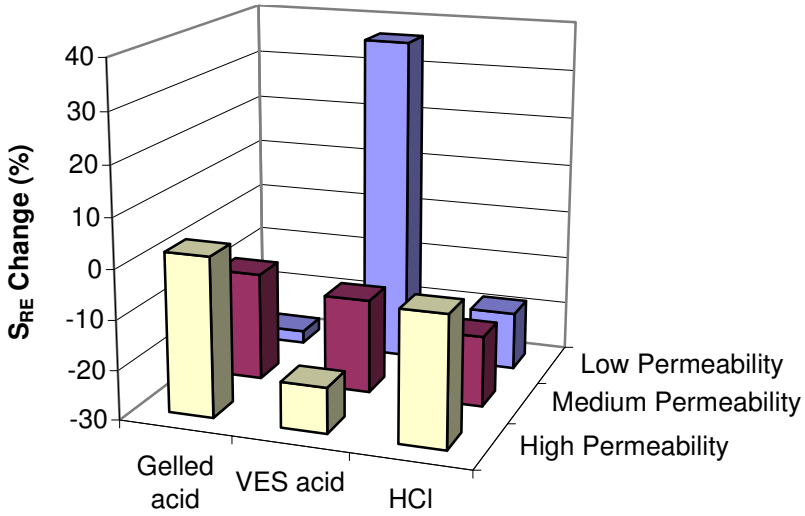

Fig. 3.56—Change in S_{RE} of three different permeability ranges of Macae limestone samples acidized at 185 °F with three different acid types.

3.4.3.5. Repeatability

As rock strength measurements have shown such a wide variation before acidizing and also after acidizing for the same rock formation, it is not expected that there will be much repeatability between repeated tests in terms of S_{RE} values. **Fig. 3.57 and Fig. 3.58** show changes in S_{RE} values for the five sets of repeated experiments. There is great variation among change in S_{RE} values of repeated tests, however most of them agree with each other in terms of whether rock was weakened or strengthened after acidizing. The results clearly show that S_{RE} measurements are not repeatable and are not suitable for relating to acidizing conditions and resulting conductivity.

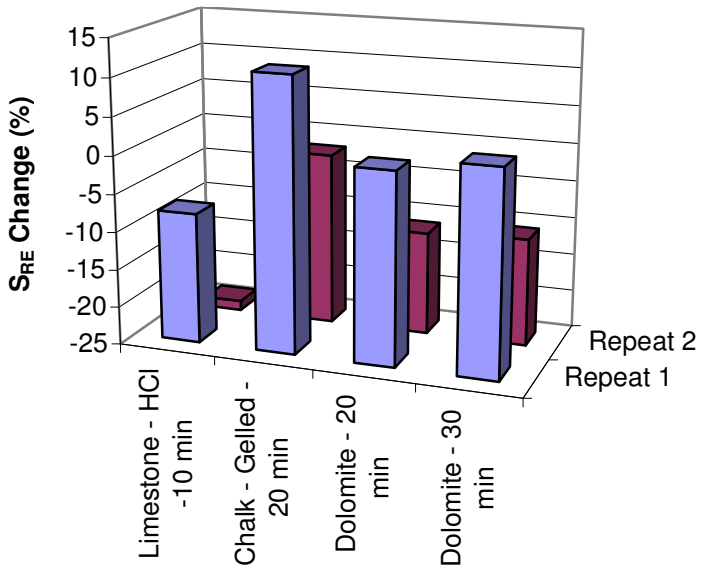

Fig. 3.57—Change in S_{RE} values of four sets of experiments repeated twice each.

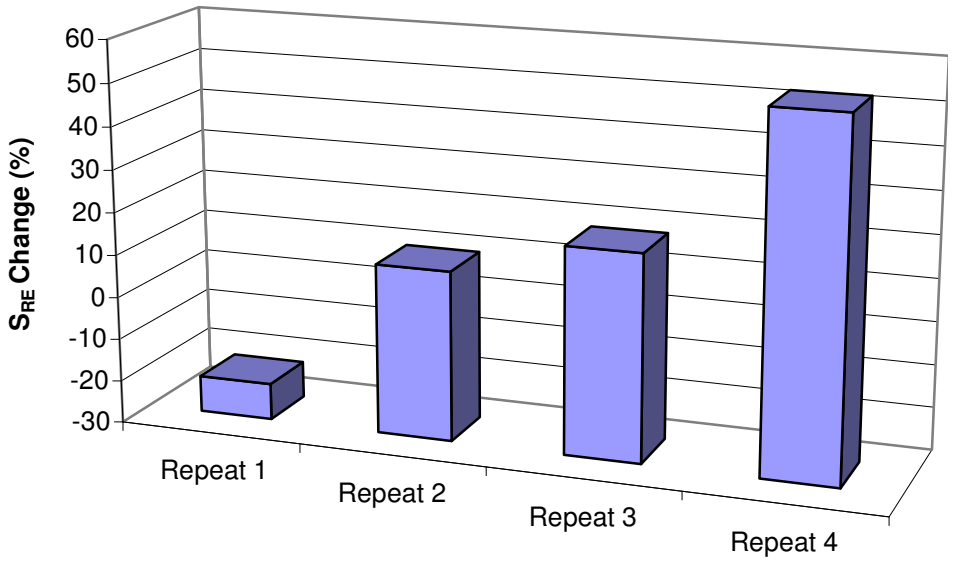

Fig. 3.58—Change in S_{RE} values of one set of experiments repeated four times with Indiana limestone samples acidized with HCl acid at 5 minute contact time.

3.4.4. Strength Measurement Errors

There were several major experimental limitations and errors that affected S_{RE} measurements. The depth of indentation was measured with a dial pentameter which did not have a good resolution. Also the pressure gauge that measured the pressure required to press the indentation into the core was not very accurate as it was based on hydraulic pressure. A template was made to determine the measurement points; however the actual measured location was sometimes not the same due to etching pattern or movement of indentation ball from the measurement point.

3.5. Fracture Conductivity

The final outcome of the experiments was measurement of resulting fracture conductivity under different closure stresses. It is essential to determine the relationship between treatment and formation parameters and final conductivity in order to better understand how to design acid fracturing treatments that result in highest possible conductivity and how to model the resulting conductivity.

3.5.1. Overall Fracture Conductivity

While three different conductivities were measured for most experiments, several experiments had only overall fracture conductivity measured. Comparison of overall to front and back section fracture conductivity for a sample experiment clearly shows that overall fracture conductivity is simply the harmonic mean of front and back fracture conductivity (**Table 3.5** and **Fig. 3.59).** However as most pressure drop occurs at the back section where fracture is much less conductive, the overall fracture conductivity is very similar to the back section fracture conductivity. The front section conductivity is very high as it has very little pressure drop due to a relatively wide open fracture aperture. The great variation of conductivity between front and back section can be well explained from surface etching pattern (**Fig. 3.60**), which shows much more etching with large open areas of flow at the front section of fracture with minimal etching at the end section of fracture length. As the overall conductivity is representative of the back section, the overall conductivity data values will be used in all future analysis.

TABLE 3.5—MEASURED CONDUCTIVITIES COMPARED TO CALCULATION OF OVERALL CONDUCTIVITY (PBC 9&10)

Closure Stress (psi)	Measured Conductivity (md-ft)			Calculated Overall Conductivity (md-ft)	
	Overall	Front	Back	Arithmetic	Harmonic
102	4,847	30,484	2,633	16,559	4,847
1,230	1,692	21,947	880	11,414	1,692
2,049	803	9,867	419	5,143	804
3,125	680	4,768	366	2,567	680
3,996	277	1,122	158	640	277
5,225	129	1,017	69	543	129

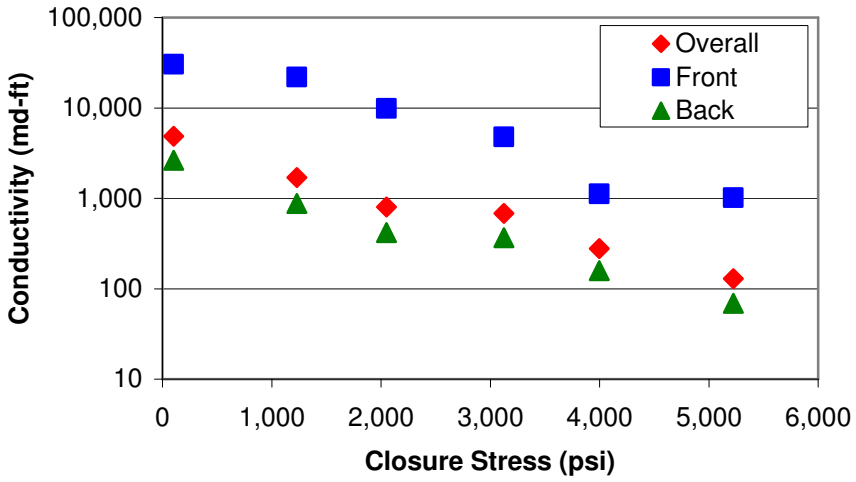

Fig. 3.59—Front, back, and overall measured conductivities as a function of closure stress for one experiment (PBC 9&10).

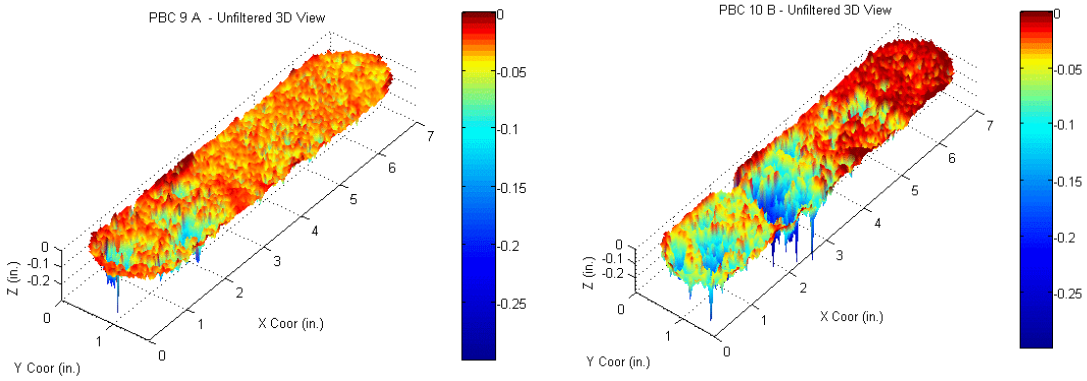

Fig. 3.60—3-D images of PBC 9 and 10 showing much more etching at the front section compared to back section.

3.5.2. Conductivity Measurement Errors

One of the main errors involved in conductivity measurements was the accuracy of pressure transducers. The accuracy of the transducers is about 0.075% of the calibrated span or upper range of reading and it is recommended not to use it below about 2 to 3 times the accuracy. As the pressure transducer reads up to about 60 psi, it should not be used for pressure drops below 0.15 psi and changes of less than 0.05 psi. However during the experiments, when the fracture had a relatively wide open width, pressure drop across the fracture face was very small at about 0.02 psi which could not be measured accurately by the pressure transducer. As a result, all the conductivity values that were measured with such small pressure drops were discarded and not discussed in the following section.

Another possible error of conductivity measurement might have been the result of some missing parts of the silicone rubber around the core near the fracture face. The rubber coating around the core sometimes did not cover the core right up to the fracture

face. As a result, during the conductivity measurement, the fluid could have been flowing through the gap between the core and API cell where the silicone coating was missing. This could have resulted in much higher conductivities than should have been measured.

3.5.3. Effect of Parameters on Conductivity

In order to improve our understanding of how acid fracturing treatment parameters influence resulting conductivity, the measured conductivities are analyzed for the effect of treatment parameters.

3.5.3.1. Acid Type Effect

There are about four different sets of experiments conducted at the same conditions except with different acid systems that can be used to analyze the effect of acid type on resulting conductivity. The conductivity values of the first set which were Indiana limestone samples acidized at about 200 ^{o}F with VES acid, emulsified acid, gelled acid, and straight HCl acid at contact times of 15, 30, and 60 minutes are shown in **Fig. 3.61, Fig. 3.62, and**, **Fig. 3.63**, respectively. However the sample acidized with emulsified acid at 30 minutes was removed from analysis as it showed channeling behavior. Also samples were acidized with straight HCl for only the contact time of 15 minutes.

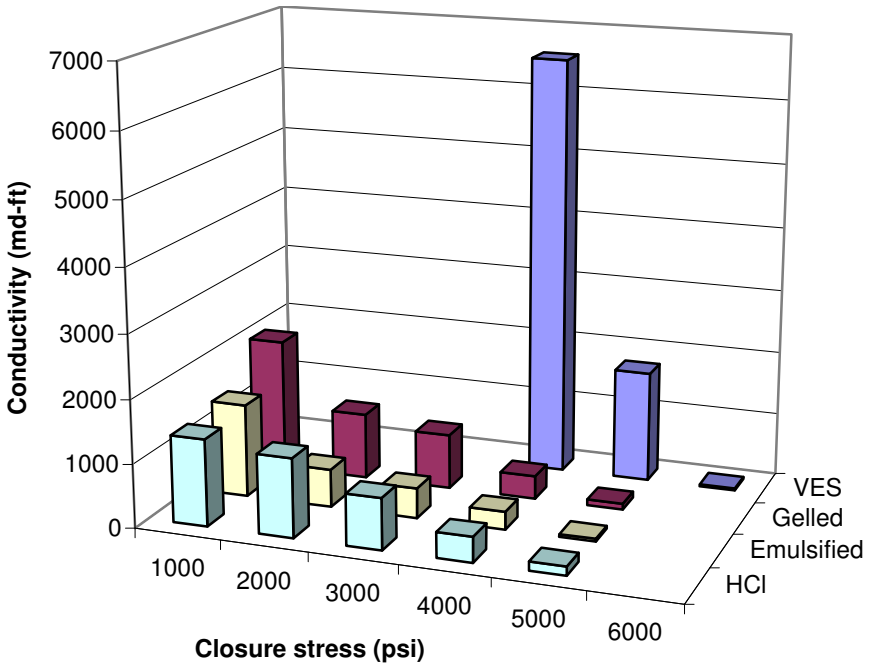

Fig. 3.61—Conductivity plot of Indiana limestone samples acidized with four different acid types at 200 °F for 15 minutes.

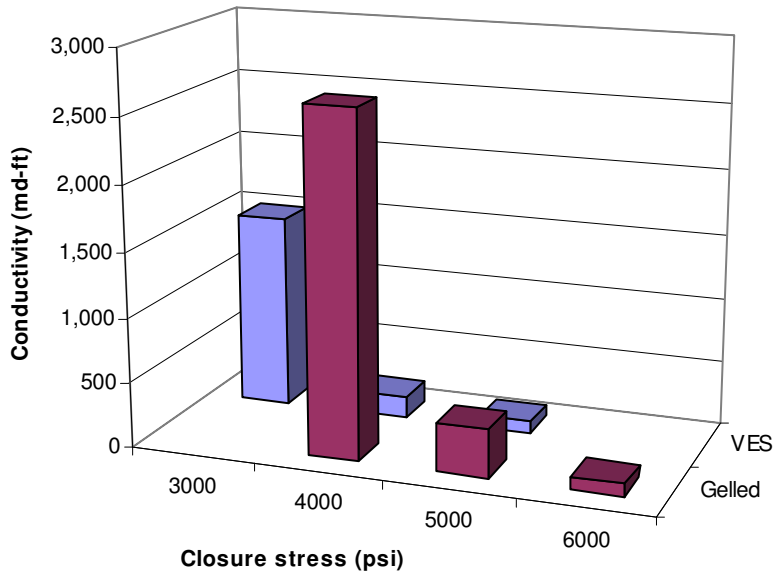

Fig. 3.62—Conductivity plot of Indiana limestone samples acidized with two different acid types at 200 °F for 30 minutes.

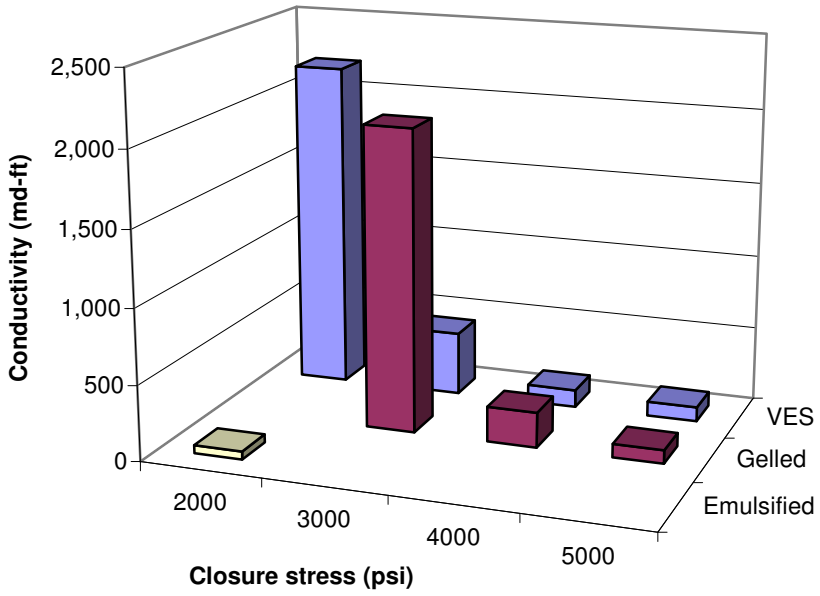

Fig. 3.63—Conductivity plot of Indiana limestone samples acidized with three different acid types at 200 °F for 60 minutes.

While the sample acidized with VES acid system had higher conductivities than all other acid systems at the shortest contact time of 15 minutes, conductivity of samples acidized with gelled acid had higher conductivity at the longer contact times of 30 and 60 minutes. From previous section on fracture width (see Fig. 3.18), it was observed that VES acidized samples had higher average fracture width open for flow at all contact times compared to the other acid systems of gelled and emulsified (straight HCl acid always resulted in higher average fracture widths). However samples acidized with gelled acid had greater amount of contact (higher contact ratios) between asperities that were holding the fracture open at the longer contact time of 30 and 60 minutes compared to VES acidized samples (see Fig. 3.39).

The reason for higher conductivity of VES acidized sample and gelled acidized samples at contact time of 15 minutes and longer times, respectively, can be explained from the combined effect of fracture width and contact ratio and illustrated by the surface profiles of fracture faces. At the short contact time of 15 minutes, VES acidized sample has more open area for flow with greater amount of asperities holding the fracture open, resulting in higher conductivities, especially at higher closure stresses. The etching pattern shows a nice valley running nearly to the end of fracture with sufficient asperities around the valley to hold it open while the gelled acidized sample has not been etched at all with almost no area open for flow (**Fig. 3.64**). However at the longer contact time of 30 and 60 minutes, VES acidized samples have been acidized to a great extent with a rather uniform fracture width along the whole length of fracture with almost no contact points, resulting in lower conductivities at higher closure stresses than gelled acid. Gelled acidized samples at 30 and 60 minute contact times show a rather rough pattern with significant open areas for flow and asperities to hold the flow area open (**Fig. 3.65 and Fig. 3.66**). Rock embedment strength measurements also support the conductivity trend as all samples have similar S_{RE} values after acidizing at the short contact time of 15 minutes, while the samples acidized with gelled acid keep higher strengths at the longer contact times of 30 and 60 minutes (see Fig. 3.50).

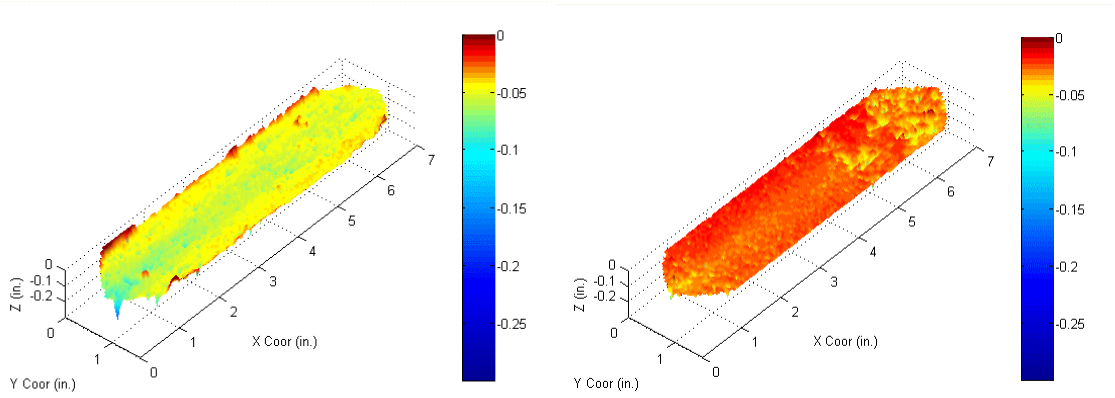

Fig. 3.64—3-D profilometer images of fracture faces for sample acidized with VES acid (left) and sample acidized with gelled acid (right) for 15 minutes.

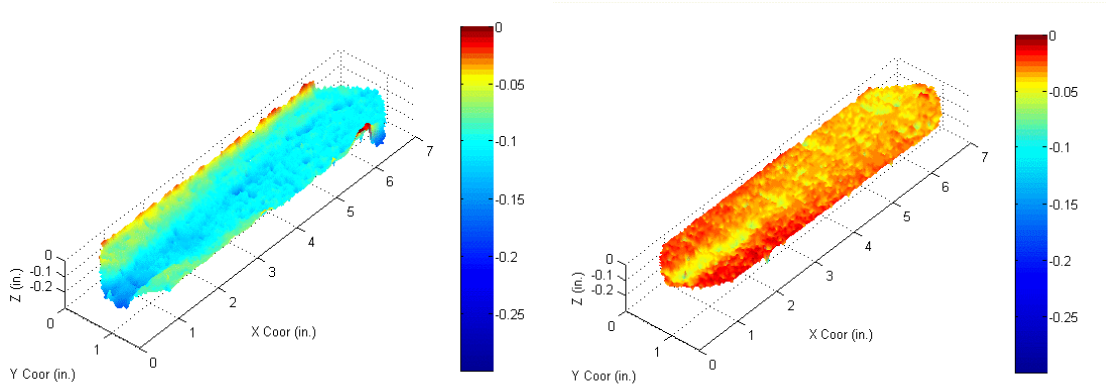

Fig. 3.65—3-D profilometer images of fracture faces for sample acidized with VES acid (left) and sample acidized with gelled acid (right) for 30 minutes.

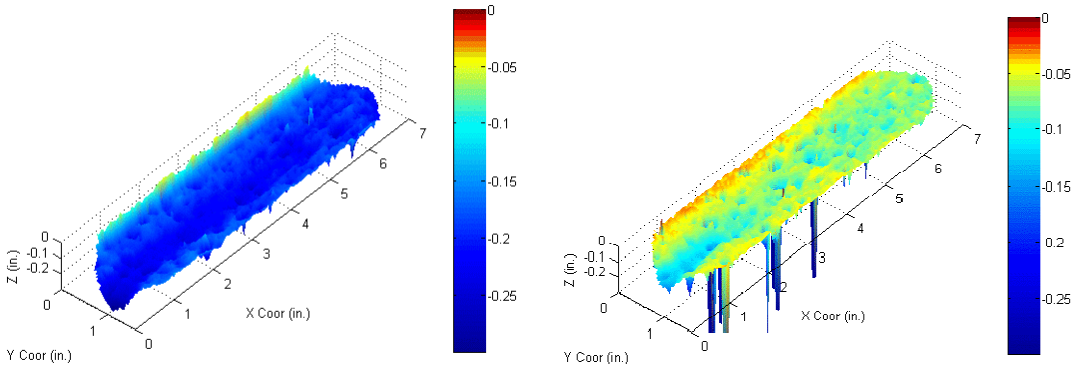

Fig. 3.66—3-D profilometer images of fracture faces for sample acidized with VES acid (left) and sample acidized with gelled acid (right) for 60 minutes.

It is also interesting to note that fracture closure occurs between 4,000 to 5,000 psi for most experiments with the exception of samples acidized with emulsified acid at contact time of 60 minutes which closed at the low closure stress of 1,000 psi. The sample acidized with emulsified acid for 60 minutes had S_{RE} after acidizing below 20,000 psi while all others were above 20,000 psi. Furthermore, the etching pattern (see **Fig. 3.67**) shows that while there is a deep channel developed in the front section of fracture, there is almost no etching from middle to end of fracture length. While the conductivity of this fracture is very high in the front section, it is almost closed at the back section, resulting in almost no conductivity. The experimental results suggest that acidized Indiana limestone samples retain enough of their rock strength to withstand closure stresses up to 4,000 psi before the asperities holding fracture open collapse completely, resulting in fracture closure.

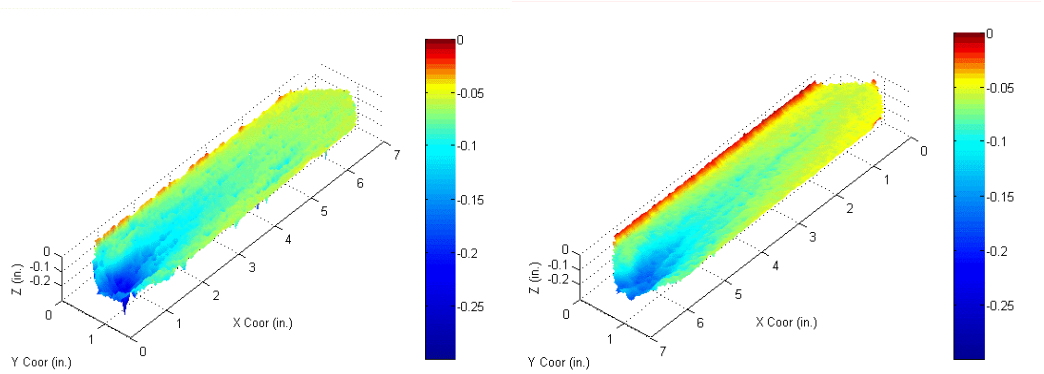

Fig. 3.67—3-D profilometer images of fracture faces for sample acidized with emulsified acid for 60 minutes.

Both emulsified and HCl acidized samples show low conductivity since etching pattern show substantial etching at front and almost no etching at end (see **Fig. 3.68**). HCl shows much more etching with a kind of irregular etching, resulting in few contact points and sections of almost no opening. On the other hand, samples acidized with emulsified acid show almost no etching for the end section of fracture, resulting in large values of contact ratio and large section with no flow capacity.

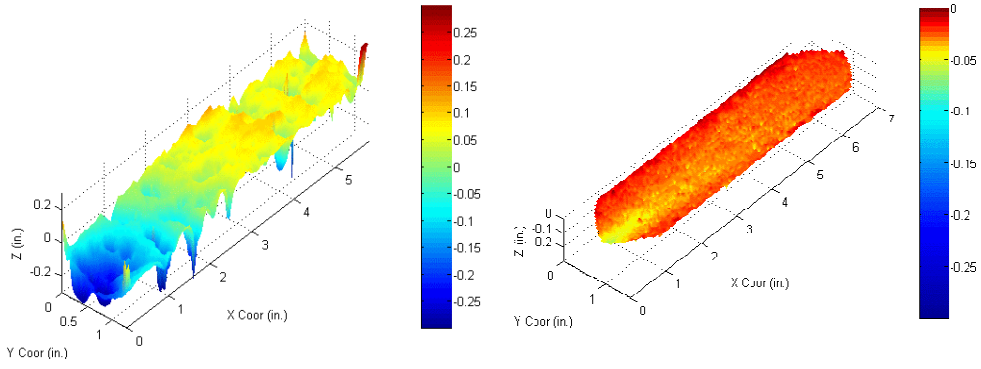

Fig. 3.68—3-D profilometer images of fracture faces for sample acidized with HCl acid (left) and with emulsified acid (right) for 15 minutes.

Experimental results recommend that it would be best to acidize Indiana limestone samples with VES acid system for relatively short contact times. Expected conductivity at closure stress of 2,000 psi for VES acidized samples at short contact times is in the range of 10,000 to 15,000 md-ft. However if Indiana limestone samples are acidized too long with VES acid system, the whole fracture face is dissolved uniformly with almost no asperities holding fracture open and also significant weakening of rock formation, resulting in low fracture conductivities. For long fractures which require to be acidized for long times, it is best to acidize with gelled acid as it results in sufficient fracture width and rough etching pattern with enough contact asperities of sufficient strength to keep the fracture open up to high closure stresses. The expected conductivity at closure stress of 2,000 psi for samples acidized with gelled acid for longer times of 30 and 60 minutes is in the range of 3,000 to 5,000 md-ft. Fracture closes between 4,000 to 5,000 psi of closure stress, regardless of contact time and acid type with the exception of emulsified acid at long contact times which weakens the rock too much, resulting in fracture closure at low stress of 2,000 psi.

A similar set of tests in terms of acid type were conducted on Texas cream chalk samples with contact times of 5, 10, and 15 minutes. However as the sample acidized with gelled acid at contact time of 15 minutes had channeling behavior, sample acidized for 20 minutes with gelled acid is compared to HCl acidized samples for 15 minutes. The conductivity data for the contact time of 5 and 15 minutes are presented in **Fig. 3.69 and Fig. 3.70**, respectively. There was limited conductivity data for sample acidized with gelled acid at 10 minutes.

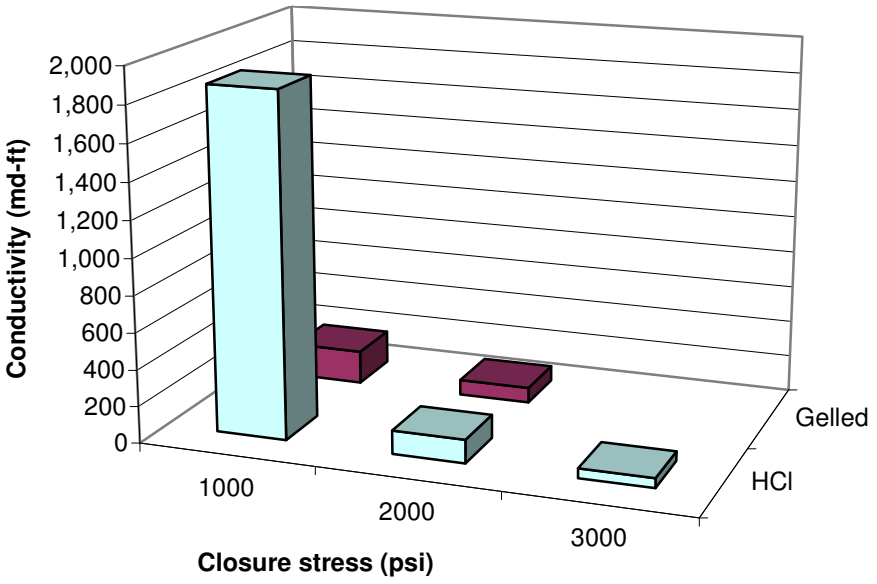

Fig. 3.69—Conductivity plot of Texas cream chalk acidized with two different acid types at 175 °F for 5 minutes.

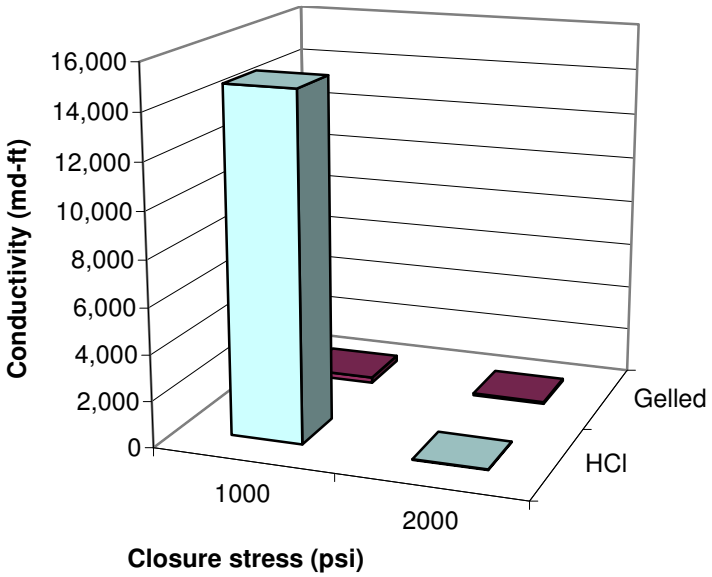

Fig. 3.70—Conductivity plot of Texas cream chalk acidized with two different acid types at 175 °F for 15 minutes.

HCl acidized samples have much higher conductivities at low closure stress of 1,000 psi, however fracture closes for both acid systems at the same closure stress which was about 2,000 psi. While HCl acidized samples had almost 5 times more average fracture width than samples acidized with gelled acid (see Fig. 3.14), gelled acidized samples had also about 5 times more contact ratio than HCl acidized sample (see Fig. 3.40). Etching pattern analysis shows that gelled acidized sample did not create much fracture width with almost no fracture opening at different areas of fracture, resulting in very low conductivity (**Fig. 3.71**). On the other hand, HCl acidized sample show considerable fracture width with few asperities to hold the fracture open, resulting in relatively high conductivity at low closure stress but a sharp drop in conductivity with higher closure stress due to limited number of asperities holding fracture. Also the HCl acidized samples had weakened the asperities to a great extent, resulting in S_{RE} values of about 20,000 psi after acidizing (see Fig. 3.50).

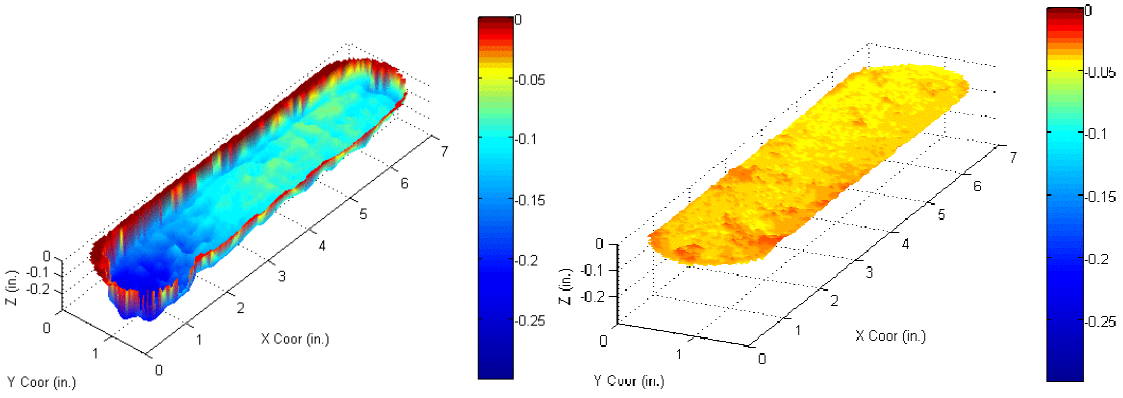

Fig. 3.71—3-D profilometer images of fracture faces for sample acidized with HCl acid (left) and sample acidized with gelled acid (right) for 5 minutes.

Experimental results suggest that straight HCl is a more appropriate acid system to use for Texas cream chalk samples as compared to gelled acid. There might be as high as 15,000 md-ft of retained conductivity with HCl acidizing at closure stresses below 1,000 psi. There is no considerable fracture conductivity at closure stresses above 2,000 psi regardless of acid type or contact time.

The last set for comparison are Macae limestone samples acidized with VES acid, gelled acid, emulsified acid, and straight HCl. There are two different permeability cores: 175 mD (medium permeability) and 350 mD (high permeability) as shown in **Fig. 3.72 and Fig. 3.73**, respectively. There was not enough conductivity data for the low permeability cores of 1 md. While only the 175 mD core was acidized with emulsified acid, there was no accurate conductivity measurement for VES acidized sample of 175 mD. While gelled and emulsified acid resulted in similar and much higher conductivities than HCl acidized samples of 175 mD permeability, VES acidized samples had larger conductivities than HCl and gelled acidized samples of 350 mD permeability.

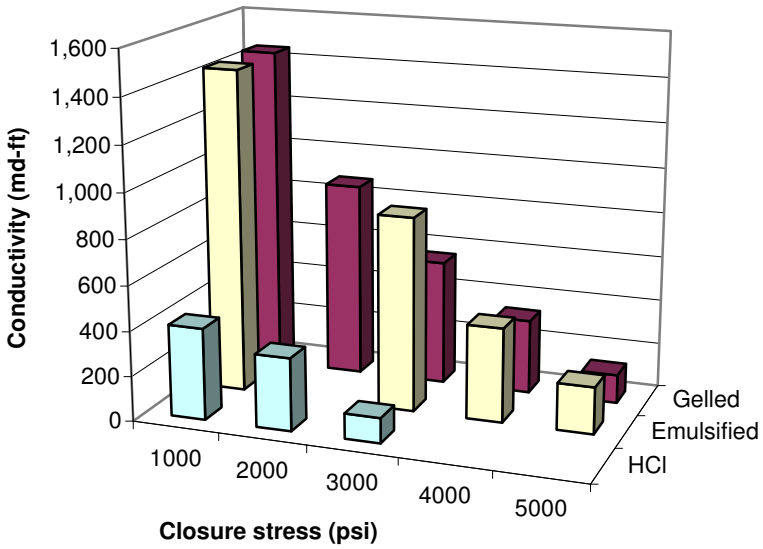

Fig. 3.72—Conductivity plot of Macae limestone samples of 175 mD permeability acidized with three acid types.

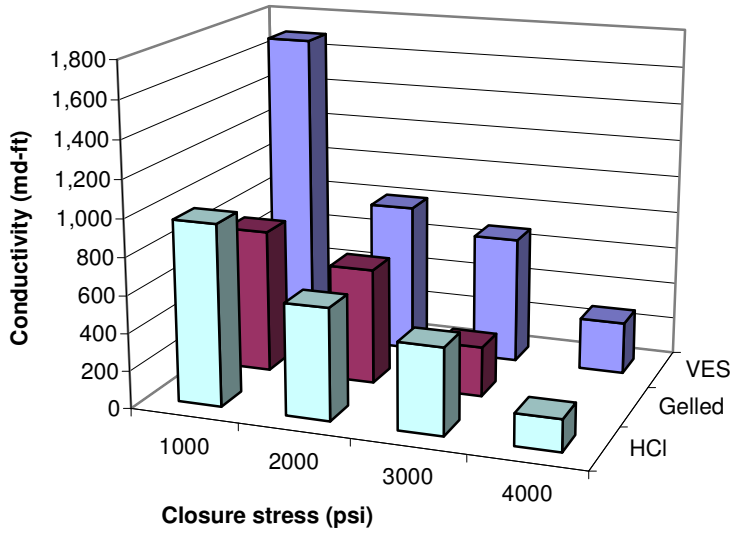

Fig. 3.73—Conductivity plot of Macae limestone samples of 350 mD permeability acidized with three acid types.

While gelled acidized sample of 175 mD permeability has high conductivity due to larger fracture width created with relatively few contact points (similar to HCl acidized sample), sample acidized with emulsified acid has high conductivity due to substantial amount of contact points keeping the fracture width which is small (even smaller than HCl acidized sample) open for flow (**Fig. 3.74**). Also as the emulsified acid has almost 5 times the contact ratio as gelled acid, it retains conductivity better than gelled acid with increasing closure stress, resulting in larger conductivities at higher closure stresses. Even though the fracture width created by HCl acid is more than that of sample acidized with emulsified acid, the etched pattern shows similar irregular pattern of etching as was observed on Indiana limestone samples by HCl acidizing (**Fig. 3.75**). This irregular etching with lots of ups and down results in large areas with almost no etching and hence no conductivity. Rock strength measurements showed similar values of S_{RE} after acidizing and amount of rock weakening as was shown in Fig. 3.56.

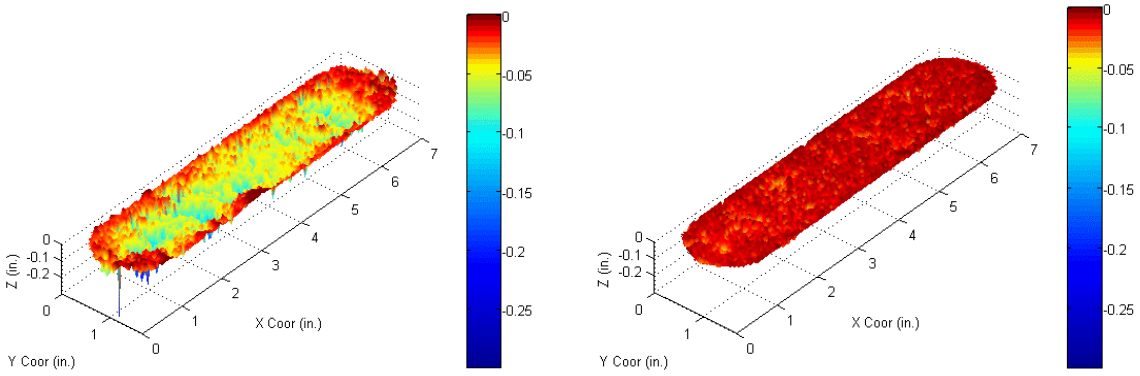

Fig. 3.74—3-D profilometer images of fracture faces for sample acidized with gelled acid (left) and sample acidized with emulsified acid (right) for 175 mD cores.

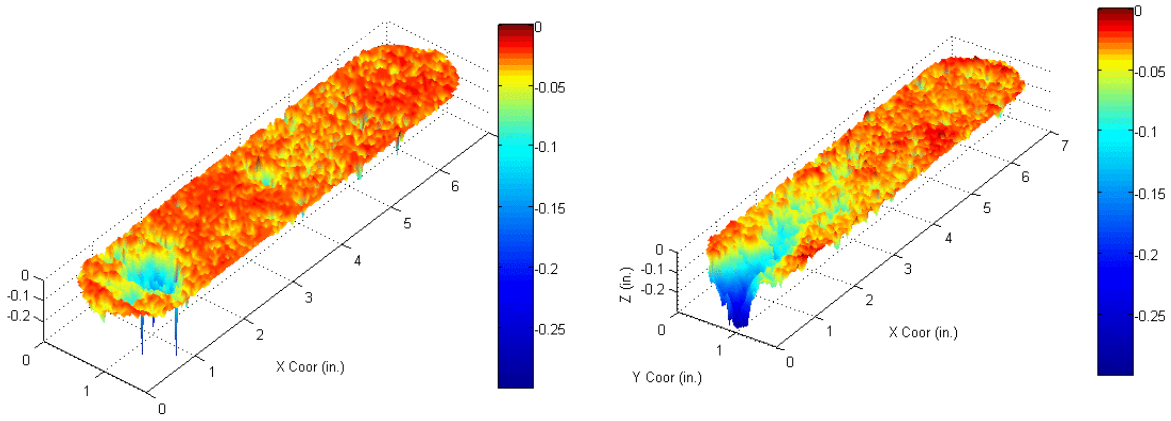

Fig. 3.75—3-D profilometer images of fracture faces for sample acidized with HCl for 175 mD cores.

Samples with 350 mD permeability had much higher conductivities when acidized with VES acid system as it created much larger fracture width than other acid systems with greater roughness and etching across most of fracture face. Etching pattern of samples acidized with gelled acid and HCl were similar with a channel at the entrance of fracture and almost no etching near the end of fracture length (**Fig. 3.76**), hence no substantial conductivity. However as the VES acidized sample was weakened more than the other samples (see Fig. 3.56), the conductivity declined much faster with increasing closure stress, resulting in similar values of conductivity among the different acid types at higher closure stresses.

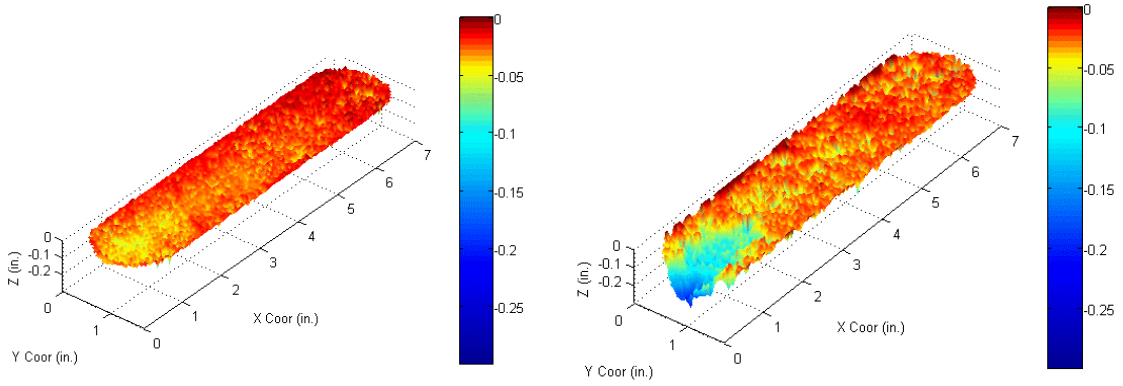

Fig. 3.76—3-D profilometer images of fracture faces for sample acidized with gelled acid (left) and with HCl acid (right) for 350 mD cores.

Experimental results suggest that the 175 mD permeability Macae limestone formation should be treated with emulsified acid as it creates a favorable etching pattern with sufficient amount of fracture width and asperities to keep fracture open while still maintaining the strength of these asperities to generate high conductivities at all different closure stresses. It would be best to treat the more permeable cores (350 md) of the same formation with VES acid system as it results in higher conductivities at low closure stresses, however the retained conductivities are similar between different acid systems at higher closure stresses due to significant amount of rock weakening with VES acid. The expected retained conductivity for both core types is only around 1,000 md-ft at closure stress of 2,000 psi. It should be noted that fracture closes between 3,000 and 4,000 psi which is between the range of fracture closure for Indiana limestone and Texas cream chalk. This is consistent with rock strength measurements which showed Macae limestone to have SRE values between those of Indiana limestone and Texas cream chalk (see Fig. 3.47).

3.5.3.2. Temperature Effect

There was only one set of experiment with Indiana limestone acidized with emulsified acid at two different temperatures of 200 and 275 ^{o}F that shows the effect of temperature (**Fig. 3.77 and Fig. 3.78**). Results clearly show that there is an increase in conductivity with temperature and also fracture closure occurs at higher closure stress with increasing temperature.

Fracture width results clearly showed significant increase with temperature (Figure 3.16), while amount of contact points was significantly reduced (Fig. 3.33). The etching pattern analysis shows that at the higher temperature of 275 ^{o}F, a deep etched channel formed along most of fracture length with adequate amount of asperities around it to keep the channel open while there was almost no etching at the end section of fracture length when acidized at the lower temperature of 200 ^{o}F (**Fig. 3.79**). Rock strength measurements also showed similar values of S_{RE} after acidized at the different temperatures (see Fig. 3.52). As a result, larger fracture widths created at higher temperature resulted in higher retained conductivity as all the acidized samples had similar rock strengths.

Results suggest that it might be beneficial to inject heated emulsified acid at high temperatures in order to create more conductive fractures without significantly weakening the rock formation. The expected retained conductivity with emulsified acid at higher temperature of 275 ^{o}F is about 2,000 md-ft at closure stress of 2,000 psi. This outcome may not be true for other acid systems and other rock formations due to different acid properties, rock-acid interactions and rock weakening.

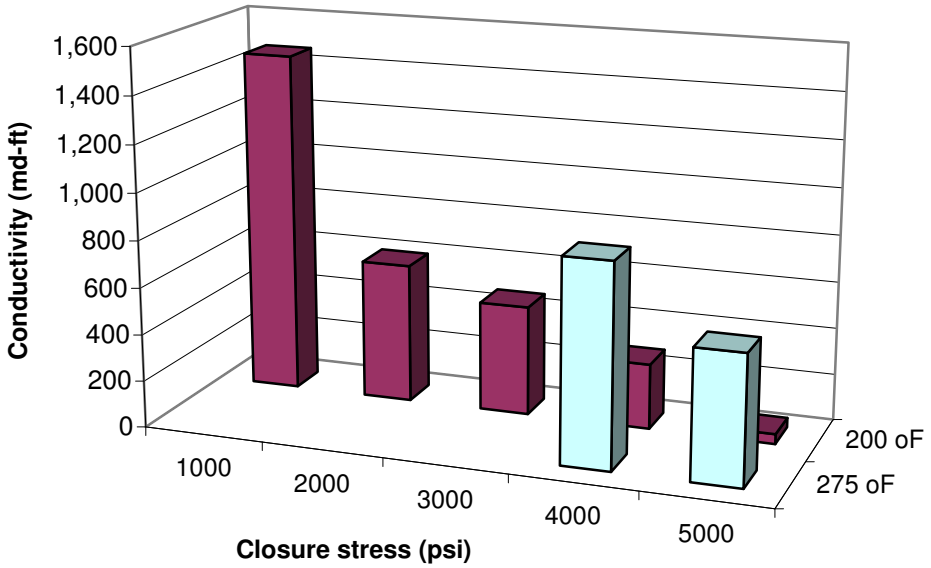

Fig. 3.77—Conductivity plot at two different temperatures for Indiana limestone samples acidized for 15 minutes.

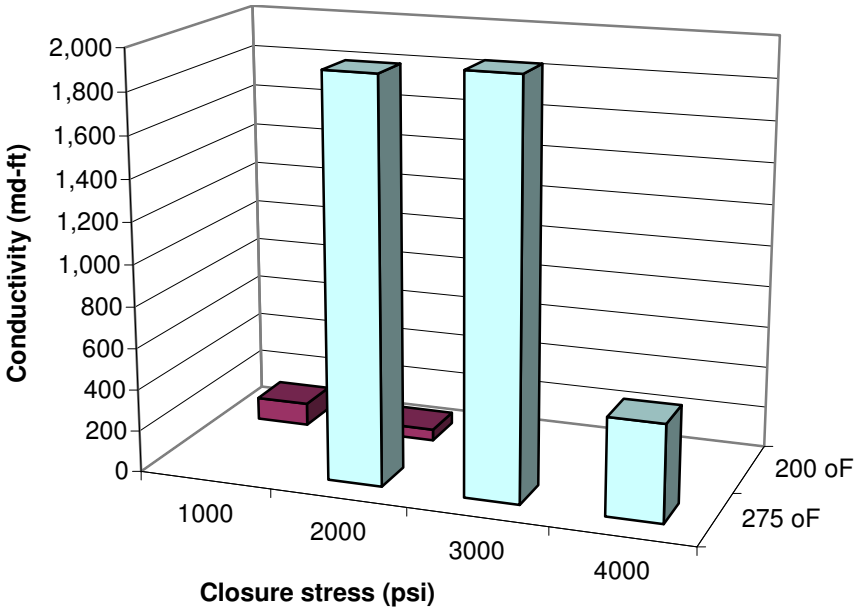

Fig. 3.78—Conductivity plot at two different temperatures for Indiana limestone samples acidized for 60 minutes.

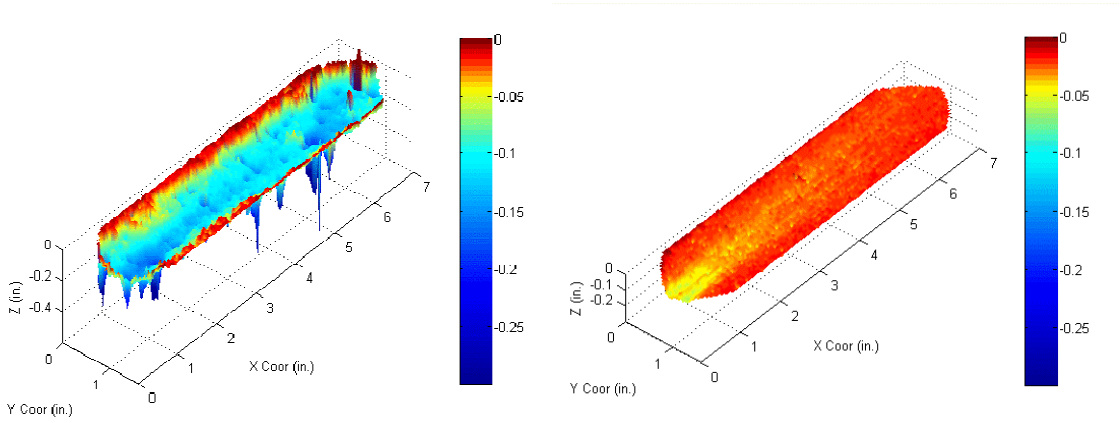

Fig. 3.79—3-D profilometer images of fracture faces for sample acidized with emulsified acid at 275 °F (left) and 200 °F (right) for 15 minutes of contact time.

3.5.3.3. Contact Time Effect

There are six different experimental sets that can be analyzed for the effect of contact time on fracture conductivity. The first four sets are Indiana limestone samples acidized with different acid systems. The conductivity plot versus closure stress for these four sets which were acidized with VES acid system, emulsified acid, gelled acid, and HCl are shown in **Figs. 3.80 through 3.83**, respectively. There is no observable trend of conductivity with contact time. There is no tendency of increased conductivity at low closure stress with increasing contact time as expected from Nierode and Kruk correlation even though all tests showed increased fracture width with contact time. There seems to be an optimum contact time for each acid system and rock type that results in maximum fracture conductivity.

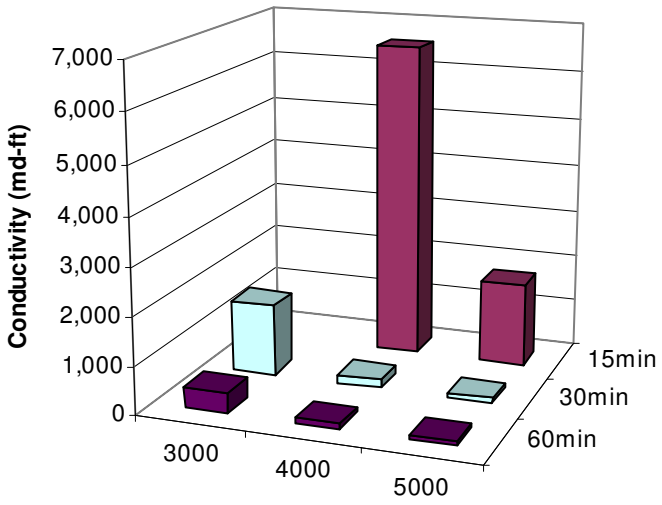

Fig. 3.80—Conductivity plot at three different contact times for Indiana limestone samples acidized with VES acid system.

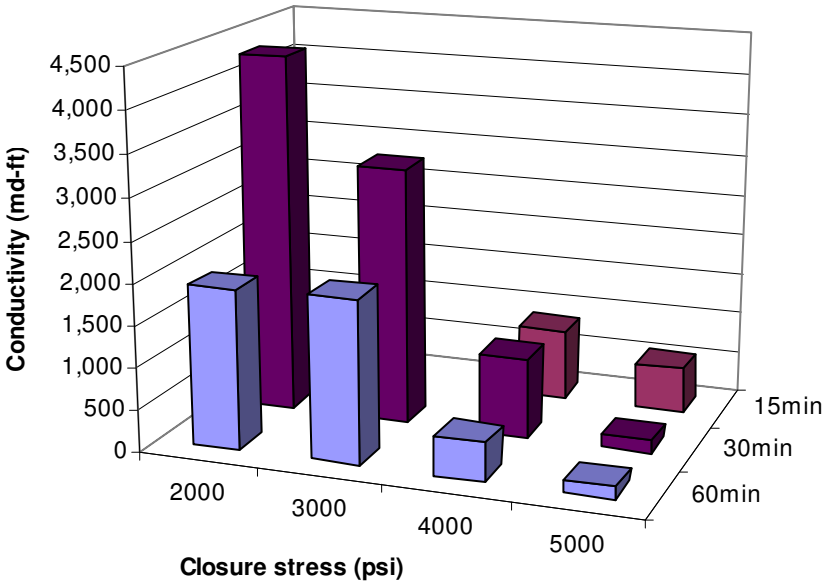

Fig. 3.81—Conductivity plot at three different contact times for Indiana limestone samples acidized with emulsified acid at 275 °F.

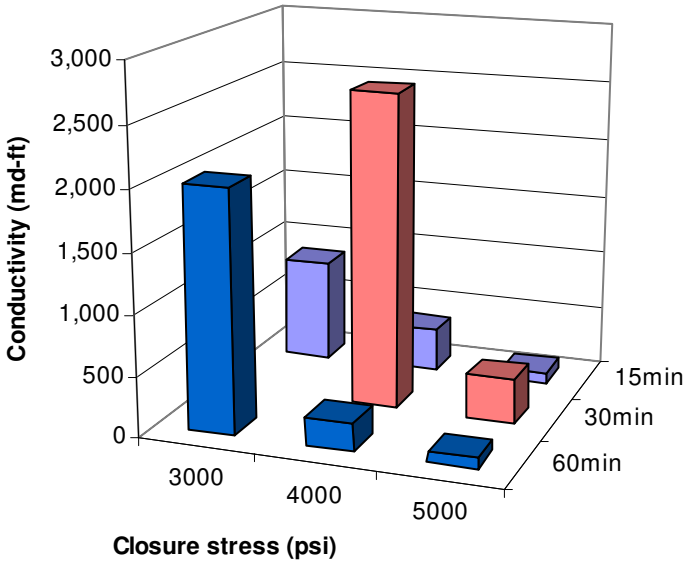

Fig. 3.82—Conductivity plot at three different contact times for Indiana limestone samples acidized with gelled acid.

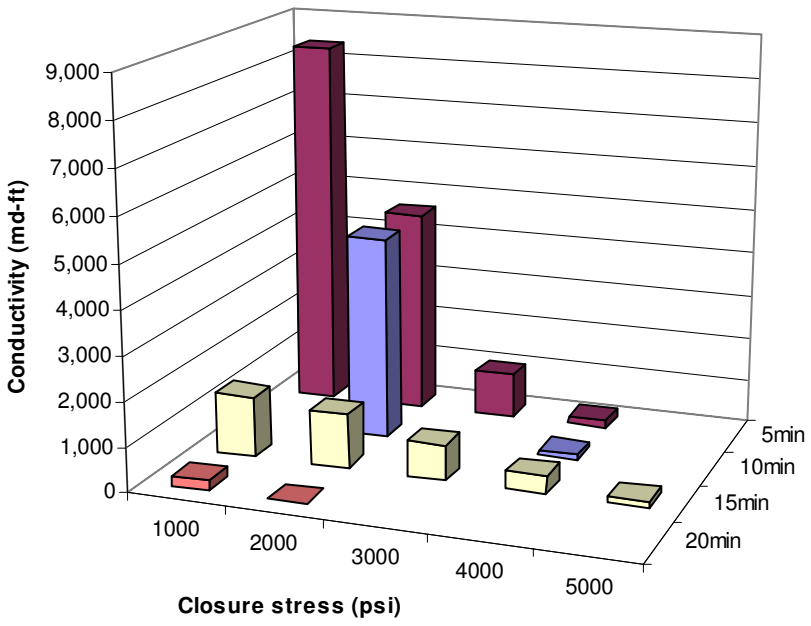

Fig. 3.83—Conductivity plot at four different contact times for Indiana limestone samples acidized with HCl acid.

Samples acidized with VES acid and straight HCl show higher conductivity at the shortest contact time. The samples acidized for the shortest contact time have the highest amount of asperities holding the fracture open even though they have less fracture width. There was a sharp decline in contact ratio with increasing contact time (see Fig. 3.30). Etched profiles for both VES and HCl acidized samples (**Fig. 3.84** and **Fig. 3.85**, respectively) show that while there is enough etched width created at the shortest contact time with significant number of asperities holding fracture open, there is too much etching with uniform etching pattern and few asperities holding fracture open at longer contact times. Also as the rock strength was reduced significantly with increasing contact time for VES and HCl acidized samples (see Fig. 3.50), the greater number of asperities holding the fracture open for samples acidized for the shortest contact time are stronger to withstand the closure stress and hence result in higher conductivities even at high closure stresses. The samples acidized with emulsified acid might be showing similar behavior as they show higher conductivities at 30 minute contact time compared to 60 minute contact time at low closure stresses.

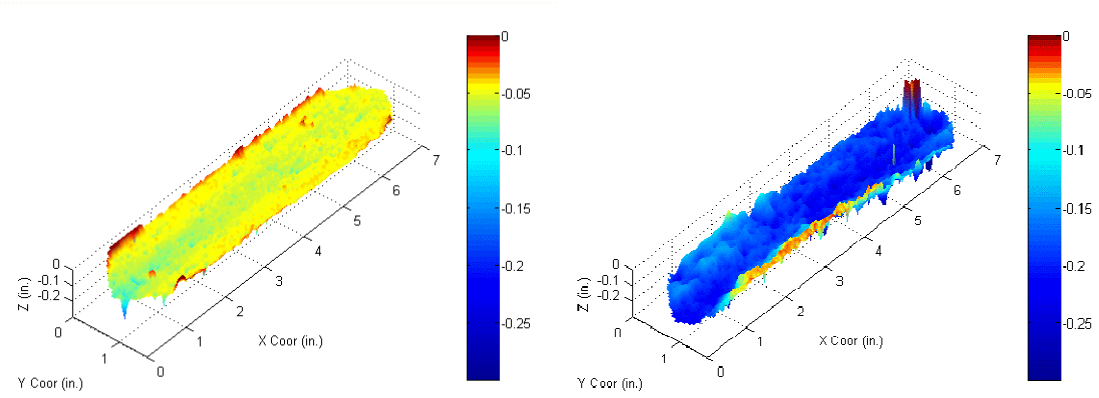

Fig. 3.84—3-D profilometer images of fracture faces for sample acidized with VES acid at 15 min (left) and 60 min (right).

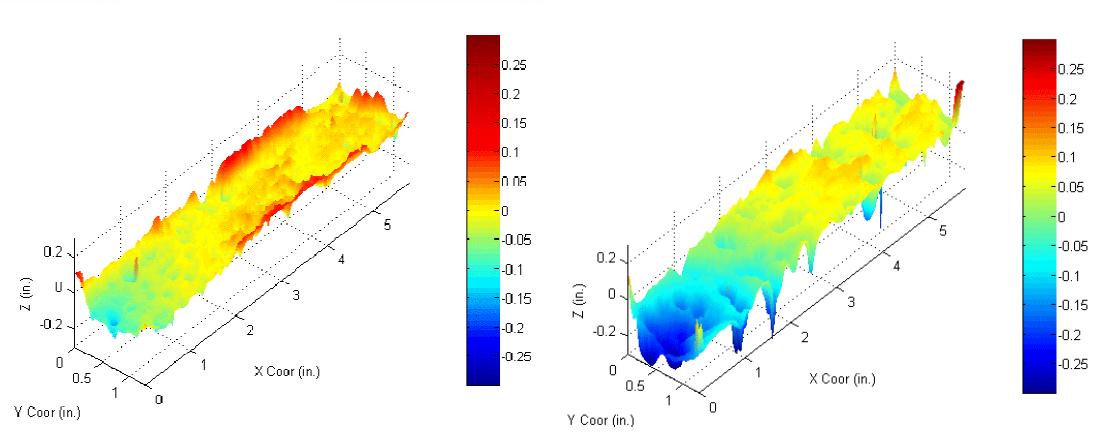

Fig. 3.85—3-D profilometer images of fracture faces for sample acidized with HCl acid at 5 min (left) and 15 min (right).

The gelled acidized samples have highest conductivity at the 30 minute contact time which is in middle of contact time range tested. While samples acidized with VES acid showed an optimum acid contact time of 15 minutes and HCl acidized samples had an optimum time of about 5 to 10 minutes, gelled acidized samples had a longer optimum contact time of 30 minutes. The change of optimal contact time depending on acid system can be well correlated to the amount of fracture face dissolution. As straight

HCl acid creates much more surface dissolution and hence fracture width compared to other acid system, short contact time of 5 to 10 minutes are enough to create enough fracture width for flow with sufficient contact areas of adequate strength to keep it open, while VES acid and emulsified acid (at 275 ^{o}F) require longer contact time of about 15 minutes to result in enough fracture width with strong and adequate asperities, resulting in maximum fracture conductivity. There is much less dissolution of Indiana limestone with gelled acid as compared to the other acid systems (see Fig. 3.18). Consequently longer contact time of 30 minute is required for gelled acid to acidize the fracture face enough to maximize resulting conductivity. It is also important to note that gelled acidized samples showed the least amount of rock weakening, which is another reason that the sample acidized at the longer contact time of 30 minute had still strong asperities to hold fracture open.

The last two sets are Texas cream chalk samples acidized with HCl and gelled acid as shown in **Fig. 3.86 and Fig. 3.87**, respectively. There was a tendency of increasing conductivity with longer contact times. While fracture closure occurred at about the same closure stress for all different contact times for HCl acidized samples (Fig. 3.86), sample acidized with gelled acid at the longest contact time of 30 minutes retained conductivity up to higher closure stress than samples acidized at shorter times (Fig. 3.87). Similar to acidizing of Indiana limestone samples with gelled acid, gelled acid requires longer contact time to create enough fracture width to maximize fracture conductivity (see Fig. 3.15).

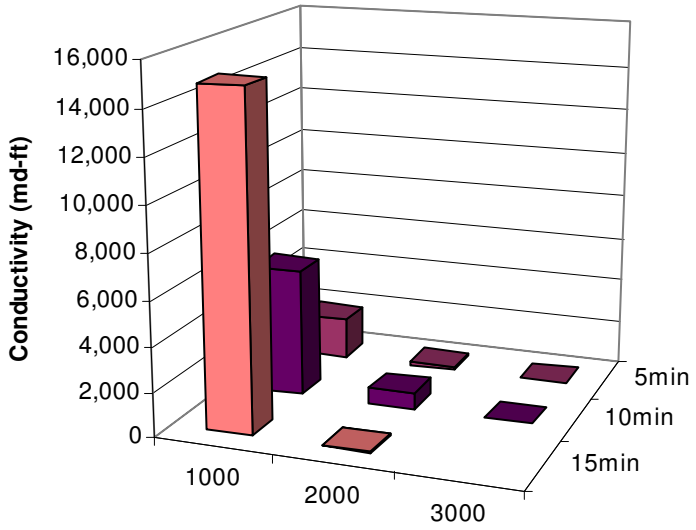

Fig. 3.86—Conductivity plot at three different contact times for Texas cream chalk samples acidized with HCl acid.

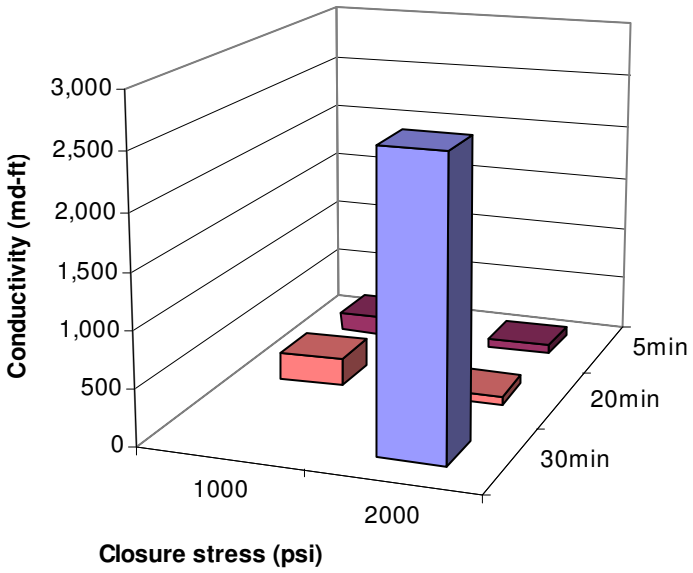

Fig. 3.87—Conductivity plot at three different contact times for Texas cream chalk samples acidized with gelled acid.

3.5.3.4. Formation Type Effect

Two different sets of experiments were acidized at the same conditions except with different rock types which can be used to analyze the effect of formation type on resulting fracture conductivity. The resulting conductivities for the two sets with one acidized for 20 minutes and the other for 30 minutes with gelled acid are shown in **Fig. 3.88 and Fig. 3.89**, respectively. Results from previous section on the effect of acid type indicated that about 30 minutes of contact is required for gelled acid to create enough fracture width to maximize resulting fracture conductivity for both Indiana limestone and Texas cream chalk. It was also observed that due to different rock strengths, fractures created on Indiana limestone closed at about 4,000 to 5,000 psi load, while Texas cream chalk fracture closed much earlier at loads between 2,000 to 3,000 psi.

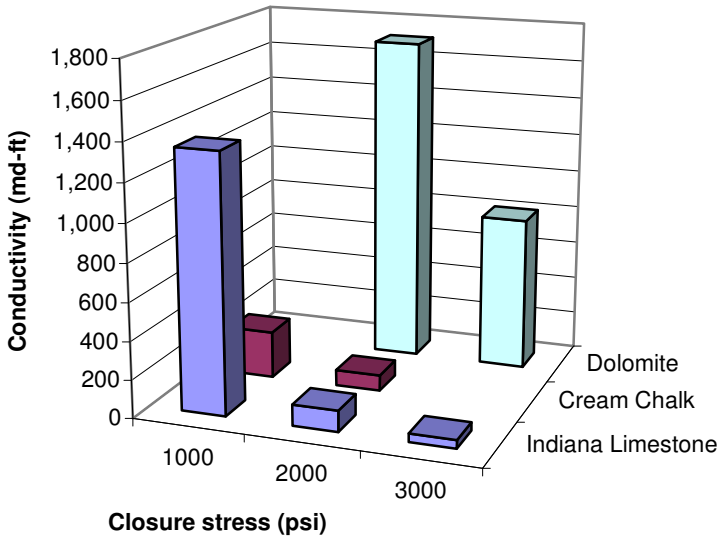

Fig. 3.88—Conductivity plot for three different formations acidized with gelled acid for 20 minutes.

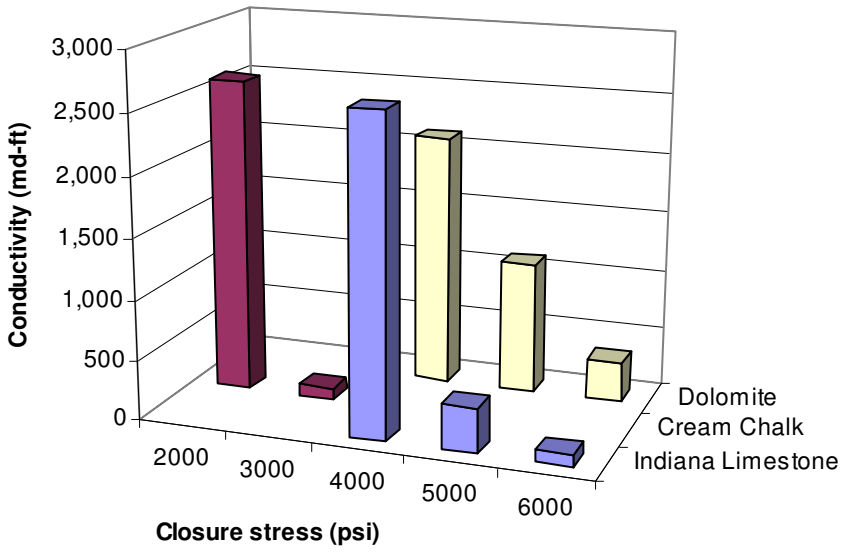

Fig. 3.89—Conductivity plot for three different formations acidized with gelled acid for 30 minutes.

Dolomite samples have the highest conductivity compared to other rock types at most closure stresses, especially at high closure stresses. Even though there is less etching and fracture width created on dolomite samples, due to the rougher etching pattern, there were considerably more distributed asperities holding the fracture open across the entire fracture length (**Fig. 3.90**). Also the asperities of dolomite are much stronger than those of other rock types (50,000 psi compared to average of 25,000 psi), allowing the fracture to withstand more closure stress before closure which was at about 6,000 psi of stress.

While gelled acid does not result in sufficient amount of etching across the entire fracture length of Indiana limestone and Texas cream chalk samples at contact time of 20 minutes, after 30 minutes of contact time, sufficient fracture width with roughness

etching pattern across the entire length of fracture is created (**Fig. 3.91**), resulting in high fracture conductivities at low closure stress. Results clearly show that conductivity is lower than that of dolomite sample even at small closure stresses for Indiana limestone and Texas cream chalk samples at contact time of 20 minutes, however conductivities of these rocks are much higher that those of dolomite with increased contact time of 30 minutes.

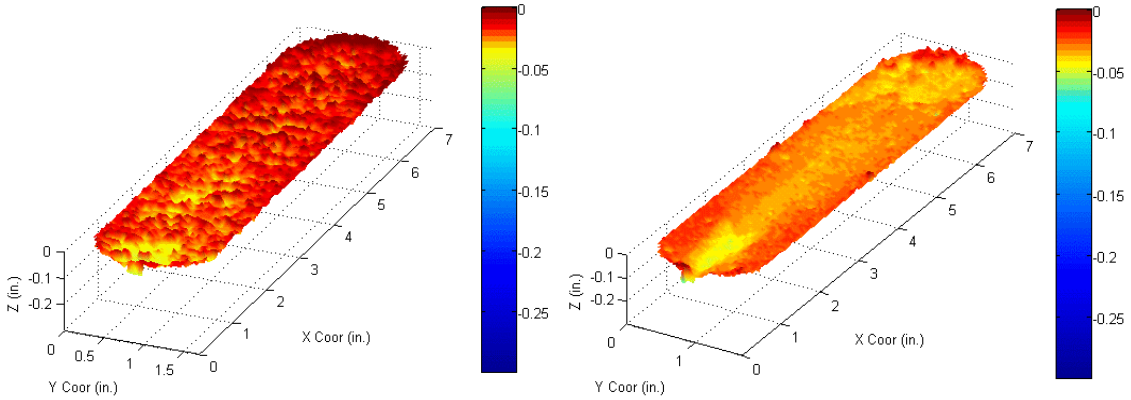

Fig. 3.90—3-D profilometer images of fracture faces for dolomite sample (left) and Texas cream chalk sample (right) acidized for 20 minutes.

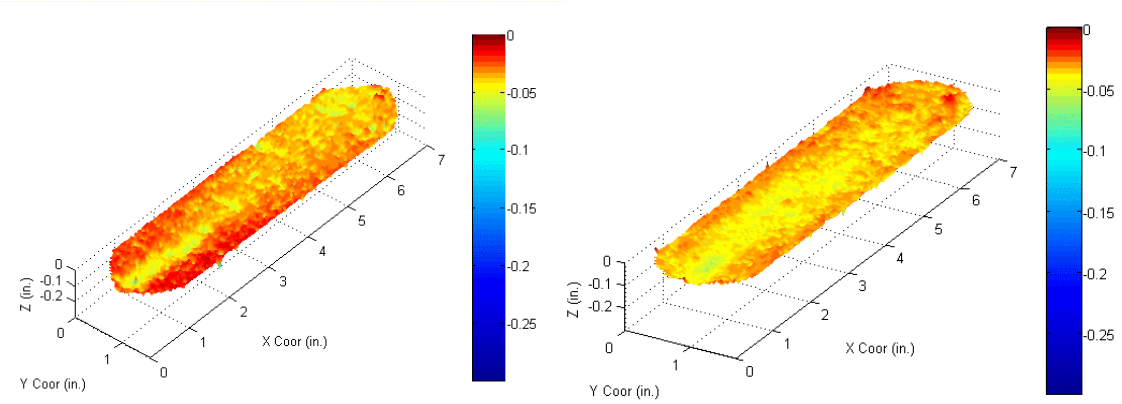

Fig. 3.91—3-D profilometer images of fracture faces for Indiana limestone sample (left) and Texas cream chalk sample (right) acidized for 30 minutes.

Clearly, formation type influences the amount of etching and etching pattern of fracture faces which in turn influences resulting fracture conductivity. Furthermore, the strength of rock formations is different and hence the rate of conductivity decline with closure stress is also different. Experimental results suggest that the stress at which fractures closes completely is around 2,000 psi, 4,000 psi and 6,000 psi for Texas cream chalk, Indiana limestone, and San Andres dolomite, respectively.

3.5.3.5. Repeatability Effect

There were several different sets of experiments repeated at exactly the same conditions in order to check on the repeatability. The plots of conductivity for the different repeat experiments are shown in **Fig. 3.92 through 3.94**. The large variation in conductivity among repeated experiments clearly shows the stochastic nature of the etching process and the difficulty in modeling resulting conductivity.

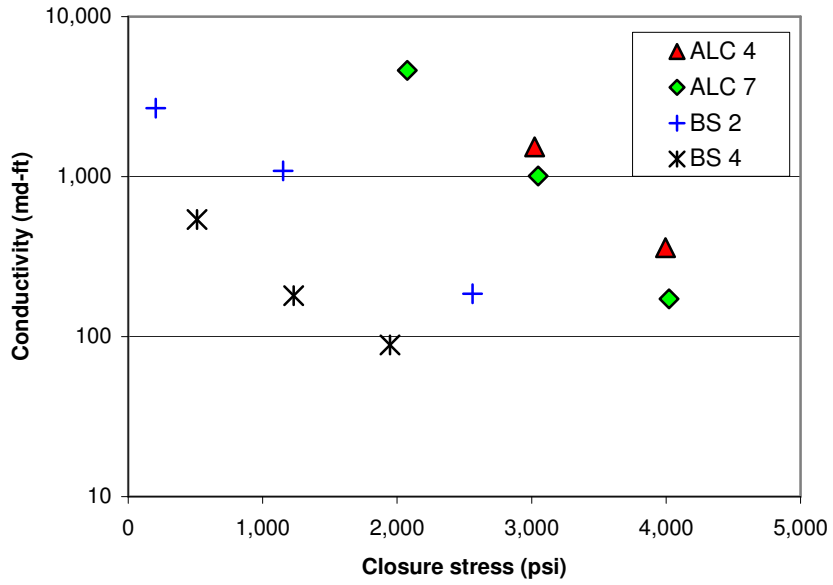

Fig. 3.92—Conductivity versus closure stress for repeated tests with Indiana limestone acidized with HCl acid at contact time of 5 minutes.

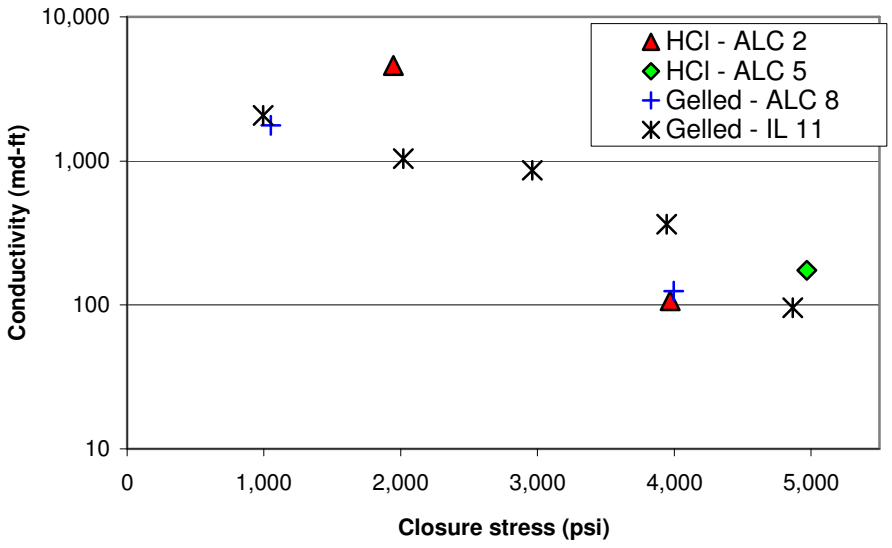

Fig. 3.93—Conductivity versus closure stress for repeated tests with Indiana limestone acidized with HCl (10 min)and gelled acid (15 min).

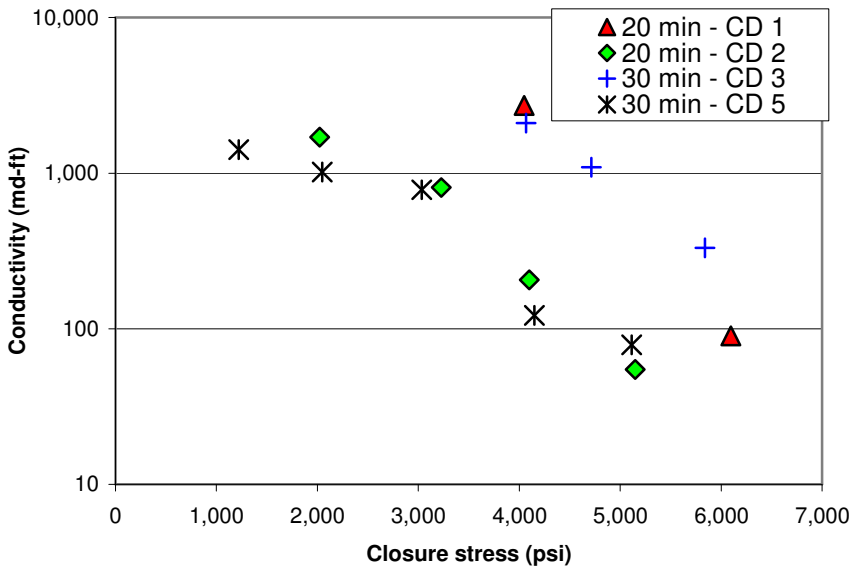

Fig. 3.94—Conductivity versus closure stress for repeated tests with San Andres dolomite acidized with gelled acid.

Majority of repeated experiments show great differences between measured conductivities with an average of one order of magnitude difference, while most repeated tests showed similar values of average fracture width. However there were some considerable differences between surface parameters. For example, ALC 2 had similar value of average fracture width but about half the contact ratio as ALC 5, which might explain that even though both had similar conductivities at lower closure stresses, ALC 2 had almost two order of magnitude less conductivity at 4,000 psi closure stress due to fracture closure as a result of lack of enough asperities to hold fracture open. The etching pattern clearly shows the difference in terms of asperities that are holding the fracture open (**Fig. 3.95**). As shown in **Fig. 3.96**, etching pattern of dolomite samples CD3 and CD5, which also showed large differences in terms of conductivity, indicates

that the rough etching pattern of CD3 with significant areas open for flow and asperities holding them open compared to rather uniform etching of CD5, resulted in much higher conductivities for CD3.

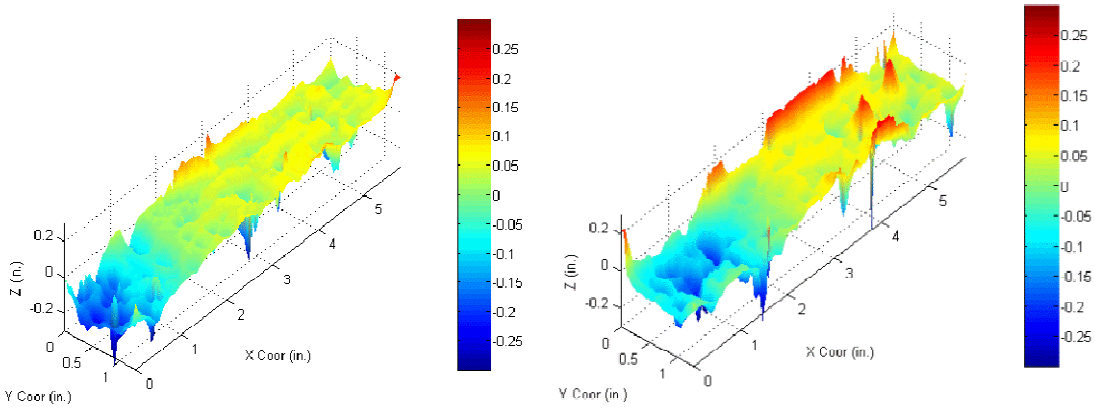

Fig. 3.95—3-D profilometer images of fracture faces for ALC 5 sample (left) and ALC 2 sample (right).

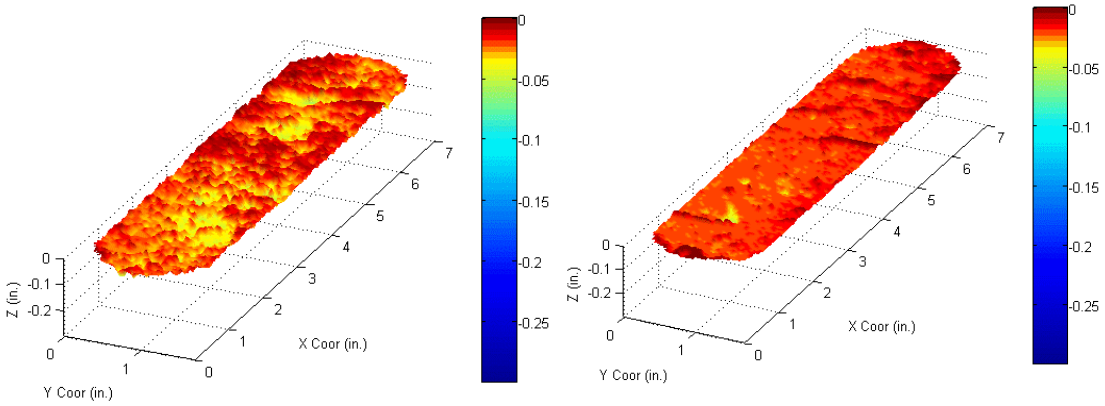

Fig. 3.96—3-D profilometer images of fracture faces for CD 3 sample (left) and CD 5 sample (right).

The reason for repeated tests that showed similar conductivities like ALC 4 and ALC 7 and also between ALC 8 and IL 11 can also be attributed to surface etching parameters and etching patterns. Even though one repeat sample had higher average fracture width than the other, it had much lower contact ratio and roughness to hold fracture open. The interaction between fracture width and contact ratio might have resulted in similar values of conductivity for these two sets of experiments. Etching pattern of ALC 4 and ALC 7 (**Fig. 3.97**) show that while ALC 4 has larger fracture width, it does not have as much asperities (lower contact ratio) to take advantage of the larger width. As ALC 7 has enough fracture width and roughness etching to have considerable conductivity, values of conductivity for ALC 4 and ALC 7 are very similar.

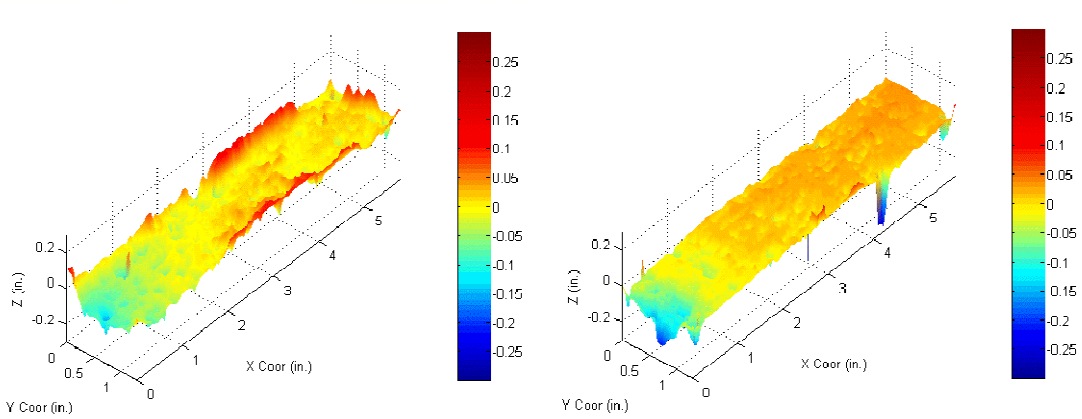

Fig. 3.97—3-D profilometer images of fracture faces for ALC 4 sample (left) and ALC 7 sample (right).

Experimental results suggest that a formation treated under the exact same condition may result in different retained conductivity due to different etching pattern

created as a result of the stochastic nature of the process. The difference between the repeated tests might also be due to some differences in core heterogeneities in terms of permeability field and mineralogy distribution, however as the samples are relatively small, there should not be much difference in permeability and/or mineralogy distribution across fracture face to cause such a significant difference in resulting conductivity. Differences in conductivity between repeated tests clearly shows the need for a conductivity model to account for etching pattern characteristics like contact ratio in addition to just average fracture width.

3.5.4. Measurement Error Bars

As there were significant differences of conductivity among majority of repeated experiments, there is no unique value of conductivity for each specific treatment and field condition. A range of possible conductivities at each specific condition should be determined rather than a specific value. In order to determine the conductivity range at each load, repeated experiments with measured conductivities under similar closure stresses were analyzed. At each load, average and standard error were calculated for each set of repeat experiments (**Table 3.6**) and plotted as shown in **Fig. 3.98**. The standard error is defined as the standard deviation divided by square root of total number of data points. The standard error describes how confident we are that the mean represents the true value and it indicates the size of uncertainty in measured values.

TABLE 3.6—ARITHMETIC AVERAGE AND STANDARD ERROR OF MEASURED CONDUCTIVITIES FOR REPEATED EXPERIMENTS

		Indiana Limestone			San Andres Dolomite	
	Average / Standard Error	Gelled at 20 min	Gelled at 30 min	HCl at 5 min	Gelled at 20 min	Gelled at 30 min
Closure stress (psi)	1000	1268 / 84				
	2000	317 / 206		2397 / 221		
	3000		1460 / 1170	852 / 447		
	4000		248 / 121	266 / 94	1467 / 1261	1110 / 988
	5000				1099 / 1044	

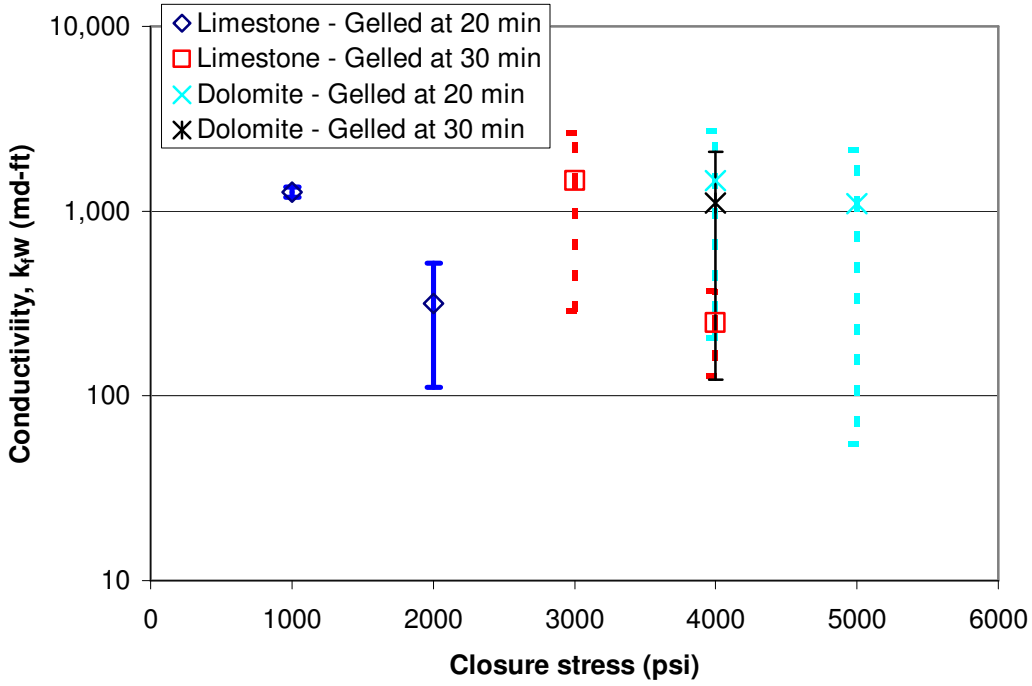

Fig. 3.98—Average conductivity values with standard error bars plotted for repeated experiments at different closure stresses.

The results show a tendency of decreasing error and more confidence in measured conductivities with increasing closure stress. There is usually little error at highest closure stresses. Also the amount of error differs among different experimental

conditions with more error for dolomite samples than limestone samples. Unfortunately, due to lack of data under same load, there is very limited information available from this analysis and we can not create a generalized error bar for conductivity measurements. However, it must be remembered that a measure value of conductivity is not an absolute value and could change up to almost one order of magnitude.

4. DEVELOPMENT OF CONDUCTIVITY CORRELATION

4.1. Approach

There are two possible methods for developing a correlation for conductivity: empirical and theoretical. Empirical method is based on experimental data which determine the important parameters and how these parameters affect the final outcome. This is a very useful methodology for processes that do not have strong theoretical basis. The current model of conductivity prediction used today in industry is an empirical model developed by Nierode and Kruk (1973) based on about 25 experiments (total of 115 data points). However such a procedure requires detailed experimental study that accounts for all important parameters influencing conductivity and ensures experiments are scaled to field conditions.

Another methodology is theoretical modeling which requires that there must be an established basis of the relationship between parameters. Such methodology was used by Gong (1997) in development of his conductivity prediction model. However, the model makes several assumptions and does not account appropriately for effect of roughness on conductivity.

As the resulting fracture conductivity from acid fracturing process depends highly on the roughness of etched fracture faces, the best method for correlation development is actually combination of an empirical method with a theoretical understanding. Theoretical understanding indicates that conductivity is influenced by parameters that determine width, roughness, closure stress and rock mechanical strength.

The approach taken here is to correlate conductivity to these parameters which were measured after acidizing in the experimental work. The correlation development will only concentrate on samples that showed roughness etchings as these are the experiments that are influenced by surface roughness. While channeling etched patterns are influenced mainly by the dimensions of channel, conductivity of uniformly etched experiments are minimal due to even etching. The turbulence and cavity etched experiments can not be correlated as they depend on turbulent flow which is difficult to analyze.

As conductivity changes with closure stress and all the surface parameters and rock strength measurements were taken before any load is placed on the fracture, it is best to correlate the initial conductivity under no closure stress to surface parameters. However as we do not have values of conductivity at zero closure stress, these must be estimated with models that predict the behavior of conductivity with closure stress. The change in conductivity with closure stress can then be related to initial surface parameters, rock strength and closure stress.

4.2. General Pattern of Conductivity

There are three main different models that describe the effect of closure stress on fracture conductivity. Two of these models have theoretical basis while one (Nierode and Kruk) is based on empirical correlation of experimental data. The three different models are:

1) Nierode and Kruk (N-K) (1973):

$$k_f w = C_1 \exp(-C_2 \sigma_c), \quad \text{..... (4.1)}$$

2) Gangi (1978):

$$\left(k_f w\right)^{1/3} = C_1 - C_2\left(\sigma_c\right)^{C_3}, \quad \text{..... (4.2)}$$

3) Walsh (1981):

$$\left(k_f w\right)^{1/3} = C_1 - C_2 \ln\left(\sigma_c\right), \quad \text{..... (4.3)}$$

where C_1 is the conductivity at zero closure stress (intercept), C_2 is the rate of conductivity change with closure stress (slope), while C_3 for the Gangi model is the exponent of closure stress which depends on distribution of surface asperities. The experimental data are fitted to these models with the constants determined for each experiment from regression analysis as summarized in **Table 4.1**. There were 15 experiments that showed roughness experiments with enough conductivity data points for analyze. There are about 60 conductivity values from these 15 experiments. The C_3 parameter in Gangi model was about 0.25 for most experiments and Gangi (1978) recommends similar value to be used. Hence, the value of C_3 parameter was fixed at 0.25 for all experiments.

TABLE 4.1—INTERCEPT (C_1) AND SLOPE (C_2) VALUES BASED ON THREE DIFFERENT MODELS

				Intercept, C_1 (md-ft)			Slope, C_2 (md-ft/psi)		
Label	**Rock type**	**Acid type**	**Time (min)**	**Gangi**	**Walsh**	**N-K**	**Gangi**	**Walsh**	**N-K**
IL 9	Indiana Limestone	Emulsified	15	26,003	124,452	3,297	3.05	5.39	0.0006
IL 11		Gelled	15	18,218	56,728	3,728	2.42	3.72	0.0006
IL 14			30	60,458	295,351	9,005	3.87	7.01	0.0007
IL 15			30	32,235	34,104	5,585	3.39	3.48	0.0010
ALC 8			15	40,913	118,035	4,549	3.93	5.31	0.0009
CD 1	San Andres Dolomite	Gelled	20	365,389	2,490,474	2,813,751	7.21	14.64	0.0017
CD 2			20	79,371	445,243	13,424	4.62	8.46	0.0010
CD 3			30	25,108	3,241,063	153,406	2.29	16.27	0.0011
CD 5			30	11,897	55,322	2,314	1.96	3.78	0.0004
PBC 11	Macae Limestone	Gelled	30	9,636	33,607	2,316	1.76	3.02	0.0005
PBC 15			20	6,839	24,294	1,419	1.66	2.78	0.0005
PBC 3		HCl	30	70,005	273,440	8,277	5.04	7.53	0.0014
PBC 7			20	72,601	104,540	3,693	4.73	4.90	0.0007
PBC 9		VES	20	20,937	88,158	3,130	2.64	4.58	0.0005
PBC 13		Emulsified	30	10,297	34,631	2,420	1.85	3.08	0.0005

The plot of calculated conductivity versus measured conductivity at all different closure stresses are shown for Nierode and Kruk, Gangi, and Walsh model in **Fig. 4.1, Fig. 4.2, Fig. 4.3**, respectively. The plots clearly show that all the models can represent the changing conductivity with closure stress with appropriate values of C_1 and C_2. It is interesting to note that while Walsh model predicts largest values of conductivity at zero closure stress, Nierode and Kruk model estimates the lowest conductivity. The values estimated by Nierode and Kruk and Gangi model are more in accordance with previous measured conductivities at zero closure stress. Both Gong (1997) and Nierode and Kruk (1973) experiments had an average of 50,000 md-ft and median of 5,000 md-ft for

conductivities under no load. Both Gangi and Nierode and Kruk model have similar average and median values while Walsh model estimates values that are one order of magnitude larger than previous experimental studies (see **Table 4.2**). Furthermore, as the total error between measured and predicted conductivities is the least for Nierode and Kruk model, it is used as the basis for correlation development.

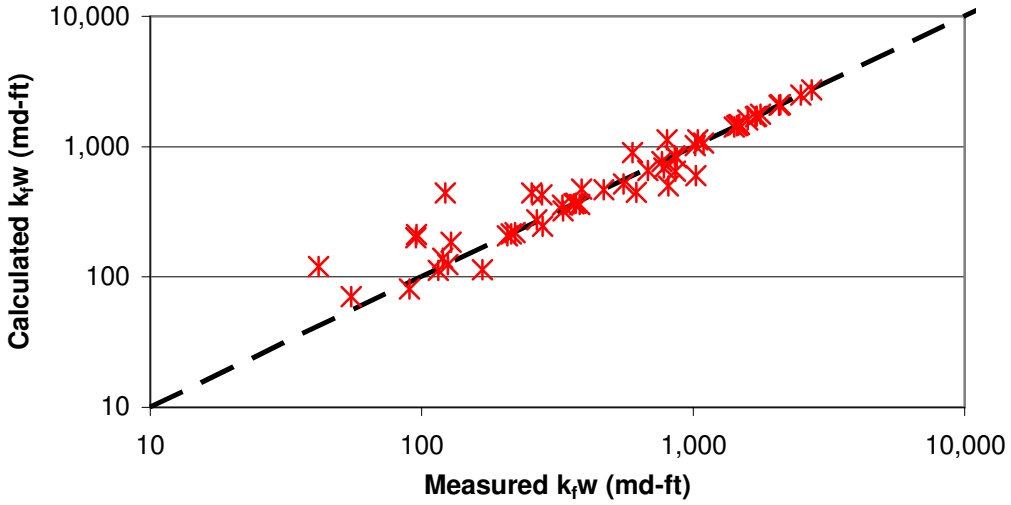

Fig. 4.1—Comparison of measured and calculated conductivity for Nierode and Kruk model.

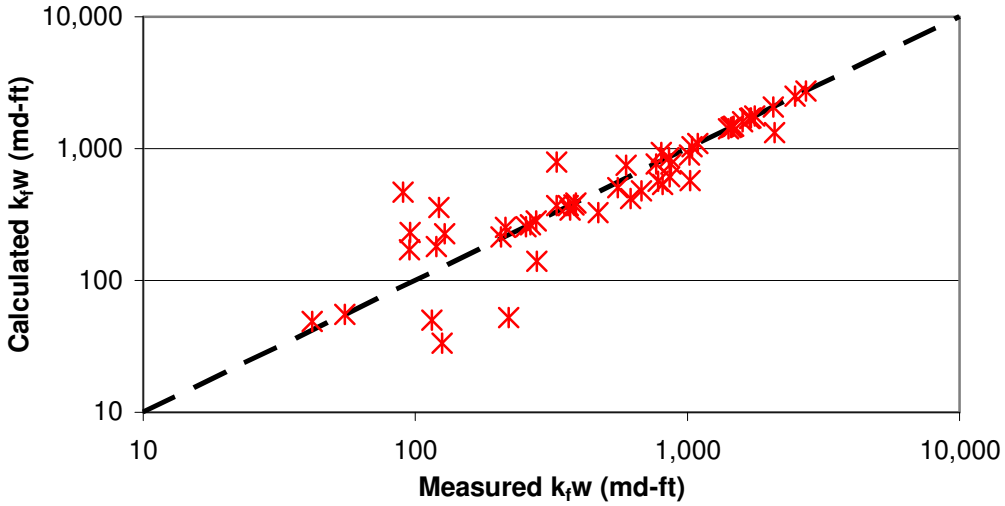

Fig. 4.2—Comparison of measured and calculated conductivity for Gangi Model.

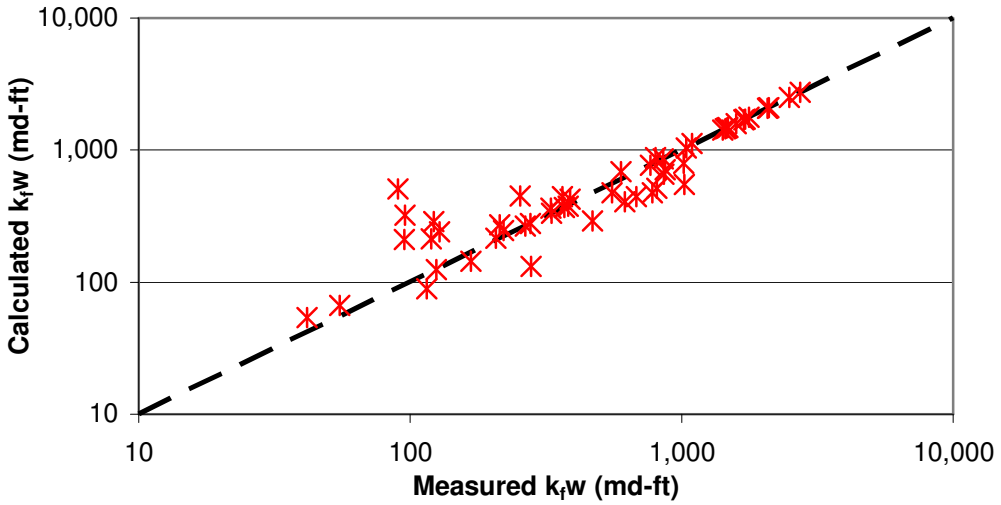

Fig. 4.3—Comparison of measured and calculated conductivity for Walsh model.

TABLE 4.2—STATISTICAL PARAMETERS OF CONDUCTIVITY AT ZERO CLOSURE STRESS PREDICTIONS FOR THE THREE DIFFERENT MODELS

	Gangi	Walsh	N-K
Median	26,003	104,540	3,728
Average	56,661	494,629	202,021
Total Error	5,379	5,908	3,435
SSE	1.7E+06	3.1E+06	7.7E+05
R^2	0.93	0.96	0.97

4.2.1. Rate of Conductivity Decline with Closure Stress (Slope)

The rate of change of conductivity with closure stress (slope, C_2 parameter in above section) should be mainly the function of rock strength that is withstanding the stress and also it might be the function of some surface parameters that describe the surface asperities that are holding the fracture open. The values of slope from Nierode and Kruk model predictions are very similar for each rock type, regardless of acid type, contact time or temperature (see **Fig. 4.4**, **Fig. 4.5**, and **Fig. 4.6**). The rate of conductivity change with closure stress seems to be only function of rock type with almost no influence of etching parameters. All Indiana limestone samples show very similar slopes around 0.0008, while all Macae limestone samples except one sample (PBC 3) show almost exactly the same slope of 0.0005. However dolomite samples show a much more scattered slopes ranging from 0.0008 to 0.0017 with two out of four samples having much different slopes.

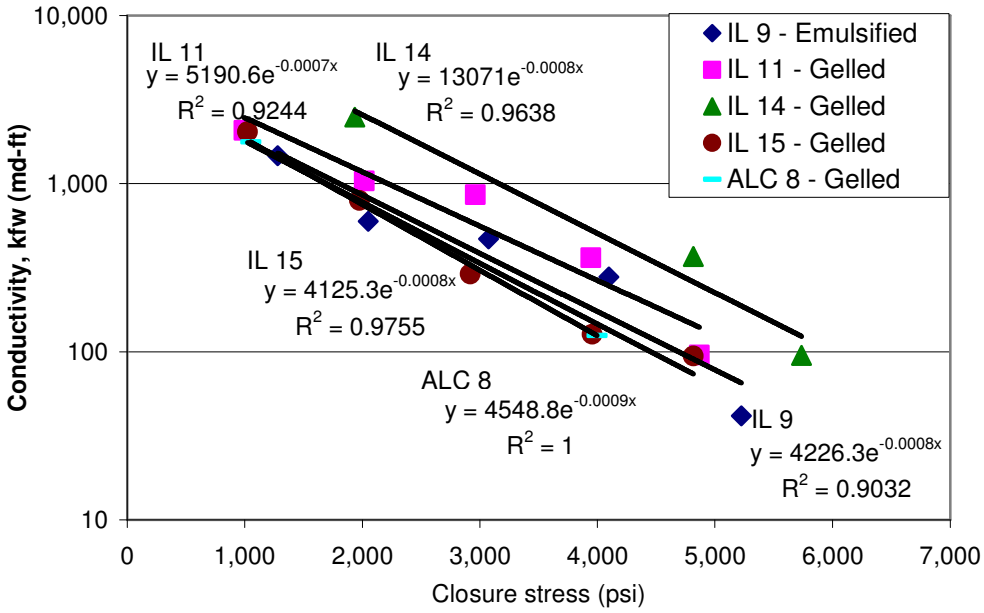

Fig. 4.4—Conductivity versus closure stress plot for Indiana limestone samples with best fit exponential trend line.

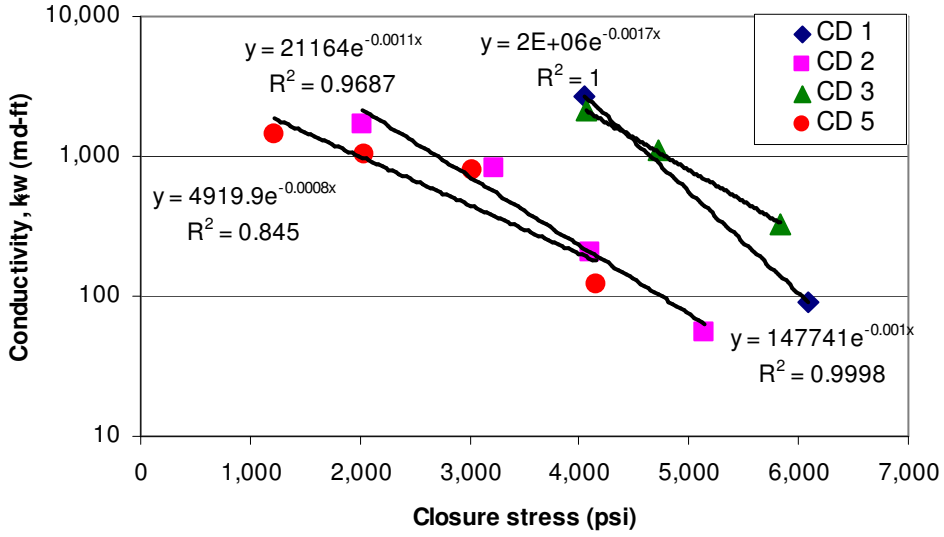

Fig. 4.5—Conductivity versus closure stress plot for San Andres dolomite samples with best fit exponential trend line.

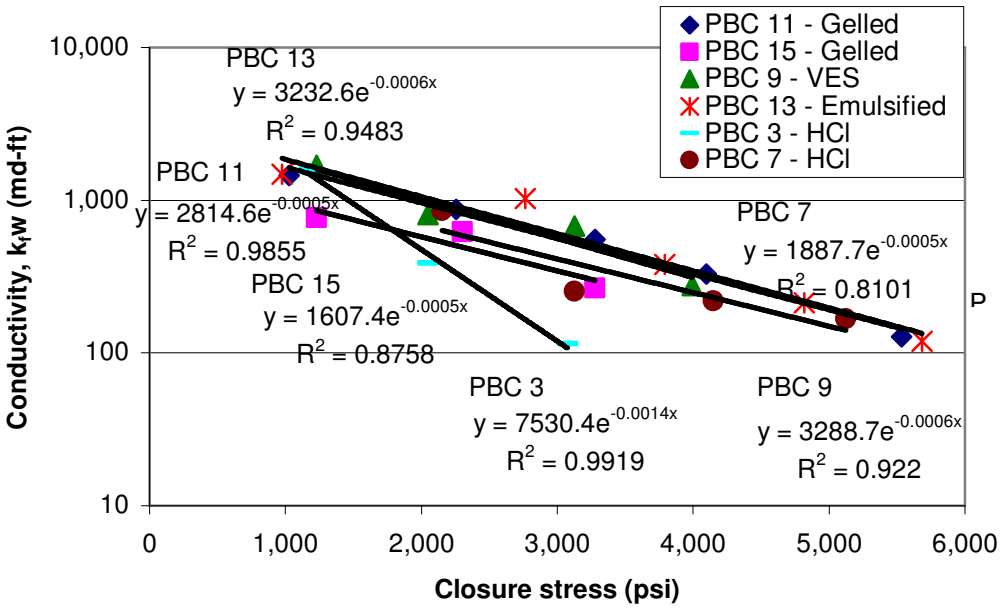

Fig. 4.6—Conductivity versus closure stress plot for Macae limestone samples with best fit exponential trend line.

As the slopes are almost the same for each rock type regardless of acid type or contact time, a fixed slope for each rock type is selected based on averaging of slopes. The fixed slopes are 0.0007, 0.0010, and 0.0005 for Indiana limestone, San Andres dolomite, and Macae limestone, respectively. The prediction of conductivity based on these fixed slope values is compared to estimation based on actual best fit slope values as shown in **Fig. 4.7**, which shows that fixing the slope does not result in significantly greater error in conductivity estimation. The total error in conductivity estimation doubled to about 7,411 md-ft for fixed slope case compared to about 3,435 md-ft with best fit slope case.

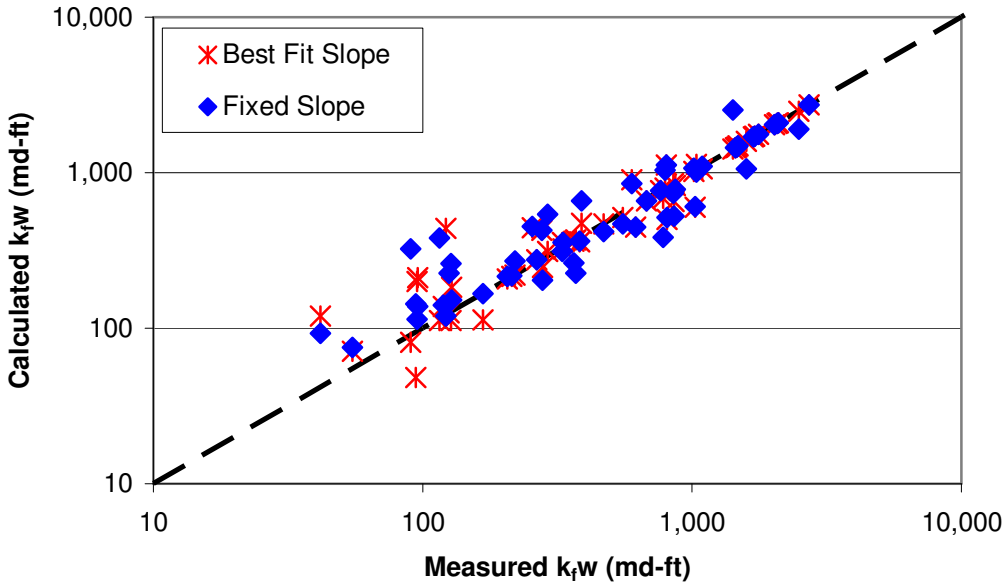

Fig. 4.7— Comparison of measured and calculated conductivity for models based on best fit slope and fixed slope.

As the slopes are based on only rock type, the slopes are correlated to average rock embedment strength values for each rock type. The best correlation is based on logarithmic function which is the same as Nierode and Kruk model, resulting in the following function for slope, C_2:

$$C_2 = -0.0063 + 0.0007 \ln(S_{RE}), \quad \text{..... (4.4)}$$

While there is great match between measured and predicted slope from above function, the correlation is based on only 3 data points which makes it relatively weak (see **Fig. 4.8**). However the logarithmic function provides much better match between rock embedment strength and slope as compared to other functional relationships.

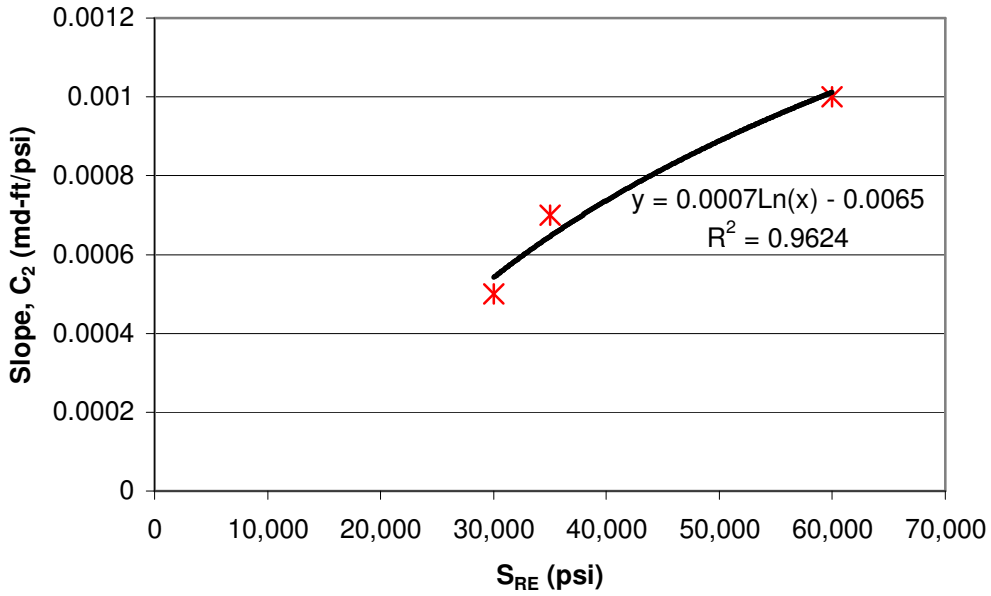

Fig. 4.8— Prediction of slope based on rock embedment strength.

However, there are major shortcomings with the relationship between rock embedment strength and slope. First of all, as it was shown in previous section, there are significant errors in actual rock embedment strength measurements and also a rather unpredictable change of conductivity with acid fracturing process. More importantly, the new correlation implies that the decline of conductivity with closure stress will be greater with increasing rock embedment strength as the slope increases with S_{RE}. Theoretically, fracture with stronger asperities should be able to maintain conductivity better and hence conductivity should decline less with closure stress as compared to a fracture with much weaker asperities. However, the rock embedment strength measurement may not be representative of actual strength of asperities as it is measured before acidizing all over the fracture face. Also etching parameters suggest that there is

more surface roughness and larger distribution of widths with decreasing rock strength which might explain the reason for lower decline of conductivity with closure stress. The etched surfaces of weaker rocks have larger relative roughness and greater distribution of asperities holding the fracture open and hence resulting in greater ability to withstand closure stress.

4.2.2. Conductivity at Zero Closure Stress (Intercept)

From theoretical understanding, fracture conductivity depends mainly on the fracture width that is open for flow. The dependence of conductivity on fracture width is to the power of 3 for smooth fractures (parallel plate flow cubic law). For a rough surface, the roughness of the surface clearly affects the flow path (Walsh, 1981; Tsang, 1984; Brown, 1987; Ge, 1997). There has been extensive work in hydrology and rock mechanics on developing a model for flow through rough-walled fractures. While many models that account for the effect of different aspects of roughness on fluid flow have been developed, none of them is comprehensive enough to predict flow through a rough fracture accurately and consistently for all situations.

There are about three different models available that relate conductivity of rough fractures at no closure stress to some surface roughness parameter. All assume the standard cubic law applies for flow through rough fractures. However the width used in the cubic equation is referred to as hydraulic width (w_h) which replaces the average fracture width ($\overline{w}$) and the hydraulic width is related to other surface roughness parameters. There are about three different roughness parameters used to modify the width, which are ratio of width to standard deviation of width ($\overline{w}/\sigma_w$), ratio of asperity

height to width ($\bar{h}/\bar{w}$), and fraction of asperities in contact with each other(α). The following models which account for these three roughness parameters are used in our study:

1) Zimmerman and Bodvarsson (1996):

$$w_h^3 = a_1 \bar{w}^3 \left[1 - 1.5 \left(\frac{\sigma_w^2}{\bar{w}^2} \right) \right], \quad \text{..... (4.5)}$$

where σ_w is the standard deviation of fracture width distribution.

2) Modified Huitt (1956):

$$w_h^3 = a_1 \bar{w}^3 \left[\frac{1}{(\bar{h}/\bar{w})} \right], \quad \text{..... (4.7)}$$

where $\bar{h}$ is the average asperity height above the flat surface of fracture.

3) Modified Walsh (1981):

$$w_h^3 = a_1 \bar{w}^3 \alpha, \quad \text{..... (4.8)}$$

where α is the fraction of asperities in contact with each other.

In addition to all the above models, simple cubic law multiplied by a constant and modified cubic law with a new exponent are also used to match measured data as shown below:

4) Cubic law:

$$w_h^3 = a_1 \bar{w}^3, \quad \text{..... (4.9)}$$

5) Modified cubic law:

$$w_h^3 = \bar{w}^{a_1}, \quad \text{..... (4.10)}$$

All models were multiplied by a constant, a_1 in order to ensure better match to experimental measurements. The constant a_1 was determined based on linear regression to give best fit between measured and predicted conductivities.

As the rate of change of conductivity with closure stress was already determined and fixed in last section (sec. 4.2.1), in order to have a more appropriate methodology to compare among models, the actual conductivity values at different closure stresses were calculated based on above models. In this manner, the models are compared in terms of how well actual measured conductivities are matched rather than based on how well the models match no closure stress conductivity values which were not actually measured. The comparison between measured and predicted conductivities are shown in **Fig. 4.9**.

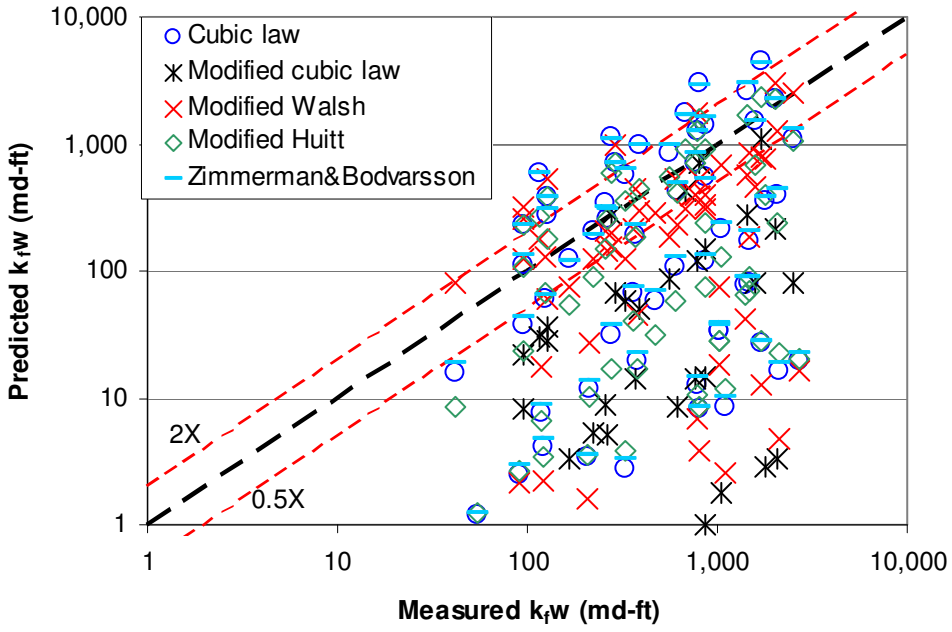

Fig. 4.9—Comparison of model's prediction to measured conductivities for all roughness etching experiments.

Analysis of the model's predictions shows that no model can predict well the measured conductivities. A closer look at the data points where the models failed to match experimentally measured conductivities well shows that these are conductivities of all of the dolomite samples and those limestone samples acidized with emulsified acid. Once the conductivity measurements of all dolomite samples and those limestone samples acidized with emulsified acid are removed, some of the models show a rather good prediction of measured conductivities as shown in **Fig. 4.10**. The models that show the better match to experimentally measured conductivities are shown only in **Fig. 4.11** in order to better see the match.

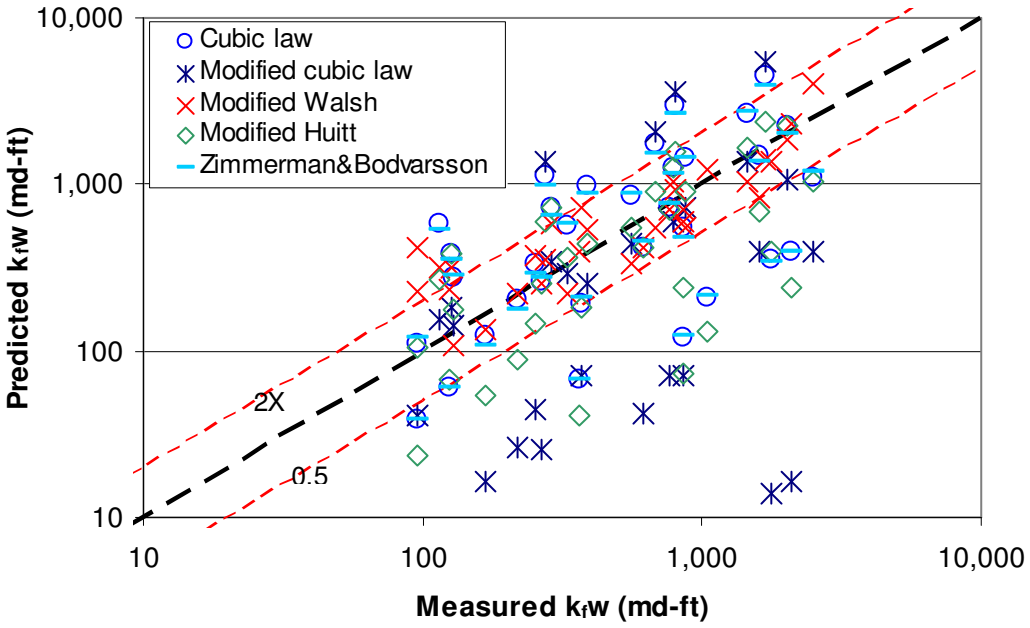

Fig. 4.10—Comparison of model's prediction to measured conductivities with dolomite samples and limestone samples acidized with emulsified acid removed.

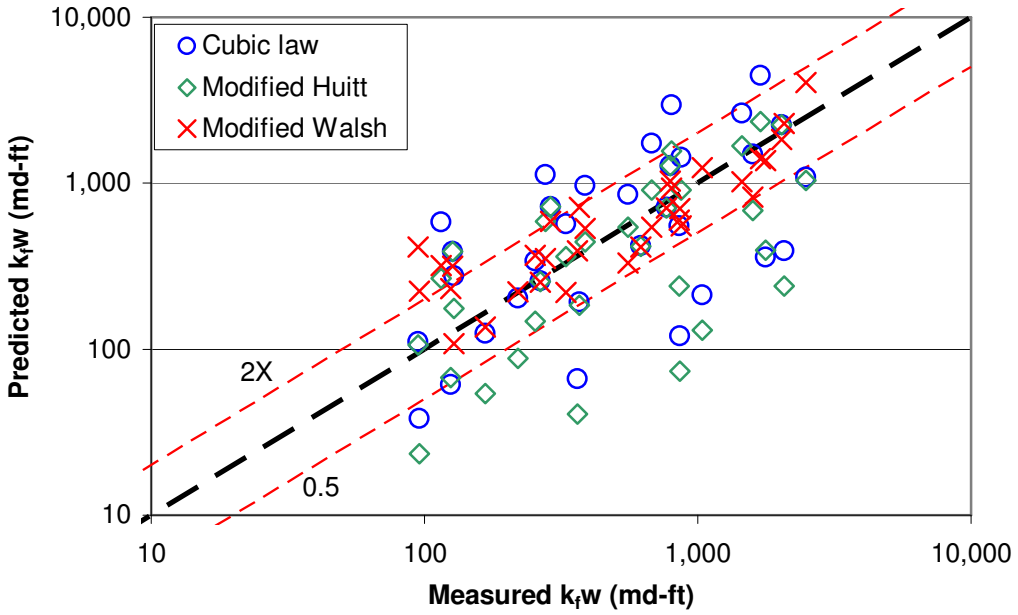

Fig. 4.11— Comparison of best match model's prediction to measured conductivities.

Results of matching between experimental data and model's predictions clear show that the model that accounts for effect of contact ratio gives the best match to experimental data. Majority of predicted conductivities are within half to double the actual measured conductivities and the total error between measured and experimental conductivities is about 7,850 md-ft as shown in **Table 4.3** (twice the error of best fit match to experimental data (see Table 4.2)).

TABLE 4.3—VALUES OF CONSTANT AND STATISTICAL FIT PARAMETERS OF SELECTED LIMESTONE EXPERIMENTS

	Cubic law	Modified cubic law	Zimmerman& Bodvarsson	Huitt (Modified)	Walsh (modified)
Constant, a_1	8.89E-04	7.09	9.88E-04	2.60E-04	0.32
Total Error	19,204	23,599	17,566	13,081	7,885
SSE	2.6E+07	4.3E+07	2.1E+07	1.2E+07	4.4E+06
R^2	0.24	0.09	0.26	0.34	0.77

The best fit model that has dependence on contact ratio indicates that conductivity increases with an increase in contact ratio. However, the original model of Walsh shows the opposite, with a decrease in conductivity with more contact ratio, as contact ratio accounts for tortuosity of fluid flow by diverting fluid around the asperities in contact. Walsh model implies that there is an increase in fluid flow tortuosity with more contact ratio and hence a decline in fluid conductance. However adequate numbers of contact points are required to keep fracture open for flow. As the measured contact ratio in our experiments are relatively small with an average of about 0.005, conductivity actually increases with greater contact ratio as the fracture can remain open over the entire length of fracture while the number of contact points is relatively low and does not impact the flow toruosity.

It is interesting to note that the modified cubic law matching resulted in an exponent of 7 in order to give best match which is more than twice the typical cubic law exponent of 3. Actually, cubic law resulted in better match to measured conductivities than the modified cubic law with exponent of 7. Also all models that accounted for

effect of some roughness parameter on conductivity gave better match that cubic law or modified cubic law.

While there are 4 different dolomite experiments with about 15 conductivity data points that can be used to develop a correlation, there are not enough experimental data points to develop a correlation for limestone samples acidized with emulsified acid. The same models as above are used to predict conductivities of dolomite samples. The comparison between prediction and measured conductivity is shown in **Fig. 4.12**.

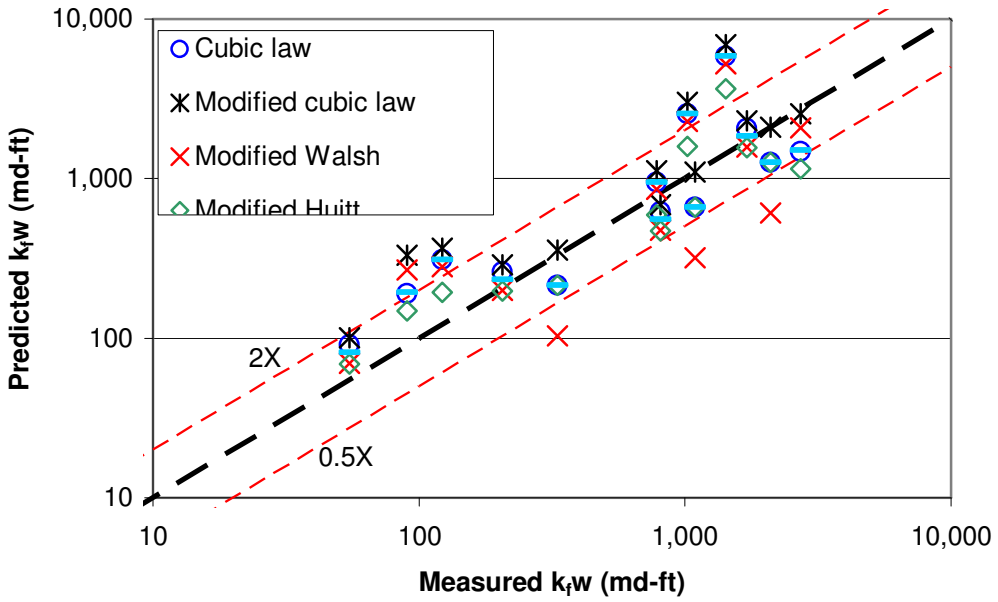

Fig. 4.12—Comparison of model's prediction to measured conductivities for dolomite samples.

While all the models give very similar matches to each other, the Huitt model that accounts for relative roughness effect gives a little better match to experimental data

compared to other models. Majority of predicted conductivities are within half to double the actual measured conductivities and the total error between measured and experimental conductivities is about 6,500 md-ft as shown in **Table 4.4** (less than twice the error of best fit match to experimental data (see Table 4.2)).

TABLE 4.4—VALUES OF CONSTANT AND STATISTICAL FIT PARAMETERS OF DOLOMITE EXPERIMENTS

	Cubic law	Modified cubic law	Zimmerman& Bodvarsson	Huitt (Modified)	Walsh (modified)
Constant, a_1	6.80E-02	3.78	7.18E-02	1.45E-02	22.74
Total Error	9,668	9,332	9,467	6,587	9,134
SSE	2.5E+07	3.5E+07	2.4E+07	8.9E+06	2.0E+07
R^2	0.22	0.32	0.22	0.33	0.24

It is interesting to note that the modified cubic law matching resulted in an exponent of 3.78 in order to give best match which is relatively close to the typical cubic law exponent of 3. Actually, cubic law resulted in similar overall match to measured conductivities compared to the modified cubic law with exponent of 3.78.

Results suggest that conductivities of dolomite samples follow much closely the cubic law than limestone samples which deviate a large degree from cubic law with an exponent of almost 7. While all samples showed roughness etching pattern, dolomite samples had a rather lower degree of roughness with smaller asperity heights and lower extent of fracture width scatter. Dolomite samples had smaller average fracture width, standard deviation of width, and relative roughness as shown in **Table 4.5**. As the

dolomite samples do not show significant amount of roughness compared to limestone samples, conductivity of dolomites follow much more closely the typical cubic law for completely smooth fractures.

TABLE 4.5—VALUES OF SURFACE PARAMETERS FOR LIMESTONE AND DOLOMITE EXPERIMENTS WITH ROUGHNESS ETCHING

	Average width (w)	Contact Ratio (α)	Standard deviation of width (σ_w)	Relative roughness (h/w)
Limestone	0.087	0.005	0.024	0.439
Dolomite	0.048	0.003	0.010	0.277

4.3. Sources of Error and Reliability

There are several major sources of error that can not be accounted for by the models. Firstly, there are no measured values of conductivity at zero closure stress and the models that estimate conductivity at no closure stress were used to match values of conductivity that were derived based on models of conductivity change with closure stress. If the measured values of conductivity at zero closure stress were available, the models would be more appropriate estimate of those measured values rather than the estimated values. Secondly, the correlations developed were based on relatively limited number of experimental data. While conductivity correlation for limestone was based on about 35 experimental measurements, dolomite correlation was developed from only about 15 data points. Furthermore, the change of conductivity with closure stress function was developed from only 3 different data points which makes it very questionable.

Even though the correlations developed in this section show certain amount of error, the errors are much less than the other previously developed correlations. Experimental values of conductivity measured by Nieorde and Kruk (1973) and also Gong (1997) were compared to estimate of those experiments using their own models. This shows the error that each of the previous correlations has in terms of how well it matched their experimental data. The comparison between measured values and calculated values of conductivity for these two correlations based on their own experimental results are shown in **Fig. 4.13** and **Fig. 4.14**, for Nierode and Kruk (1973) and Gong (1997), respectively. There are clearly large errors in the development of both Nierode and Kruk and also Gong correlations as they both show large discrepancies between their models estimate of conductivity and measured values of conductivity that were used to develop their correlation. Almost half of the predicted conductivities are over two times larger or half the value of measured conductivities, while in our correlation, less than 10% of predicted conductivities were in this range.

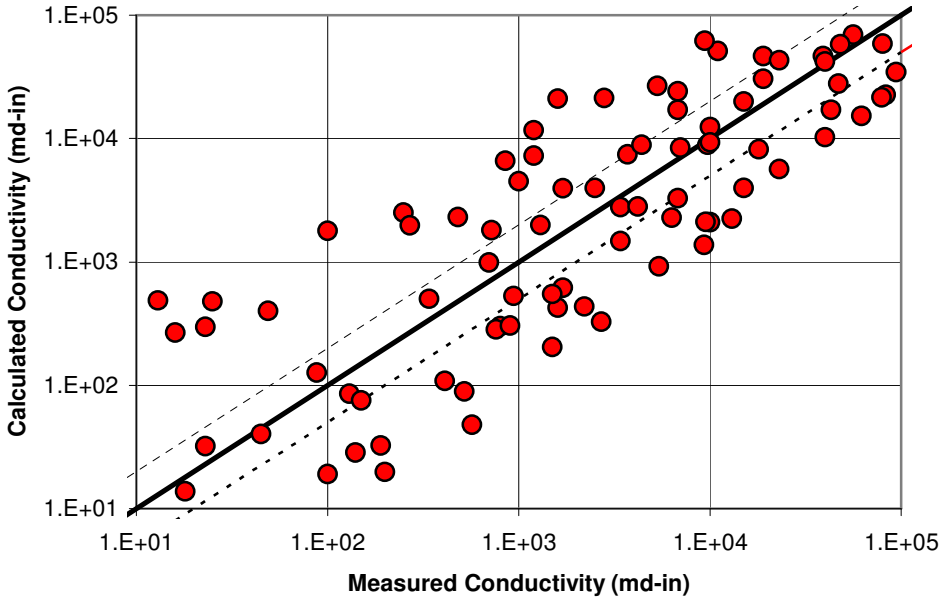

Fig. 4.13—Conductivity predictions of Nierode and Kruk's experimental data using their own correlation.

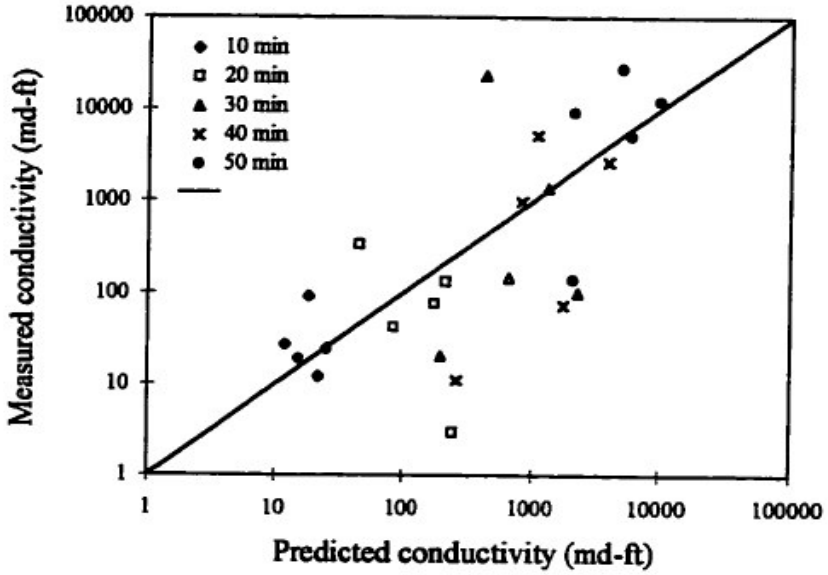

Fig. 4.14—Conductivity predictions of Gong's experimental data using Gong's own correlation.

4.4. Comparison with Prediction from Other Models

As one of the main objectives of this study was to develop a more accurate conductivity prediction correlation, the new model must be compared to previous models. There are two well known models of fracture conductivity. While Nierode and Kruk (1973) model is simple, easy to use and has been used extensively in industry, Gong (1997) model is not easily applicable, however it includes more parameters that are not included in Nierode and Kruk model. In order to compare our results, we calculate conductivity using these two models for only limestone samples as Gong model was based on only limestone experiments and also our model shows the need for different modeling for dolomite samples.

In the Nierode and Kruk model, the width used is the average width as it has been shown by Schechter (1992) that actual ideal width is approximately equal to mean ideal width for Peclet numbers above 5. However our Peclet number is about 3 where the actual width could be up to 3 times the mean width. For our comparison, we used the average width of fracture that was also used in our modeling. Furthermore, the value of S_{RE} used in the equation is not clear whether it is before or after acidizing rock strengths. As the slopes for each rock type were very similar, a general value of S_{RE} for each rock type was used in the correlation, similar to our modeling.

The correlation of Gong (1997) does not state how to obtain the initial conductivity at zero closure stress, however he used the simple cubic law to obtain it in his dissertation. We also calculated it based on cubic law with average width. We also used the best fit intercept values from Table 4.1 as the initial conductivity in order to

improve the correlation. The kurtosis used in the correlation is of the asperity heights as stated by Gong (1997). However as the values of kurtosis measured in our experiments were relatively large with values up to 100, while Gong (1997) states that kurtosis values should be in the range of -1 to 1, we fixed kurtosis values to be in the same narrow range by using linear regression between measured and fixed kurtosis values. The value of the stress correction factor, c is stated to be between 2 and 4 and depends on the shape and size of surface irregularities. As there is no mention of how to calculate c, we correlated it to relative roughness defined as ($\overline{h}/\overline{w}$) using linear regression to ensure values of c are between 2 and 4. Furthermore, the model requires rock yield stress which is not available. As Gong (1997) used rock yield stress in the range of 5,000 to 6,000 psi for limestone samples, we also fixed it in the same range by correlating it to general S_{RE} values for each rock type.

Comparison between measured and calculated conductivities for the three models (our model, Nierode and Kruk, and Gong (based on both cubic law estimate and best fit determined initial conductivity) are shown for all closure stresses in **Fig. 4.15**. The results show that our model estimates much better the experimental data than the other models. While Gong model results are much less accurate with rather large scatter in predicted conductivities, Nierode and Kruk correlation shows much better estimate of measured conductivities with less scatter in predictions.

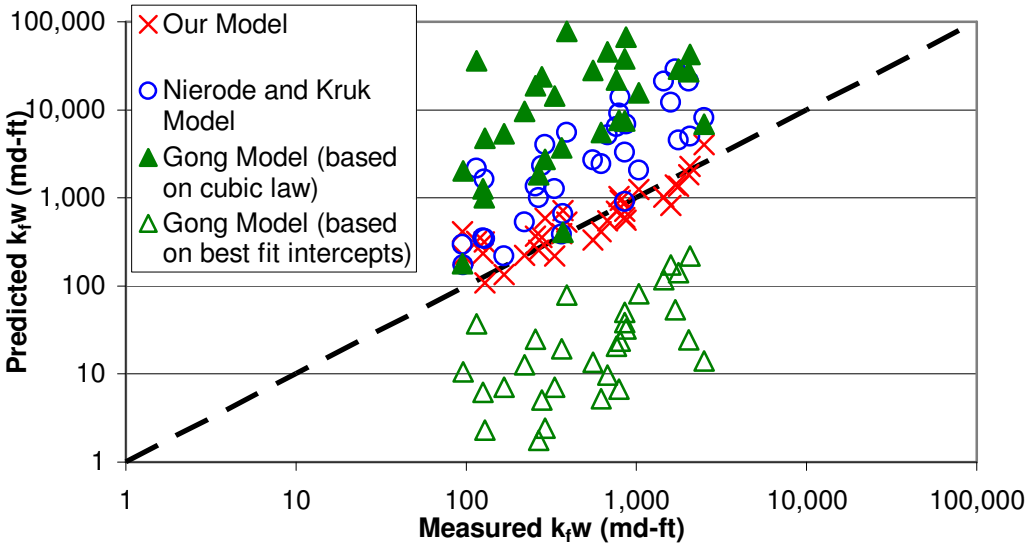

Fig. 4.15—Comparison between measured and calculated conductivities using our model, Nierode and Kruk correlation, and Gong model for all closure stresses.

Both Nierode and Kruk correlation and Gong model based on cubic law estimate of initial conductivity over predict measured conductivities, which might be the result of measured widths not being the actual widths that should be used in their equations. These two model's definition of fracture width might be different from the method that we have used to measure fracture width. In order to improve the predictions from these two models, measured fracture width was modified based on linear regression to obtain best fit to measured conductivities. The result of modified fracture width used in above two models is shown in **Fig. 4.16**, which also shows our model for comparison purpose. The new fracture widths used are 0.52 and 0.28 times the measured fracture widths for Nierode and Kruk correlation and Gong model, respectively. The models now show much closer match of experimentally measured conductivities, however there is still

much more scatter and error in the models compared to our model as shown in **Table 4.6**.

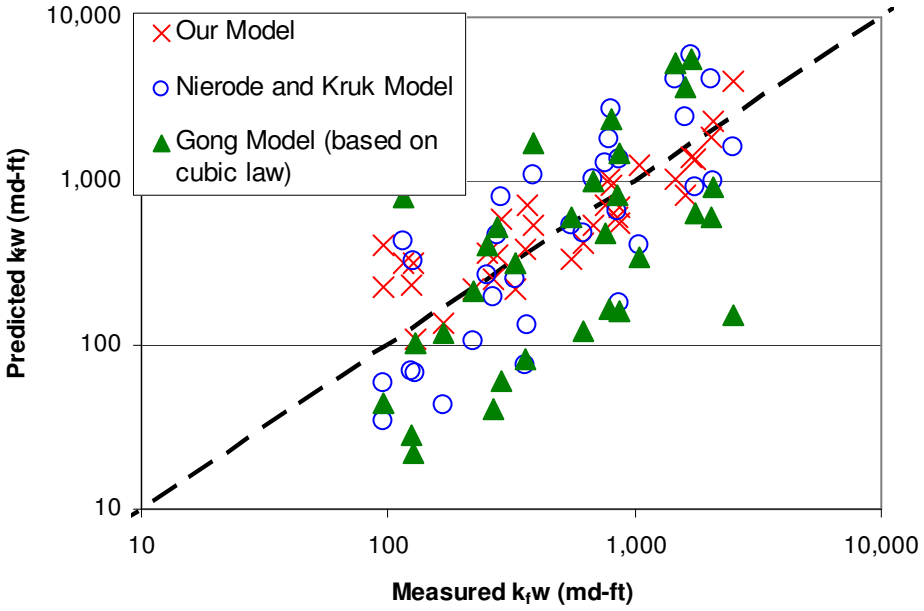

Fig. 4.16—Comparison between measured and calculated conductivities with modified fracture width for Nierode and Kruk and Gong models.

TABLE 4.6—VALUES OF STATISTICAL FIT PARAMETERS FOR DIFFERENT CONDUCTIVITY MODELS

	Our model	N-K	Modified N-K	Gong	Modified Gong
Total Error	7,885	151,552	21,678	1,289,060	25,141
SSE	4.4E+06	2.1E+09	4.0E+07	1.8E+11	5.1E+07
R^2	0.77	0.43	0.43	0.20	0.20

4.5. New Developed Correlation Advantages

The newly developed correlation offers great advantages over previous conductivity correlations. The new correlation has shown the necessity for modeling resulting conductivity of limestone and dolomite samples separately. As acid fracturing of limestone samples results in much more rougher surfaces with greater degree of deviation from smooth surface, resulting conductivity depends highly on roughness parameters, especially contact ratio. However dolomite samples etch more uniformly with lower degree of roughness, hence cubic law is appropriate for conductivity prediction.

Clearly Nierode and Kruk correlation which assumes conductivity at zero closure stress to be a function of just the fracture width is not appropriate for rough walled fractures like limestone samples. The discussion in section 4.2.2 indicated that conductivity depends on some surface parameters that describe the roughness pattern like contact ratio and relative roughness.

5. CONCLUSIONS AND RECOMMENDATIONS

5.1. Conclusions

A laboratory facility to conduct acid fracturing experiments scaled to field conditions with measurement of all important parameters that influence resulting conductivity was designed and tested. The effect of different treatment parameters on resulting conductivity was established which were:

1. There is an optimal acid system for each formation which depends on closure stress and treatment schedule.

2. Conductivity even at low closure stress sometimes declines with increasing contact time; hence there is an optimal contact time for each formation and acid, depending on closure stress levels.

3. Formations respond differently to same treatment with greatest difference among them in the rate of conductivity decline with closure stress due to differences of formation strengths.

4. Temperature of the formation seems to have significant influence on resulting conductivity, especially on initial conductivity at low closure stress.

The etching pattern analysis clearly showed that there are three main modes of dissolution: surface roughness, channeling, and turbulence etching. Each etching pattern type has its own unique pattern of conductivity and must be modeled separately.

A new correlation for conductivity based on surface etching parameters for roughness pattern was developed. The new correlation reveals the following important conclusions:

1. Initial conductivity at no closure stress is a function of contact ratio in addition to just the average fracture width.

2. The rate of conductivity decline with closure stress is mainly a function of rock strength and very similar for each rock type.

The newly developed model was validated against experimental data which showed relatively good match compared to other available conductivity models. There was much less scatter and error in estimation of conductivity with new model. Furthermore, the new conductivity model shows the necessity in including surface etching roughness parameters like contact ratio for calculation of conductivity as the average fracture width can not predict retained conductivities.

5.2. Recommendations

It is clear from almost all studies on acid fracturing that treatment affects rock strength and rock strength is a very important factor controlling the rate of conductivity decline with closure stress. While we measured rock embedment strength of acidized cores, the measurements did not show any trend and showed wide variation. It is recommended to measure other parameters that describe the strength of rocks like Young's modulus and rock yield stress in a more precise manner to develop a better understanding of rock strength influence on resulting conductivity.

As results have clearly indicated that conductivity at zero closure stress is controlled by surface roughness parameters, it would be beneficial to perform more detailed characterization of roughness and relate it to resulting conductivity. It would be

helpful to characterize surface roughness after each closure stress load in order to also determine the effect of stress on roughness and hence on resulting conductivity.

As etching patterns showed much more etching at the inlet of the fracture and acid consumption calculations showed little acid consumed during reaction, our experiments represent conditions near wellbore. It is recommended to use some percentage of spent acid in the acidizing process in order to represent conditions further down a real fracture.

REFERENCES

Abass, H.H., Al-Mulhem, A.A., and Mirajuddin, K.R. 2006. Acid Fracturing or Proppant Fracturing in Carbonate Formation? A Rock Mechanic's View, paper SPE 102590 presented at the 2006 SPE Annual Technical Conference and Exhibition, San Antonio, Texas, 24-27 September.

Anderson, M.S., and Fredrickson, S.E. 1989. Dynamic Etching Tests Aid Fracture-Acidizing Treatment Design, *SPE Production Engineering* **4** (4): 443-449.

Barron, A.N., Hendrickson, A.R., and Wieland, D.R. 1962. The Effect of Flow on Acid Reactivity in a Carbonate Fracture, *JPT* **14** (4): 409-415.

Bartko, K.M., Conway, M.W., Krawietz, T.E., Marquez, R.B., and Oba, R.G.M. 1992. Field and Laboratory Experience in Closed Fracture Acidizing the Lisburne Field, Prudhoe Bay, Alaska, paper SPE 24855 presented at the 1992 Annual Technical Conference and Exhibition, Washington, D.C., 4-7 October.

Bartko, K.M., Nasr-El-Din, H.A., Rahim, Z., and Al-Muntasheri, G.A. 2003. Acid Fracturing of a Gas Carbonate Reservoir: The Impact of Acid Type and Lithology on Fracture Half Length and Width, paper SPE 84130 presented at 2003 SPE Annual Technical Conference and Exhibition, Denver, Colorado, 5-8 October.

Beg, M. S., Kunak, A. O., Gong, M., Zhu, D., and Hill, A. D. 1996. A Systematic Experimental Study of Acid Fracture Conductivity, paper SPE 31098 presented at the 1996 SPE International Symposium on Formation Damage Control, Lafayette, Louisiana, 14-15 February.

Broaddus, G.C., Knox, J.A., and Fredrickson, S.E. 1968. Dynamic Etching Tests and Their Use in Planning Acid Treatments, paper SPE 2362 presented at the 1968 Oklahoma Regional Meeting of SPE of AIME, Stillwater, Oklahoma, 25 October.

Conway, M.W., Asadi, M., Penny, G.S., and Chang, F. 1999. A Comparative Study of Straight/Gelled/Emulsified Hydrochloric Acid Diffusivity Coefficient Using Diaphragm Cell and Rotating Disk, paper SPE 56532 presented at 1999 SPE Annual Technical Conference and Exhibition, Houston, Texas, 3-6 October.

De Rozieres, J., Chang, F.F., and Sullivan, R.B. 1994. Measuring Diffusion Coefficients in Acid Fracturing Fluids and Their Application to Gelled and Emulsified Acids, paper SPE 28552 presented at the 1994 SPE Annual Conference and Exhibition, New Orleans, LA, 25-28 September.

Economides, M.J., Hill, A.D., and Ehlig-Economides, C. 1994. *Petroleum Production Systems*, Upper Saddle River, New Jersey: Prentice Hall Petroleum Engineering Series, 412.

Gangi, A.F. 1978. Variation of Whole and Fractured Porous Rock Permeability with Confining Pressure, *Int. J. Rock Mech. Min. Sci. Geomech. Abstr.* **15**, 249-257.

Gong, M. 1997. Mechanical and Hydraulic Behavior of Acid Fractures – Experimental Studies and mathematical Modeling, Ph.D. dissertation, The University of Texas, Austin, Texas.

Gong, M., Lacote, S., and Hill, A.D. 1998. New Model of Acid-Fracture Conductivity Based on Deformation of Surface Asperities, paper SPE 39431 presented at the 1998 SPE International Formation Damage Symposium, Lafayette, Louisiana, 18-19 February.

Howard, G. C and Fast, C. R. 1970. *Hydraulic Fracturing*, SPE Monograph Vol. 2, Henry L. Doherty Series. New York. SPE of AIME, 203.

Lund, K., Fogler, H.S., and McCune, C.C. 1973. Acidizing-I. The Dissolution of Dalcite in Hydrochloric Acid, *Chemical Engineering Science* **28**, 691-700.

Lund, K., Fogler, H.S., McCune, C.C., and Ault, J.W. 1975. Acidizing-II. The Dissolution of Calcite in Hydrochloric Acid, *Chemical Engineering Science* **30**, 825-835.

Malagon, C. 2007. The Texture of Acidized Fracture Surfaces-Implications for Acid Fracture Conductivity, Master's thesis, Texas A&M University., College Station, Texa

Melendez, M.G. 2007. The Effects of Acid Contact Time and Rock Surfaces on Acid Fracture Conductivity, Master's thesis, Texas A&M University., College Station, Texas.

Nasr-El-Din, H.A., Al-Driweesh, S. M., Metcalf, A. S., and Chesson, J. 2006. Fracture Acidizing: What Role Does Formation Softening Play in Production Response? paper SPE 103344 presented at the 2006 SPE Annual Technical Conference and Exhibition, San Antonio, Texas, 24-27 September.

Nasr-El-Din, H.A., Al-Ghamdi, A.H., Al-Qahtani, A.A., and Samuel, M.M. 2008. Impact of Acid Additives on the Rheological Properties of a Viscoelastic Surfactant and Their Influence on Field Application, *SPE Journal* **13** (1): 35-47.

Navarrete, R.C., Miller, M.J., and Gordon, J.E. 1998. Laboratory and Theoretical Studies for Acid Fracture Stimulation Optimization, paper SPE 39776 presented at the 1998 SPE Permian Basin Oil and Gas Recovery Conference, Midland, Texas, 23-26 March.

Nierode, D.E., and Kruk, K.F. 1973. An Evaluation of Acid Fluid Loss Additives, Retarded Acids, and Acidized Fracture Conductivity, paper SPE 4549 presented at the 1973 Annual Fall Meeting, Las Vegas, Nevada, 30 September–3 October.

Pursell, D. A. 1987. Laboratory Investigation of Inertial Flow in High Strength Fracture Proppants, Master's thesis, Texas A&M University, College Station, Texas.

Shaughnessy, C.M., and Kunze, K.R. 1981. Understanding Sandstone Acidizing Leads to Improved Field Practices, *JPT* **33** (7): 1196-1202.

Van Domelen, M.S. 1992. Optimizing Fracture Acidizing Treatment Design by Integrating Core Testing, Field Testing, and Computer Simulation, paper SPE 22393 presented at the 1992 SPE International Meeting on Petroleum Engineering, Beijing, China, 24-27 March.

Van Domelen, M.S., Gdanski, R.D., and Finley, D.B. 1994. The Application of Core and Well Testing to Fracture Acidizing Treatment Design: A Case Study, paper SPE 27621 presented at the 1994 European Production Operations Conference and Exhibition, Aberdeen, U.K., 15-17 March.

Walsh, J.B. 1981. Effect of Pore Pressure and Confining Pressure on Fracture Permeability, *Int. J. Rock Mech. Min. Sci. Geomech. Abstr.* **18**, 429-435.

Williams, B.B., Gidley, J.L., and Schechter, R.S. 1979. *Acidizing Fundamentals*, Richardson, TX, Society of Petroleum Engineers.

Williams, B.B., and Nierode, D.E. 1972. Design of Acid Fracturing Treatments, *JPT* **24** (7): 849-859.

Wong, C.S., Tishchenko, P.Y., and Johnson, W.K. 2005. Solubility of Carbon Dioxide in Aqueous HCl and NaHCO3 Solutions from 278 to 298 K, *J. Chem. Eng. Data* **50**, 817-821.

Zimmerman, R.W., and Bodvarsson, G.S. 1996. Hydraulic Conductivity of Rock Fractures, *Transport in Porous Media* **23**, 1-30.

Zou, C.L. 2006. Development and Testing of an Advanced Acid Fracture Conductivity Apparatus, Master's Thesis, Texas A&M University, College Station, Texas.

VITA

Name:	Maysam Pournik
Address:	3702 Westfield Drive, College Station, TX 77845
Email Address:	maysamp@tamu.edu
Education:	M.EN., Chemical Engineering, University of Birmingham, United Kingdom, June 2001 M.S., Petroleum Engineering, The University of Texas at Austin, TX, USA, May 2004 Ph.D., Petroleum Engineering, Texas A&M University, TX, USA, December 2008